SCHOOL OF
CIVIL ENGINEERING

INDIANA
DEPARTMENT OF TRANSPORTATION

JOINT HIGHWAY RESEARCH PROJECT

FHWA/IN/JHRP-95/16
Final Report

IMPACT ANALYSIS OF VEHICLES ON OZONE GENERATION IN THE INDIANAPOLIS METROPOLITAN STATISTICAL AREA

Ouattara Fatogoma
Robert B. Jacko

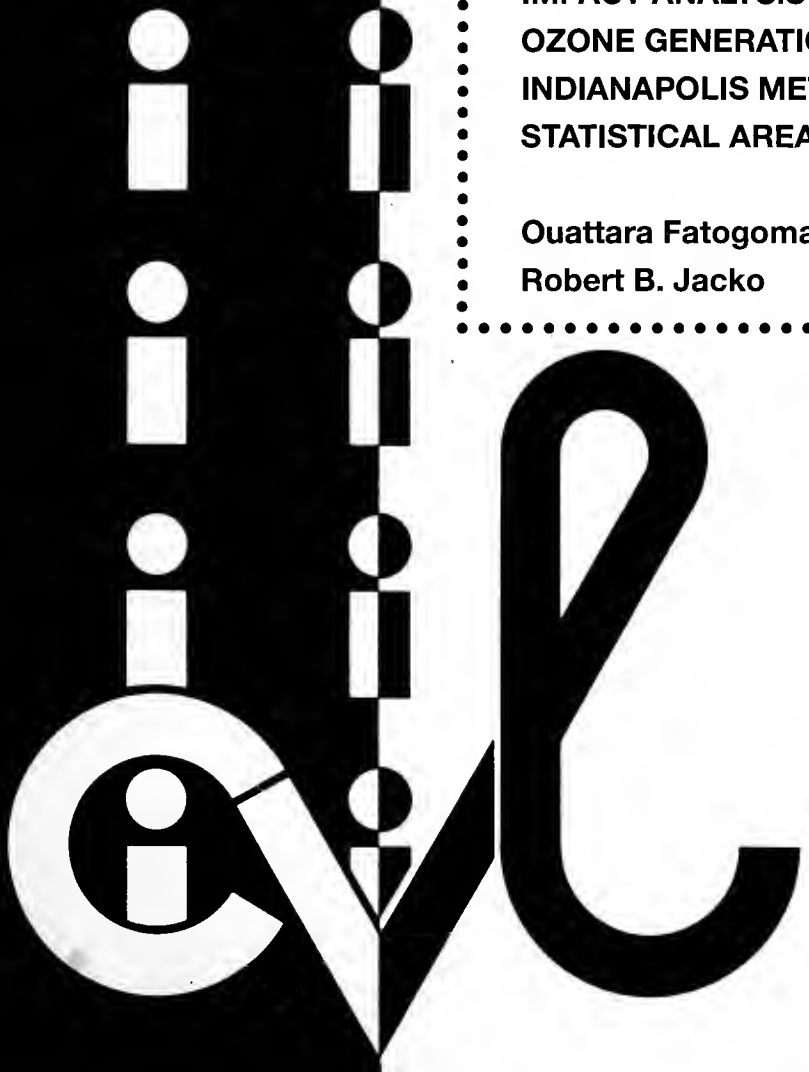

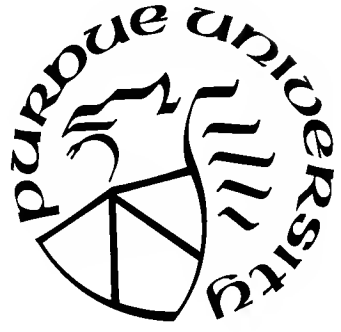

PURDUE UNIVERSITY

Final Report

Impact Analysis of Vehicles on Ozone Generation In the Indianapolis Metropolitan Statistical Area

FHWA/IN/JHRP-95/16

Prepared by

Outtara Fatagoma, Ph.D.
Research Assistant

and

Robert B. Jacko, Ph.D., P.E.
Professor

Environmental Engineering
School of Civil Engineering
Purdue University

Joint Highway Research Project

Project No. C-36-37
File No. 9-10-38

Prepared in Cooperation with the
U.S. Department of Transportation
and
Federal Highway Administration

Purdue University
West Lafayette, IN 47907
September 1, 1996

TECHNICAL REPORT STANDARD TITLE PAGE

1. Report No.	2. Government Accession No.	3. Recipient's Catalog No.
FHWA/IN/JHRP-95/16		

4. Title and Subtitle	5. Report Date
Impact Analysis of Vehicles on Ozone Generation in the Indianapolis Metropolitan Statistical Area	September, 1996
	6. Performing Organization Code

7. Author(s)	8. Performing Organization Report No.
Ouattara Fatogoma and Robert Jacko	FHWA/IN/JHRP-95/16

9. Performing Organization Name and Address	10. Work Unit No.
Joint Highway Research Project Civil Engineering Building Purdue University West Lafayette, Indiana 47907-1284	11. Contract or Grant No. HPR-2108

12. Sponsoring Agency Name and Address	13. Type of Report and Period Covered
Indiana Department of Transportation State Office Building 100 North Senate Avenue Indianapolis, IN 46204	Final Report
	14. Sponsoring Agency Code

15. Supplementary Notes

Prepared in cooperation with the Indiana Department of Highways and Federal Highway Administration.

16. Abstract

Motor vehicles are one of the largest emitters of ground-level ozone precursors - volatile organic compounds (VOCs) and nitrogen oxides (NO_x) - into the atmosphere. Consequently, the Clean Air Act Amendment of 1990 requires the implementation of transportation control measures in order to reduce ground-level ozone precursor emissions and alleviate the ozone air quality problems.

This research investigates the relative effects of motor vehicle emissions of VOCs and No_x on hourly average concentrations of ground level ozone in the Indian Airshed Model (UAM-1V). The Findings of the research study are presented. This includes the results of the data analyses leading to the modeling domain definition, episodes selection, and the different UAM-IV inputs development, as well as the modeling results including the UAM-IV performance evaluation and the sensitivity analyses on VOCs and No_x emission reductions.

17. Key Words	18. Distribution Statement
tropospheric ozone, mobile source emission, urban airshed model, ozone modeling.	No restrictions. This document is available to the public through the National Technical Information Service, Virginia, 22161

19. Security Classif. (of this report)	20. Security Classif. (of this page)	21. No. of Pages	22. Price
Unclassified	Unclassified	119	

Form DOT F 1700.7 (8-69)

Table of Contents

List of Tables

List of Figures

1. Introduction

1.1. Introduction

Unlike the other criteria pollutants[1], ground-level ozone is not directly emitted into the atmosphere. It is a secondary pollutant which is formed as a result of photochemical reactions involving the primary pollutants such as volatile organic compounds (VOCs) and nitrogen oxides (NO_x) which are largely emitted by motor vehicles. Evidence from scientific studies indicate that ground-level ozone adversely affect human respiratory system, damage crops and trees and other materials. Since ozone is not directly emitted into the atmosphere, its control strategies are not obvious and depend on well-calibrated urban-scale air quality models such as the Urban Airshed Model (UAM-IV).

In this research project, the UAM-IV was used along with other emission and meteorological models such as Mobile5a, Biogenic Emissions Inventory System (BEIS), and Diagnostic Wind Model (DWM) to simulate hourly average concentration of ground-level ozone and assess the contribution of motor vehicle emissions of VOCs and NO_x on the generation of ground-level ozone in the Indianapolis Metropolitan Statistical Area (MSA). In this final report, the findings of the research efforts are presented, especially, the results of the data analyses leading to the modeling domain definition, episodes selection, and the different UAM-IV inputs development as well as the modeling results including the UAM-IV performance evaluation and the sensitivity analyses on VOCs and NO_x emissions reductions. In addition, a summary of the chemistry of ground-level ozone formation and an overview of the UAM-IV are also presented.

1.2. Summary of Ground-Level Ozone Chemistry

Ground-level ozone is produced by reactions involving VOCs and NO_x driven by the sun's ultra-violet radiation (UV). By convention, NO_x represents the sum of nitric oxide (NO) and nitrogen dioxide (NO_2) excluding other reactive nitrogen species such as the nitrate radical ($NO_3^{\bullet}$), dinitrogen pentoxide (N_2O_5), nitrous acid (HONO),

---

[1] Particulate matters (PM), sulfur oxides (SO_x), nitrogen oxides (NO_x) volatile organic compounds (VOCs), carbon monoxide (CO), and lead (Pb).

peroxyacetyl nitrate (PAN), other organic nitrates, and nitrites. These excluded nitrogen species have very short lifetimes and are rapidly formed from, or converted to NO or NO_2. VOCs are organic compounds which participate in atmospheric photochemical reactions. These include any organic compound other than methane, ethane, methylene chloride, and many chlorofluorocarbons (CFCs) which are inert in the lower atmosphere.

The photolysis of NO_2 generates an oxygen atom (O) and NO.

$$NO_2 + h\nu \rightarrow O + NO \quad (1)$$

where $h\nu$ represents a photon of UV light. The oxygen atom from Reaction 1 can form ozone by reacting with molecular oxygen and any other molecule M (usually O_2 or N_2).

$$O + O_2 + M \rightarrow O_3 + M \quad (2)$$

NO formed in Reaction 1 can react with ozone to yield NO_2 and O_2.

$$NO + O_3 \rightarrow NO_2 + O_2 \quad (3)$$

Reactions 1, 2, and 3 combine in a cycle (NO_2 cycle) where ozone is created and then destroyed leaving the initial NO_2 and O_2 molecules. Therefore, the sum of the above three reactions is zero except for a lost photon. However, VOCs break this cycle by converting NO back to NO_2 as in Reaction 3 without destroying ozone, through free-radical (chain) transfer reactions such as

$$OH^{\bullet} + VOC \rightarrow RO_2^{\bullet} + H_2O \quad (4)$$

$$RO_2^{\bullet} + NO \rightarrow NO_2 + RO^{\bullet} \quad (5)$$

$$RO^{\bullet} + O_2 \rightarrow RCHO + HO_2^{\bullet} \quad (6)$$

$$HO_2^{\bullet} + NO \rightarrow NO_2 + OH^{\bullet} \quad (7)$$

R is a part of an organic molecule, $RO_2^{\bullet}$ is an organic peroxy radical, $RO^{\bullet}$ is a carbonyl radical, RCHO is an aldehyde molecule, $OH^{\bullet}$ is the hydroxyl radical, and $HO_2^{\bullet}$ is the hydroperoxy radical. This VOC cycle begins and ends with the $OH^{\bullet}$ radical in which there is no net increase or decrease in the number of radicals. The NO_2 generated in the cycle can then react photochemically as in Reactions 1 and 2 to give ozone. Free radicals usually originate from photolysis reactions. The most important reactions that generate many radicals are

$$O_3 + h\nu \rightarrow O_2 + O(^1D) \quad (8)$$

$$O(^1D) + H_2O \rightarrow 2OH^{\bullet} \quad (9)$$

$$RCHO + h\nu \rightarrow RO_2^{\bullet} + HO_2^{\bullet} \quad (10)$$

$O(^1D)$ is an oxygen atom that has been electronically exited to the ^1D state.

An important reaction that removes both radicals and NO_x is

$$OH^{\bullet} + NO_2 \rightarrow HNO_3 \quad (11)$$

where HNO_3 is the nitric acid molecule.

The hydroxyl radical is very important in ground-level ozone chemistry. All organic compounds, carbon monoxide, and several nitrogen species react with $OH^{\bullet}$ in the atmosphere. Reaction of $OH^{\bullet}$ with organic compounds is an oxidation process in which the parent compound is reduced in size to form a series of relatively long-lived intermediate species until only CO_2 and H_2O remain. When NO_2 reacts with $OH^{\bullet}$, the $OH^{\bullet}$ is diverted from the VOC cycle because $OH^{\bullet}$ is consumed (Equation 11). By consuming instead of generating radicals, the reaction of $OH^{\bullet}$ with NO_2 retards the rate of ozone formation. The rate at which $OH^{\bullet}$ reacts with NO_2 depends on the product of $OH^{\bullet}$ concentration, NO_2 concentration, and the reaction rate. Similarly, the rate at which $OH^{\bullet}$ reacts with VOC depends on the product of $OH^{\bullet}$ concentration, VOC concentration, and the reaction rate. Therefore, the ratio of VOC to NO_2 determines whether $OH^{\bullet}$ reacts predominantly with VOC or NO_2. $OH^{\bullet}$ reacts at equal rates with VOC and NO_2 when the VOC-to-NO_2 ratio attains a particular value. This value is a function of the rate constants for the reactions of VOC and NO_2 with $OH^{\bullet}$. It varies from 5:1 to 10:1 depending on location. If the VOC-to-NO_2 ratio is less than the particular value, reaction of $OH^{\bullet}$ with NO_2 predominates over the reaction of $OH^{\bullet}$ with VOC. In this case $OH^{\bullet}$ is removed by NO_2, no new radicals are generated, and ozone production is low. When the ratio is greater than the particular value, $OH^{\bullet}$ reacts with VOC, photolysis of intermediate products generates new radicals, and ozone production is enhanced.

Thousands of reactions (~30,000) relate to ground-level ozone formation. However, Reaction 1 through 11 as condensed, can explain all the important observed ozone related daytime chemical phenomena.

At night, ozone and NO_x are lost through reactions involving trace species such as $NO_3^{\bullet}$ and N_2O_5. NO_2 and ozone react to form $NO_3^{\bullet}$ which then reacts with another NO_2 molecule to form N_2O_5. Reaction with water converts N_2O_5 into two molecules of nitrous acid (HONO).

$$NO_2 + O_3 \rightarrow NO_3^{\bullet} + O_2 \tag{12}$$

$$N_2O_5 + H_2O \rightarrow 2HONO + 2O_2 \tag{13}$$

$$NO_3^{\bullet} + NO_2 \rightarrow N_2O_5 \tag{14}$$

This set of reactions decreases the concentration of both NO_2 and ozone. Other trace nitrogen compounds play important roles at night. There are PAN, organic nitrates, and nitrophenols. Furthermore, ozone is destroyed through physical processes such as dry deposition, aerosol scavenging, and dilution with cleaner air.

1.3. Overview of the UAM-IV

The UAM-IV is a three-dimensional Eulerian model designed to calculate the concentrations of air pollutants by simulating the physical and chemical processes in the atmosphere that affect pollutant concentrations. The basis of the UAM-IV is the atmospheric diffusion equation.

$$\frac{\partial C_i}{\partial t} + \frac{\partial (uC_i)}{\partial x} + \frac{\partial (vC_i)}{\partial y} + \frac{\partial (wC_i)}{\partial z} = \frac{\partial}{\partial x}(k_x \frac{\partial C_i}{\partial x}) + \frac{\partial}{\partial y}(k_y \frac{\partial C_i}{\partial y}) + \frac{\partial}{\partial z}(k_z \frac{\partial C_i}{\partial z}) + R_i + S_i + D_i + W_i \tag{15}$$

where, $C_i(x,y,z,t)$ is the concentration of pollutant i, u, v, and w are the horizontal and vertical wind speed components, $k_x = k_y$ (homogeneous atmospheric boundary layer) is the horizontal turbulent diffusion coefficients, k_z is the vertical turbulent exchange coefficient, $R_i(C_1, C_2, \ldots C_n, T)$ is the net rate of production of pollutant i by chemical reaction of n pollutants, $S_i(x, y, z, t)$ is the emission rate of pollutant i, $D_i(x,y,z,t)$ and $W_i(x, y, z, t)$ are the net rate of removal of pollutant i due to surface uptake and wet deposition processes

respectively. This equation is derived from the conservation of mass of a single pollutant of concentration C_i (x,y,z,t) from n chemically reactive species in a fluid. It represents a mass balance of the relevant emissions, transport, diffusion, chemical reactions, and removal processes. In this equation, all concentrations and velocities are mean and time-average quantities.

1.3.1. Treatment of the Processes of the Atmospheric Diffusion Equation in the UAM-IV

The UAM-IV employs finite differencing numerical techniques for the solution of the atmospheric diffusion equation and boundary conditions which constitute n coupled, nonlinear partial differential equations in four dimensional space (x,y,z,t). The region to be simulated is divided into a three-dimensional grid with constant lengths in the x and y directions. Vertical layer thicknesses are defined based on the diffusion break, the top of the region, the number of layers below and above the diffusion break, and the minimum layer thickness. The UAM-IV solves the atmospheric diffusion equation stepwise by using the method of fractional steps. At each integration time step, the terms in the equation that represent the different atmospheric processes are solved separately in several steps. First, the advection/diffusion in the x- direction is solved. Second, the advection/diffusion in the y-direction is solved. Third, the emissions are injected and the vertical advection/diffusion is solved. Finally, the chemical transformations of the pollutants are performed.

1.3.1.1. Chemistry Process

In the treatment of atmospheric chemistry, the carbon-bond (CB-IV) approach is used to condense the kinetic mechanisms into a usable number of species and reactions (Gery *et al*, 1989). In this approach, organic compounds are grouped according to bond types (carbon single bonds, carbon double bonds, or carbonyl bonds). In the first step, the extended mechanism, the reactions of four different types of species are treated: inorganic species, organic species that because of their unique chemistry or special importance in the environment are treated explicitly, organic species that are represented by carbon bond surrogates, and organic species that are represented by molecular surrogates. The

inorganic reactions describing the chemistry of ozone, various NO_x species, and HO_x radicals are represented explicitly with no lumping. Formaldehyde, the simplest of the organic carbonyl species, formed during the oxidation of almost all organic species is represented explicitly. Ethene and isoprene are also treated explicitly because ethene which reacts slower than the other alkenes, constitutes a large fraction of hydrocarbon emissions and isoprene is the most prominent of the biogenic hydrocarbon emissions. Carbon bond surrogates are used to describe the chemistry of three different types of carbon bonds. The single-bonded one -carbon atom surrogate PAR (paraffin) represents the chemistry of alkanes and most of the alkyl groups. The carbon bond surrogate OLE (olefin), which contains two carbon atoms, represents the carbon-carbon double bonds that are found in 1-alkenes. The surrogate ALD2 which also contains two carbons atoms represents the -CHO group and adjacent carbon atom in acetaldehyde and higher aldehydes. It also represents 2-alkenes since these species react very quickly in the atmosphere to produce aldehyde products. The chemistry of aromatic hydrocarbons is represented by two molecular surrogates. The surrogate TOL (toluene) is a seven-carbon species used to characterize monoalkylbenzene structures. XYL (xylene) an eight-carbon surrogate represents dialkylbenzenes and trialkylbenzenes. In the second step, the condensed mechanism, four types of techniques are used to further condense the ozone chemistry to an useful form of 86 reactions and 33 state species to be used in air quality simulation models: elimination of unimportant reactions and products, creation of an universal peroxy radical, mathematical and algebraic manipulations to limit the number of reactions, and lumping of secondary reaction products. Table 1.1 shows the CB-IV species names and descriptions. The CB-IV is implemented in the UAM-IV by using quasi-steady-state assumptions for the low-mass fast-reacting species and the Crank-Nicholson numerical algorithm for the remaining species for the simultaneous solution of the differential equations representing each species. The Crank-Nicholson numerical algorithm utilizes the rate of change of each species and a Jacobian matrix relating the changes in each species to all others.

Table 1.1. Reactive species names and descriptions in the CB-IV chemical mechanism (From USEPA, 1990b).

Species Name	Representation
Nitric oxide	NO
Nitrogen dioxide	NO2
Nitrogen trioxide (nitrate radical)	NO3
Dinitrogen pentoxide	N2O5
Nitrous acid	HONO
Nitric acid	HNO3
Peroxynitric acid (HO_2NO_2)	PNA
Oxygen atom (singlet)	O1D
Oxygen atom (triplet)	O
Hydroxyl radical	OH
Water	H2O
Ozone	O3
Hydroperoxy radical	HO2
Hydrogen peroxide	H2O2
Carbon monoxide	CO
Formaldehyde ($CH_2=O$)	FORM
High molecular weight aldehydes (RCHO, R>H)	ALD2
Peroxyacyl radical ($CH_3C(O)OO\cdot$)	C2O3
Peroxyacyl nitrate ($CH_3C(O)OONO_2$)	PAN
Paraffin carbon bond (C-C)	PAR
Secondary organic oxy radical	ROR
Olefinic carbon bond (C=C)	OLE
Ethene ($CH_2=CH_2$)	ETH
Toluene ($C_6H_5-CH_3$)	TOL
Cresol and higher molecular weight phenols	CRES
Toluene-hydroxyl radical adduct	TO2
Methylphenoxy radical	CRO
High molecular weight aromatic oxidation ring fragment	OPEN
Xylene ($C_6H_4-(CH_3)_2$)	XYL
Methylglyoxal ($CH_3C(O)C(O)H$)	MGLY
Isoprene	ISOP
NO-to-NO_2 operation	XO2
NO-to-nitrate operation	XO2N
Total	33

1.3.1.2. Advective Transport Process

Since pollutants are transported by the mean or bulk motion of the air, the advection of pollutants is treated by specifying the horizontal wind fields for each grid cell and each vertical layer at a specified time. The wind inputs are defined by interpolating surface and upper air observations or through the use of diagnostic or prognostic wind models. In the UAM-IV, the Diagnostic Wind Model (DWM) is used for this purpose (USEPA, 1990d). The DWM requires gridded terrain heights, domain-mean wind data, and domain scale stability information. The domain-mean wind is adjusted for the kinematic effects of terrain (lifting and acceleration of the air flow over terrain obstacles), and the thermodynamically generated slope flows, and blocking effects. Then an objective analysis scheme is used to incorporate the available observations to define the final wind field within a specified radius of influence.

1.3.1.3. Turbulent Diffusion Process

Turbulent diffusion is treated under the assumption that dispersion of pollutants is proportional to the concentration gradient in space (K-theory). The proportionality factors are the eddy diffusivity coefficients. Since mean gradient in the x and y-directions can be neglected in comparison to those in the z direction, then $k_x = k_y \approx 0$ (this assumption further simplifies the atmospheric diffusion equation). In the present version of the UAM-IV, the eddy diffusivity constants for the vertical column of cell at a particular grid location are calculated using the Businger scheme (Businger *et al*, 1971) for stable conditions and the Lamb polynomials (Lamb *et al*, 1975) for neutral and unstable conditions.

1.3.1.4. Surface Removal Process

Ozone is removed from the surface layer by such features as vegetation through the process of dry deposition. In the UAM-IV, dry deposition is treated as a two-step process (Killus, 1984): the transfer of ozone through the atmosphere to the surface and uptake of ozone by vegetation and other materials at the surface. The deposition rate is obtained by the flux of ozone directed towards the surface.

1.3.1.5. Treatment of Emissions

In the treatment of emissions, hourly and gridded area (including mobile and biogenic) and low level point source emissions of VOCs, NO_x, CO, SO_x, and Particulate matters are injected into the first surface-based vertical layer. The hourly and gridded elevated point source emissions are injected into the vertical layers above ground level. In this differentiation, the effective plume rise of a point source is compared to the user-imposed vertical cutoff level. The area source emissions are allocated to grid cells using surrogate distribution factors such as population distribution, land use, and road type. Point source emissions are allocated by defining the geographical coordinates of the sources. Hydrocarbon speciations are developed by using VOCs speciation profiles for various source categories.

1.3.2. Operation of the UAM-IV

The core UAM-IV model is a standard FORTRAN program written for the IBM mainframe computers. It is approximately 15,000 lines long and contains 80 subroutines that simulate the processes of the atmospheric diffusion equation. It requires thirteen different input files (Figure 1.1) broken down into meteorological, emission, initial and boundary condition, chemistry parameters, and simulation control data files. CHEMPARAM contains information about the chemical species to be simulated, including reaction rate constants, upper and lower bounds, activation energy, and reference temperature. SIMCONTROL contains the simulation control information, such as the time of the simulation, file option information, default information, and information on integration and chemistry time steps. DIFFBREAK specifies the daytime mixing height or nighttime inversion height for each column of cells at the beginning and end of each hour of the simulation. REGIONTOP specifies the height of each column of cells at the beginning and end of each hour of the simulation. If this height is greater than the mixing height, the cell or cells above the mixing height are assumed to be within an inversion. METSCALARS contains the hourly values of the meteorological parameters that do not vary spatially. These scalars are the NO_2 photolysis rate constant, the concentration of

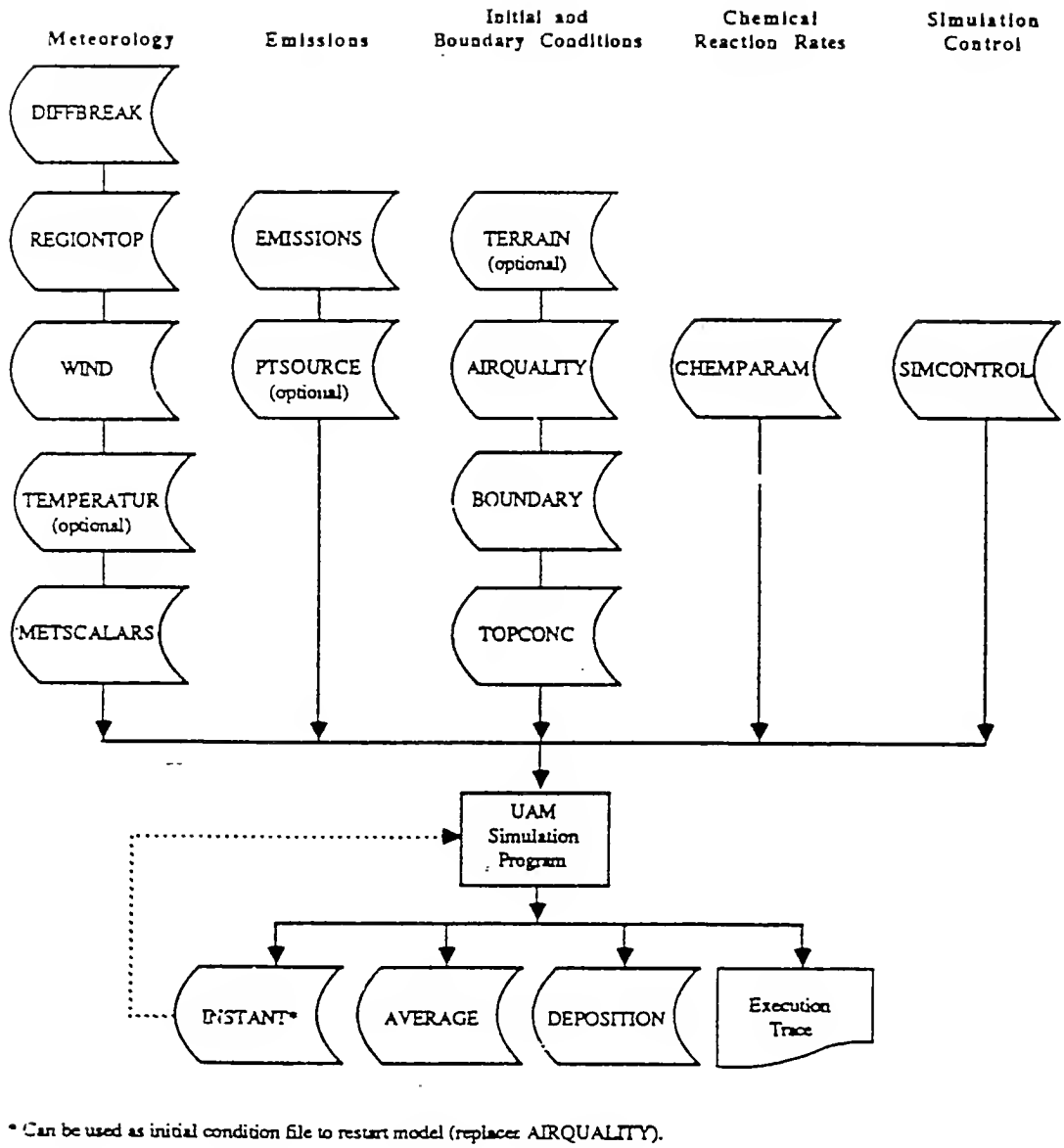

Figure 1.1. Schematic description of the UAM-IV input and output files (From USEPA, 1990b).

water vapor, the temperature gradient above and below the inversion base, the atmospheric pressure, and the exposure class. TEMPERATUR contains the hourly temperature for each surface layer grid cell. WIND contains the x and y components of the wind velocity for every grid cell for each hour of the simulation. The maximum wind speed for the entire grid and average wind speed at each boundary for each hour are also included in this file. TERRAIN contains the value of the surface roughness and deposition factor for each grid cell. AIRQUALITY defines the initial concentrations of each species for each grid cell at the start of the simulation. BOUNDARY contains information on the modeling region boundaries as well as the concentration of each species that is used as the boundary condition along each boundary segment at each vertical level. TOPCONC defines the concentration of each species for the area above the modeling region. These concentrations are the boundary conditions for vertical integration. EMISSIONS specifies the ground-level emissions of NO, NO_2, reactive hydrocarbons (speciated into seven Carbon-Bond Mechanism categories), and CO for each grid cell for each hour of the simulation. PTSOURCE contains information on point sources (stack height, temperature and flow rate, the plume rise, the grid cell into which the emissions are emitted) and the emissions rates for NO, NO_2, reactive hydrocarbons (speciated into seven Carbon-Bond Mechanism categories), and CO for each point source for each hour. The output files consist of four different files describing the simulated concentrations in all grid cells for all species at each time step, the computed average concentrations for the specified time interval, the deposition value in all grid cells for all species at each time step, and the execution trace.

1.4. Model Set up at Purdue University

The UAM-IV package was successfully set up on the Purdue University IBM 3090 mainframe computer by simulating a test case furnished by the United States Environmental Protection Agency (USEPA). In doing so, many program syntaxes were changed and/or transformed in order to fit the operating requirement of the Purdue IBM 3090 running under the VM/CMS operating system. The test case consisted of an application of the UAM-IV to the Atlanta, Georgia area. The only meteorological and air

quality data available were routine data from a very sparse network of monitors. The modeling domain consisted of a 40 by 40 array of 4 Km square grid cells. The modeling episode was only thirty two hours long from June 3 to 4, 1984. In the simulation process, default boundary conditions were assumed and the top of domain was considered clean.

2. Raw Data Analyses

2.1. Sources of Air Quality and Meteorological Data

In 1990, there were eight continuous ozone monitoring sites, two continuous NO_x monitoring sites, and three continuous CO monitoring sites throughout the Indianapolis MSA. Table 2.1 to 2.3 and Figure 2.1 show their locations and characteristics. As it can be seen, the three most southern of the ozone monitoring sites were located in rural areas, the three most northern in suburban areas, and the last two in between were located in the city of Indianapolis. Continuous ultra violet monitors were used at all of these sites to measure hourly average concentrations of ground-level ozone. Surface meteorological data in the modeling domain originated from the four observation sites listed in Table 2.4. The three sites associated with ozone monitors measured only wind speed, wind direction, and surface temperature whereas the Indianapolis airport site measured a complete surface meteorological parameters. There were no upper air observation sites located within the modeling domain. Therefore, the closest upper air observation sites surrounding the domain were used in this study. Table 2.5 summarizes the locations and characteristics of these sites.

Table 2.1. Continuous ozone monitoring sites in the Indianapolis MSA in 1990.

Site #	County	Address	UTME (Km)	UTMN (Km)	Lat (d/m/s)	Lon (d/m/s)	Setting
18-005-0004	Barthm	5841 N. Rd 500W	586	4350	39/15/38	86/00/24	Rural
18-109-0003	Morgan	Paragon Elem Sch	537	4361	39/23/47	86/34/02	Rural
18-097-0042	Marion	8327 Mann Road	564	4389	39/38/46	86/14/55	Rural
18-097-0057	Marion	1321 S. Harding	570	4400	39/44/56	86/11/11	Urban
18-097-0073	Marion	6125 E. 16th St	580	4405	39/47/21	86/03/39	Urban
18-097-0050	Marion	Trailer Crt Row B	584	4412	39/51/30	86/01/13	Suburb
18-059-0003	Hancock	Fortville Mpl Bdg	599	4421	39/56/05	85/50/27	Suburb
18-057-1001	Hamilton	186th St, High Sch	585	4434	40/03/21	86/00/04	Suburb

Table 2.2. Continuous NO_x monitoring sites in the Indianapolis MSA in 1990.

Site #	County	Address	UTME (Km)	UTMN (Km)	Lat (d/m/s)	Lon (d/m/s)	Setting
18-097-0057	Marion	1321 S.Harding	570	4400	39/44/56	86/11/11	Urban
18-097-0073	Marion	6125 E. 16th St	580	4405	39/47/21	86/03/39	Urban

Table 2.3. Continuous CO monitoring sites in the Indianapolis MSA in 1990.

Site #	County	Address	UTME (Km)	UTMN (Km)	Lat (d/m/s)	Lon (d/m/s)	Setting
18-097-0034	Marion	1 W. Washington	572	4402	39/46/00	86/09/30	Urban
18-097-0072	Marion	50 N. Illinois St	572	4402	39/46/05	86/09/36	Urban
18-097-0073	Marion	6125 E. 16th St	580	4405	39/47/21	86/03/39	Urban

Table 2.4. Surface meteorological observation sites in the Indianapolis MSA in 1990.

Site #	County	Address	UTME (Km)	UTMN (Km)	Lat (d/m/s)	Lon (d/m/s)	Setting
18-107-0001	Montgomery	Nucor Steel Plant	515	4424	39/58/12	86/49/49	Rural
18-097-0057	Marion	1321 S. Harding	570	4400	39/44/56	86/11/11	Urban
18-097-0073	Marion	6125 E. 16th St	580	4405	39/47/21	86/03/39	Urban
93819	Marion	Indy/Int'l Airport	570	4398	39/43/59	86/16/10	Urban

Table 2.5. Upper Air meteorological observation sites used in the study.

Upper Air Station #	Station Name	State	Lat (o)	Lon (o)	Zone
14842	Peoria/Greater Peoria Arpt	Illinois	40.667	89.683	6
14826	Flint/Bishop Arpt	Michigan	42.967	83.75	5
13840	Wright Patterson/AFB	Ohio	39.817	84.05	5
03816	Paducah/WSO Arpt	Kentuky	37.067	88.767	6

2.2. Sources of Emission Data

The emission data used in this study consisted of actual county level summertime emission rates of VOCs, NO_2, CO, SO_2, and particulate matters from area, mobile, biogenic, and point sources. The point, area, and mobile source emissions of VOCs, NO_2, and CO for Marion County were inventoried by the Indianapolis air pollution control section (IAPCS) as part of their 1990 revised state implementation plan (SIP). The biogenic emissions of VOCs for the entire modeling domain and the mobile and area sources emissions of VOCs, NO_2, and CO for the remaining counties were developed and inventoried in this project. The point source emissions of SO_2 and particulate matters were obtained from the USEPA aerometric information retrieval system (AIRS). Figure 2.2.a to 2.2.c summarize the total emission distributions. The contribution of mobile sources in the total emissions is very high. Mobile sources in Marion County alone account for 46%, 40%, and 75% respectively of the total VOCs, NO_x, and CO emissions in the Indianapolis MSA.

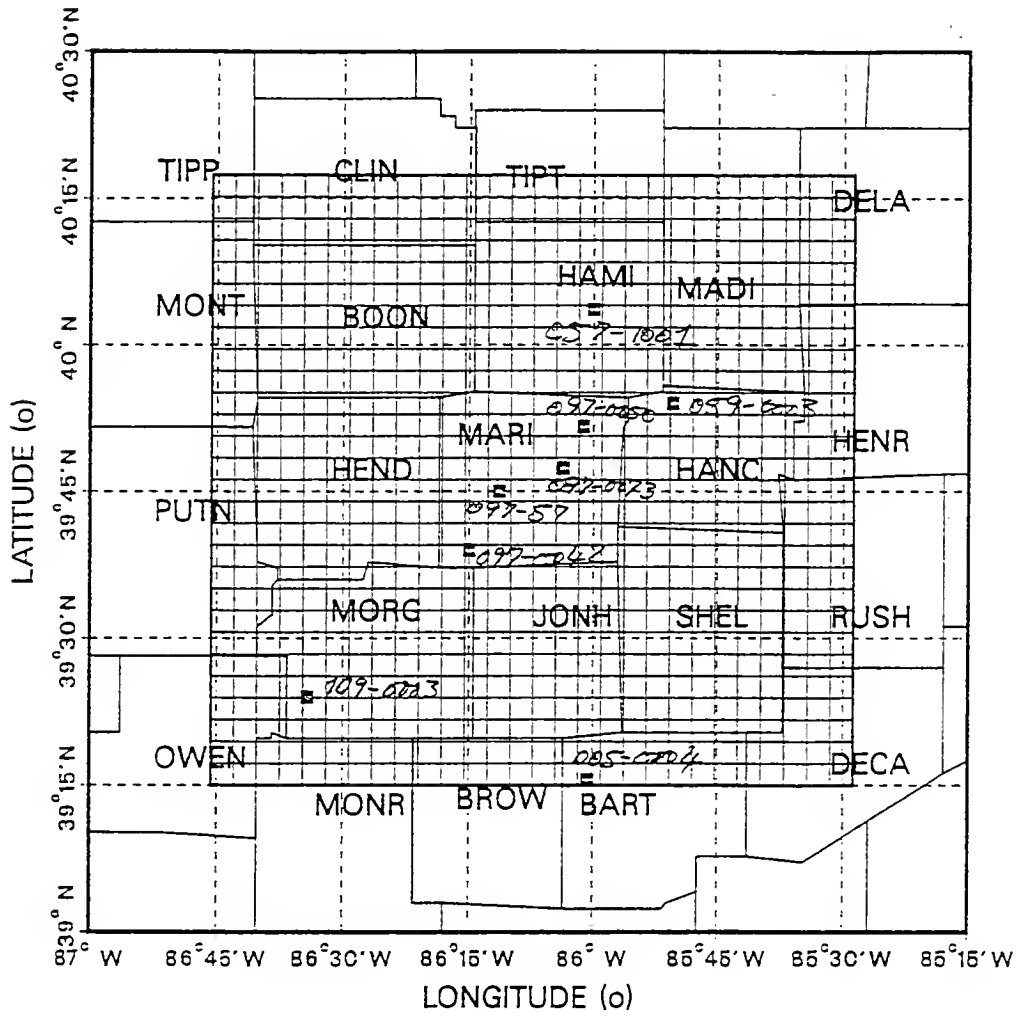

Figure 2.1. Modeling domain including ozone monitoring sites locations and grid cell array (Domain = 112 km×112 km, grid cells = 4 km×4 km, ■ = ozone sites).

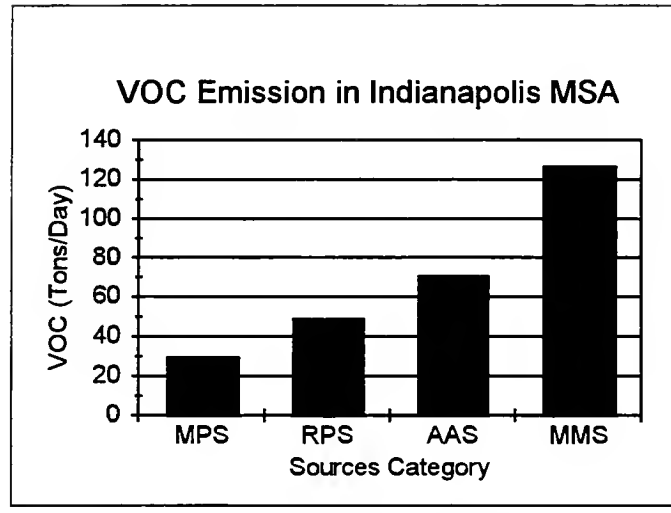

Figure 2.2.a. 1990 VOCs emissions in the Indianapolis MSA by source category (MPS=Marion Co. Point sources, RPS=Rest of the Cos. Point sources, AAS=all Cos. Area sources, MMS=Marion Co. Mobile sources).

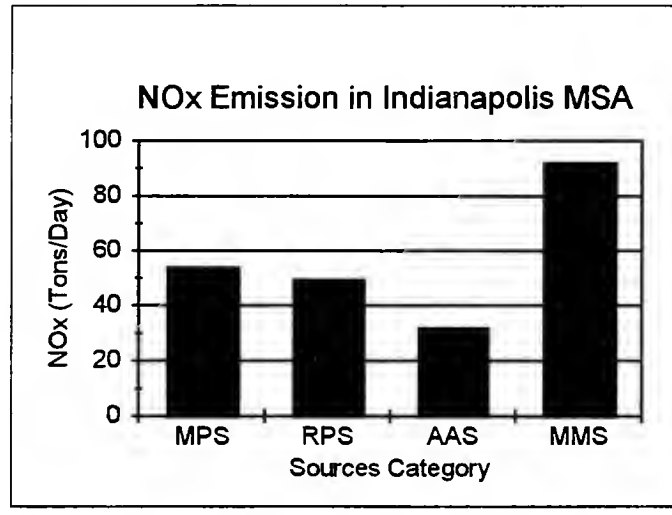

Figure 2.2.b. 1990 NOx emissions in the Indianapolis MSA by source category (MPS=Marion Co. Point sources, RPS=Rest of the Cos. Point sources, AAS=all Cos. Area sources, MMS=Marion Co. Mobile sources).

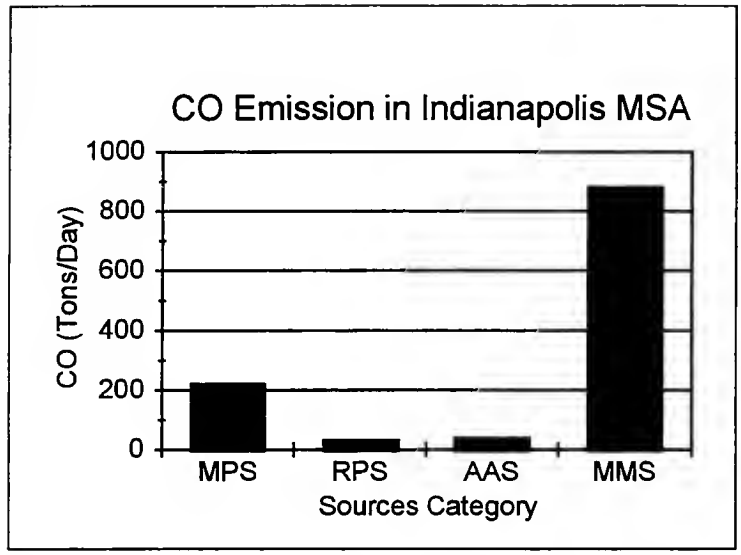

Figure 2.2.c. 1990 CO emissions in the Indianapolis MSA by source category (MPS=Marion Co. Point sources, RPS=Rest of the Cos. Point sources, AAS=all Cos. Area sources, MMS=Marion Co. Mobile sources).

2.3. Modeling Domain Definition

In this research study, the entire Indianapolis metropolitan statistical area was chosen as the modeling domain. It includes entirely or parts of the following counties: Bartholomew, Boone, Clinton, Delaware, Hamilton, Hancock, Hendricks, Henry, Johnson, Madison, Marion, Monroe, Montgomery, Morgan, Putnam, Rush, Shelby, Tippecanoe, and Tipton. The terrain is relatively simple with an average elevation of approximately 700 feet above mean sea level. With the exception of the large urban area of Indianapolis, the land use throughout the modeling domain is mainly agricultural or residential. The domain origin is located at UTM coordinates 520 Km easting and 4,350 Km northing in zone 16 and extends 112 Km in the east and north directions.

Because of the relatively low resolution of observed meteorological and air quality data throughout the domain, the computational storage and time, and the model formulation inconsistencies for very small grid dimensions, horizontal grid square dimensions of 4 Km by 4 Km were selected for this study. Therefore, the modeling domain was horizontally divided up to a 28 by 28 array of 4 Km square grid cells (Figure 2.1). This relatively large grid cell dimension should smooth out the emission gradients, wind fields, mixing heights, which in turn should lead to a smoothing of the predicted ozone concentration field (USEPA, 1991). To minimize the effect of dilution, and for a better representation of plume released above the mixing height, high vertical resolution must be used. In this study, the USEPA methodology was used. Five vertical layers were considered. Two layers below the mixing height and three above. The extent of these layers varied spatially and temporally during the modeling episode. However, as recommended by USEPA, the minimum thickness of the layers below the diffusion break and that of the layers above should be 50 m and 150 m respectively. The thickness of these five layers together represented the modeling region top.

2.4. Modeling Episodes Selection

In this study, unlike in a SIP demonstration where efforts are directed at ozone exceedence days only over many ozone seasons, only the months of June and July 1990 were looked upon in choosing ozone modeling episodes. This was based on the

assumption that these two months were climatologically the warmest in the region of interest and were the most likely to present ozone episode conditions for several consecutive days. Moreover, 1990 summertime emission inventories of VOCs, NO_2, and CO for parts of the study region already existed.

Table 2.6 shows the valid recording hours for each station during the months of June and July 1990. The database was 85.56% to 99.31% complete in June and 81.59% to 99.46% in July. Consequently, it could be used for episodes selection and model performance evaluation.

Table 2.6. Valid recording hours for hourly average ozone concentrations for each site.

O3 Sites	County	Year 1990 Days	% Valid	June 1990 Hours	% Valid	July 1990 Hours	%Valid
18-005-0004	Bartholomew	179	83.64	715	99.31	740	99.46
18-109-0003	Morgan	193	90.19	616	85.56	703	94.49
18-097-0042	Marion	176	82.24	678	94.17	690	92.74
18-097-0057	Marion	180	84.11	685	95.14	696	93.55
18-097-0073	Marion	167	78.04	715	99.31	638	85.75
18-097-0050	Marion	170	79.44	617	85.69	607	81.59
18-059-0003	Hancock	183	85.51	686	95.28	708	95.16
18-057-1001	Hamilton	178	83.18	681	94.58	695	93.41

The maximum one-hour average ozone concentration varied from 0.090 ppm to 0.119 ppm for all the stations in June and from 0.093 ppm to 0.103 ppm in July. Meanwhile, the mean one-hour average concentration varied from 0.031 ppm to 0.041 ppm in June and from 0.036 ppm to 0.037 ppm in July (Table 2.7).

Table 2.7. One-hour average ozone concentration peaks at each site.

		Year 1990		June 1990		July 1990	
Site ID	County	Max(ppm)	Mean(ppm)	Max(ppm)	Mean(ppm)	Max(ppm)	Mean(ppm)
18-005-0004	Bartholomew	0.1190	0.0380	0.1190	0.0400	0.0950	0.0370
18-109-0003	Morgan	0.1030	0.0360	0.1020	0.0370	0.1030	0.0370
18-097-0042	Marion	0.1030	0.0370	0.1030	0.0390	0.0970	0.0370
18-097-0057	Marion	0.0970	0.0320	0.0970	0.0340	0.0930	0.0360
18-097-0073	Marion	0.1190	0.0350	0.0900	0.0310	0.0950	0.0380
18-097-0050	Marion	0.1250	0.0400	0.1120	0.0410	0.0970	0.0380
18-059-0003	Hancock	0.1060	0.0370	0.1060	0.0410	0.1000	0.0360
18-057-1001	Hamilton	0.1060	0.0360	0.1006	0.0400	0.1000	0.0370

Figure 2.3.a to 2.3.h show the diurnal variations of one-hour average ozone concentration hourly maxima and means for the months of June and July 1990, for each site. Figure 2.3.a to 2.3.h also show the variations of one-hour average ozone concentration daily maxima for the months of June and July, 1990. As it can be seen, ozone concentration peaked in the early afternoon when vigorous and deep convective mixing existed as a result of very high solar radiation and temperature which in turn enhanced ozone photolytic chemistry. At night, ozone concentration rapidly reached its low.

The methodology designed to select ozone episodes in this study was based on the following approach. First, the days of highest one-hour average ozone concentration daily maximum for each and every station were identified. Second, the most frequent of these days considering all the stations was determined. This day was a candidate for the day of primary interest in the episode. Third, the meteorological synoptic scale parameters for at least two consecutive days including the target day as the end of the episode was studied. Finally, if the period presented typical atmospheric conditions for ozone episode, then it was selected as a modeling episode. If it did not, the second most frequent day of highest one-hour average ozone concentration daily maximum was studied. A typical ozone episode includes a period of light wind, high temperature, and a strong subsidence producing local high ozone concentration levels, followed by a period of southerly or southwesterly winds which can transport ozone and ozone precursors to downwind receptor sites. From Figures 2.3.a to 2.3.h, June 28 and June 13, 1990 represented the first and second most frequent days of highest one-hour average ozone concentration daily maximum. The atmospheric conditions for the periods of June 12-13, and June 25-28, 1990 were very favorable for ozone episode conditions. Therefore, these two periods were considered as ozone modeling episodes in the present study. However, most of the tasks in this project, especially model performance evaluations and emissions sensitivity analyses were conducted using the June 25-28, 1990 episode.

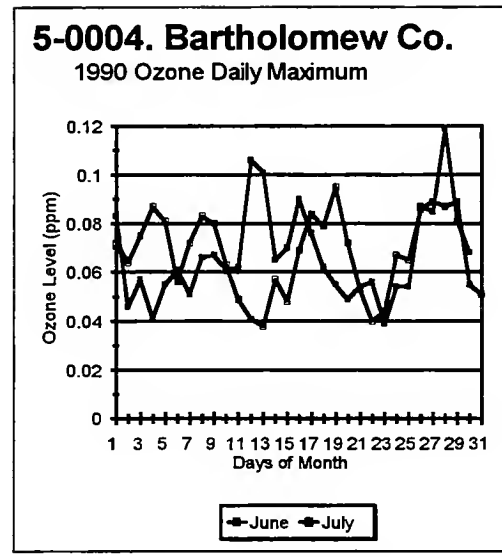

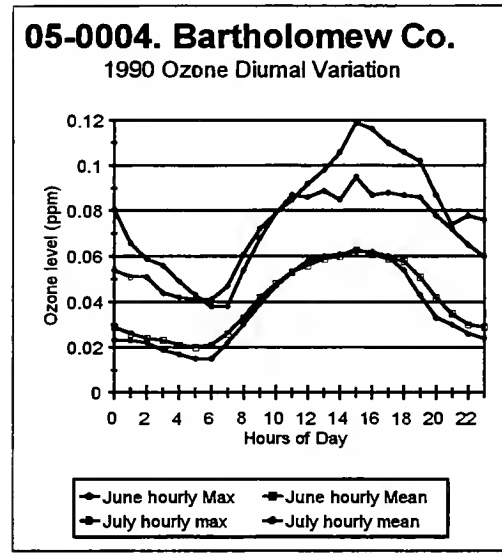

Figure 2.3.a. Time evolution of one-hour average ozone concentration daily maximum (above) and hourly maximum and mean (below) in June and July 1990 for monitoring station 18-0005-0004.

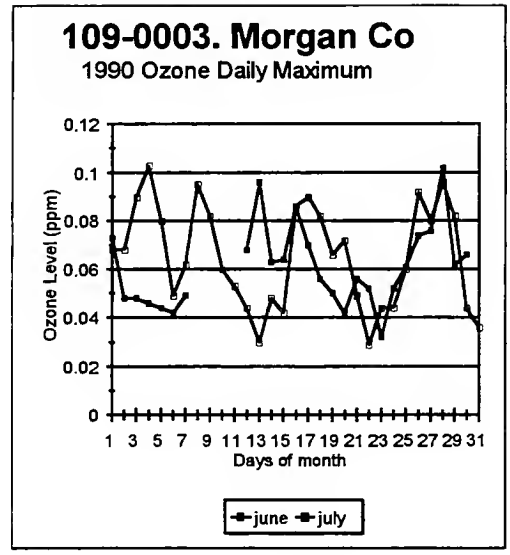

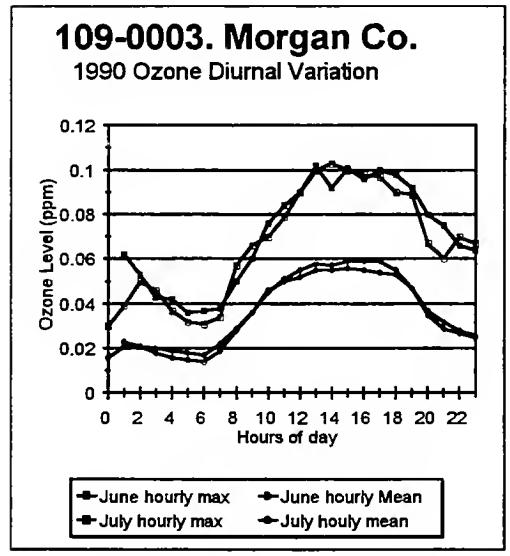

Figure 2.3.b. Time evolution of one-hour average ozone concentration daily maximum (above) and hourly maximum and mean (below) in June and July 1990 for monitoring station 18-109-0003.

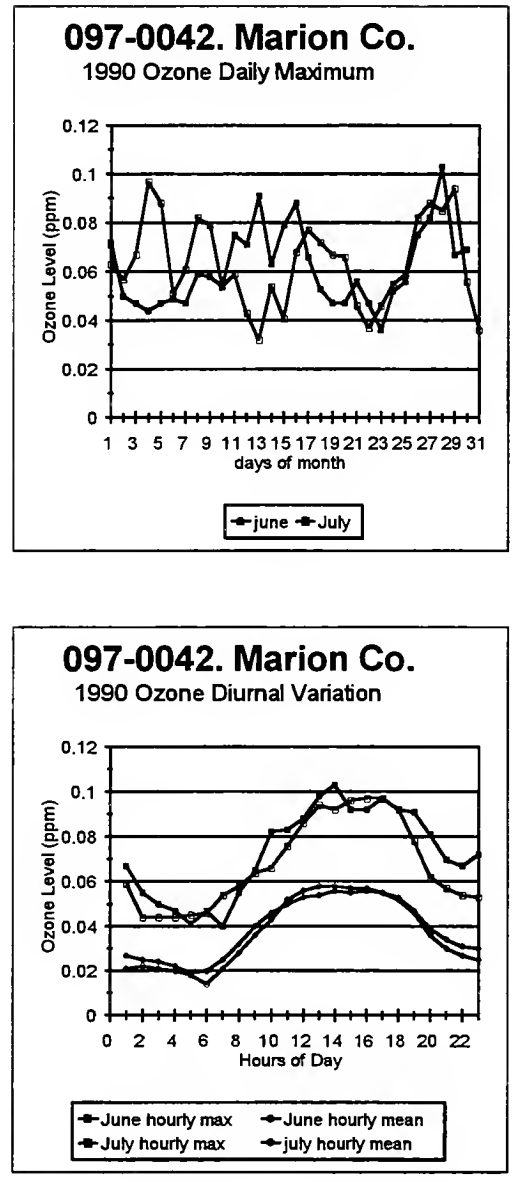

Figure 2.3.c. Time evolution of one-hour average ozone concentration daily maximum (above) and hourly maximum and mean (below) in June and July 1990 for monitoring station 18-097-0042.

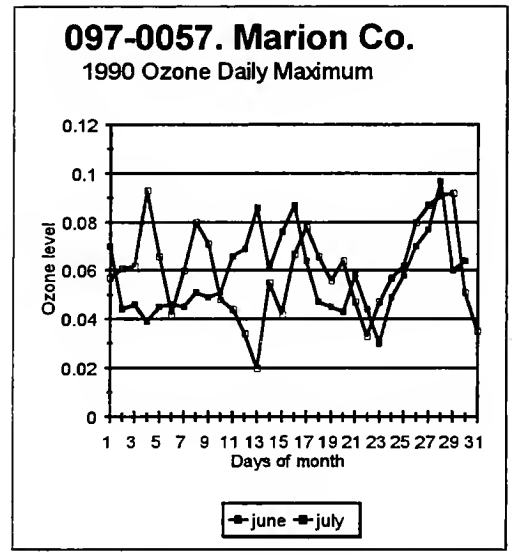

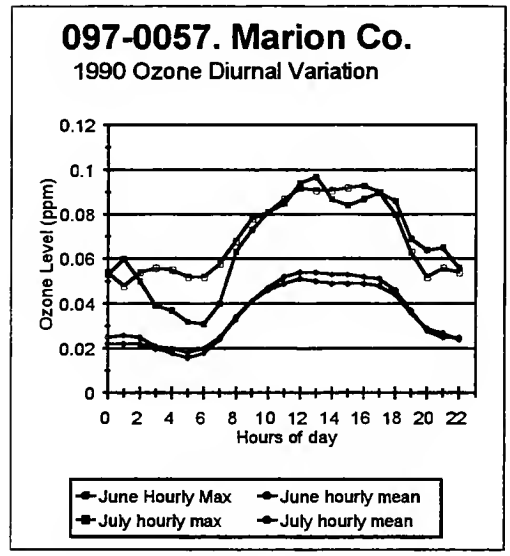

Figure 2.3.d. Time evolution of one-hour average ozone concentration daily maximum (above) and hourly maximum and mean (below) in June and July 1990 for monitoring station 18-097-0057.

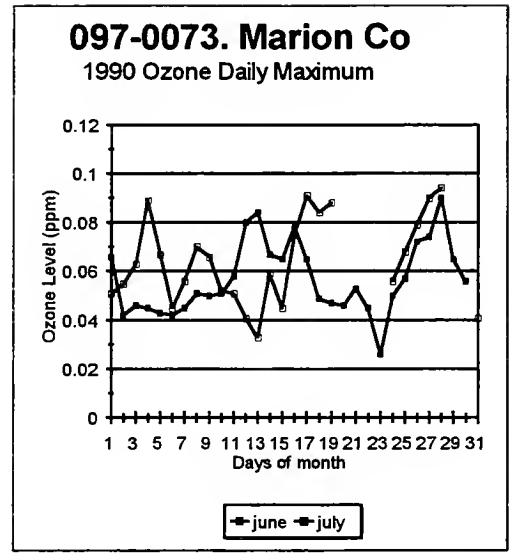

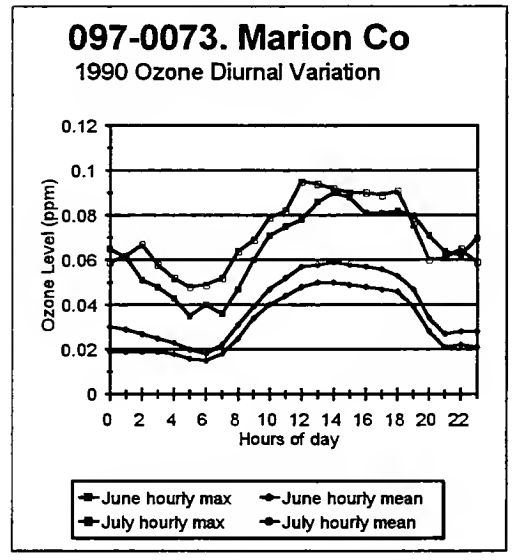

Figure 2.3.e. Time evolution of one-hour average ozone concentration daily maximum (above) and hourly maximum and mean (below) in June and July 1990 for monitoring station 18-097-0073.

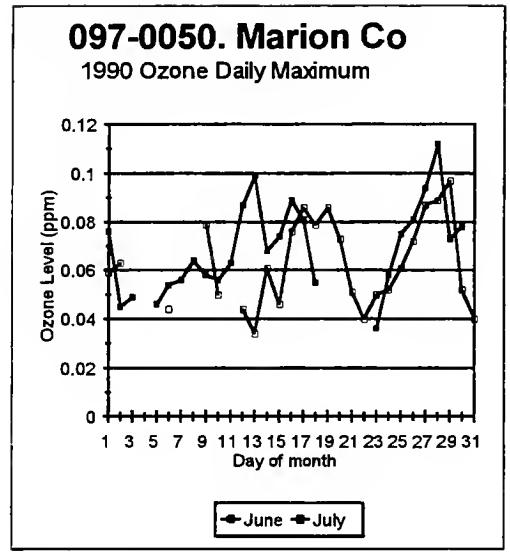

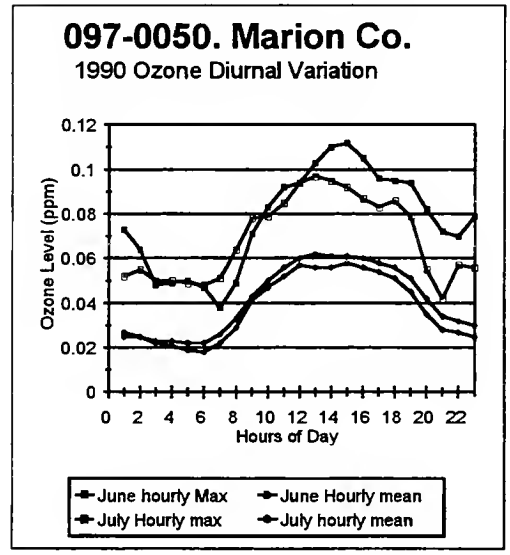

Figure 2.3.f. Time evolution of one-hour average ozone concentration daily maximum (above) and hourly maximum and mean (below) in June and July 1990 for monitoring station 18-097-0050.

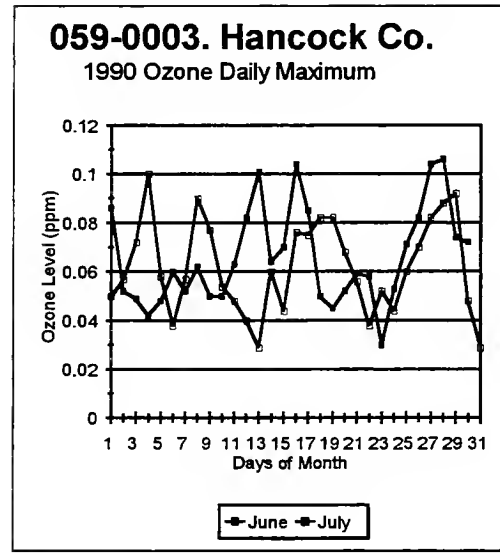

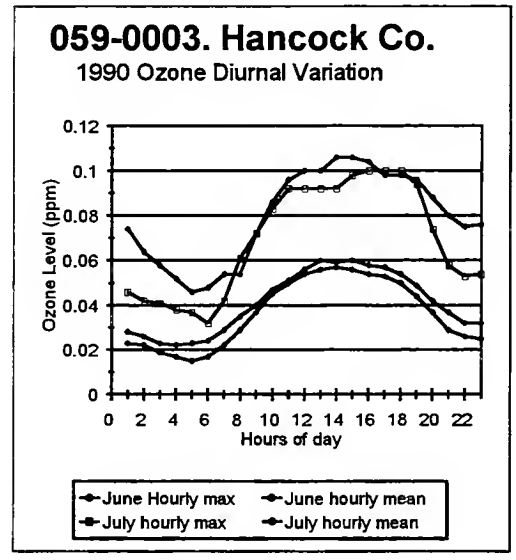

Figure 2.3.g. Time evolution of one-hour average ozone concentration daily maximum (above) and hourly maximum and mean (below) in June and July 1990 for monitoring station 18-059-0003.

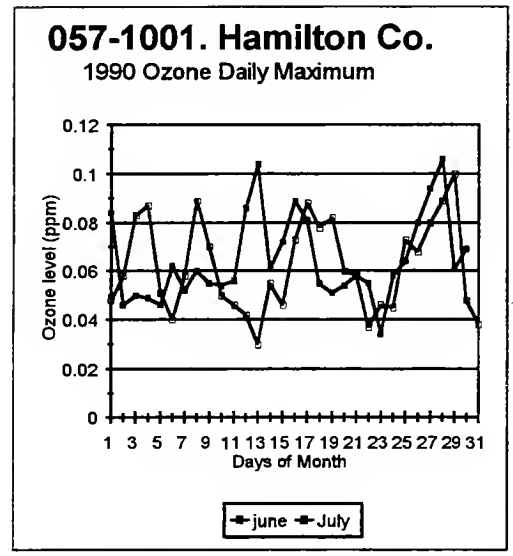

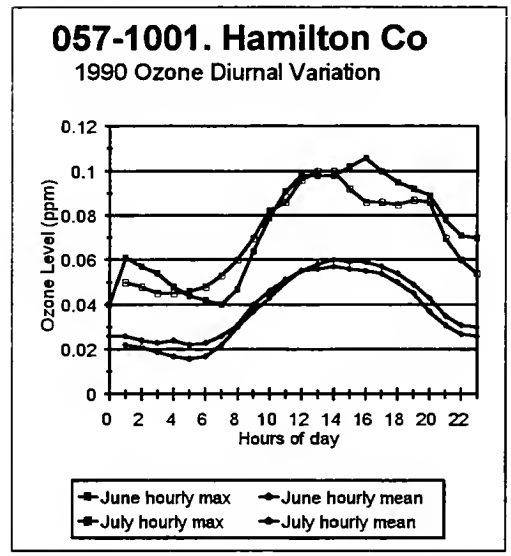

Figure 2.3.h. Time evolution of one-hour average ozone concentration daily maximum (above) and hourly maximum and mean (below) in June and July 1990 for monitoring station 18-057-1001.

2.5. Episodes Characteristics

2.5.1. Synoptic Scale Meteorology of the June 25-28, 1990 Episode

The synoptic scale meteorological pattern that developed to result in the ozone episode of June 25 to 28, 1990 began with the southward motion of a strong cold front across the domain on June 23, 1990. As depicted in Figures 2.4.a to 2.4.f, the 7:00 A.M. Eastern standard time (EST) U.S. surface weather map shows a strong low pressure center located over northeastern Michigan with a cold front extending from central New York, down deep to the southeastern United States and continuing westward into Texas. A band of precipitation extended from the low pressure center, north to Canada and south to near Indianapolis. On that day, the maximum temperature in the modeling domain was 77°F. A high pressure located over southern Nebraska followed the low pressure system eastward. Then, the winds were mainly from the west. This pattern persisted into June 24, 1990. However, the high pressure system moved a little bit southeasterly. By June 25, 1990, the high pressure system was located south east of the domain at the border of Kentucky and West Virginia influencing the modeling domain by its northwest quadrant. The wind flow consequently shifted to the southwest and was light. The maximum temperature did not change. On June 26, 1990, the high pressure center was located at the eastern border of West Virginia. At 7:00 A.M. EST, the winds were light and from the southeast but shifted to a southwesterly direction later that day. The maximum ambient temperature increased to 85°F. The dew point temperature also increased. At 7:00 A.M. EST, it was 58°F. This synoptic regime persisted onto June 27, 1990 with the advent of a light precipitation and a slight shift of the winds to the west. The maximum surface temperature increased to 90°F. On June 28, 1990, the high pressure center was back into the West Virginia area. The winds were light and mainly from the southwest. The maximum temperature on that day was 93°F and the dew point temperature at 7:00 A.M. EST was 69°F. The wind rose plot (Figure 2.5) of the Indianapolis international airport weather report for the period of June 25 to 28, 1990 shows that on average, the prevailing wind was from the southwest and mostly light.

SATURDAY, JUNE 23, 1990

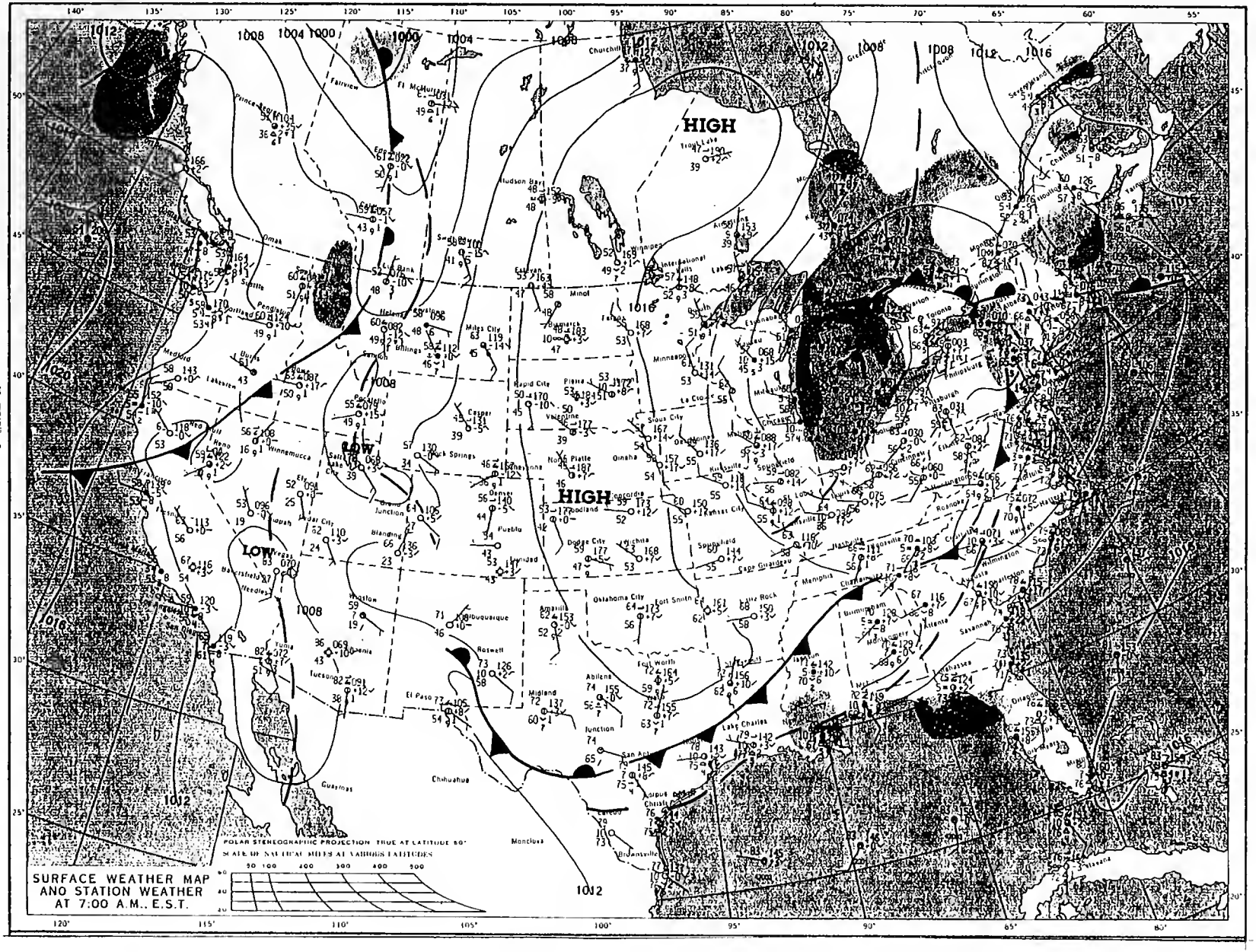

SUNDAY, JUNE 24, 1990

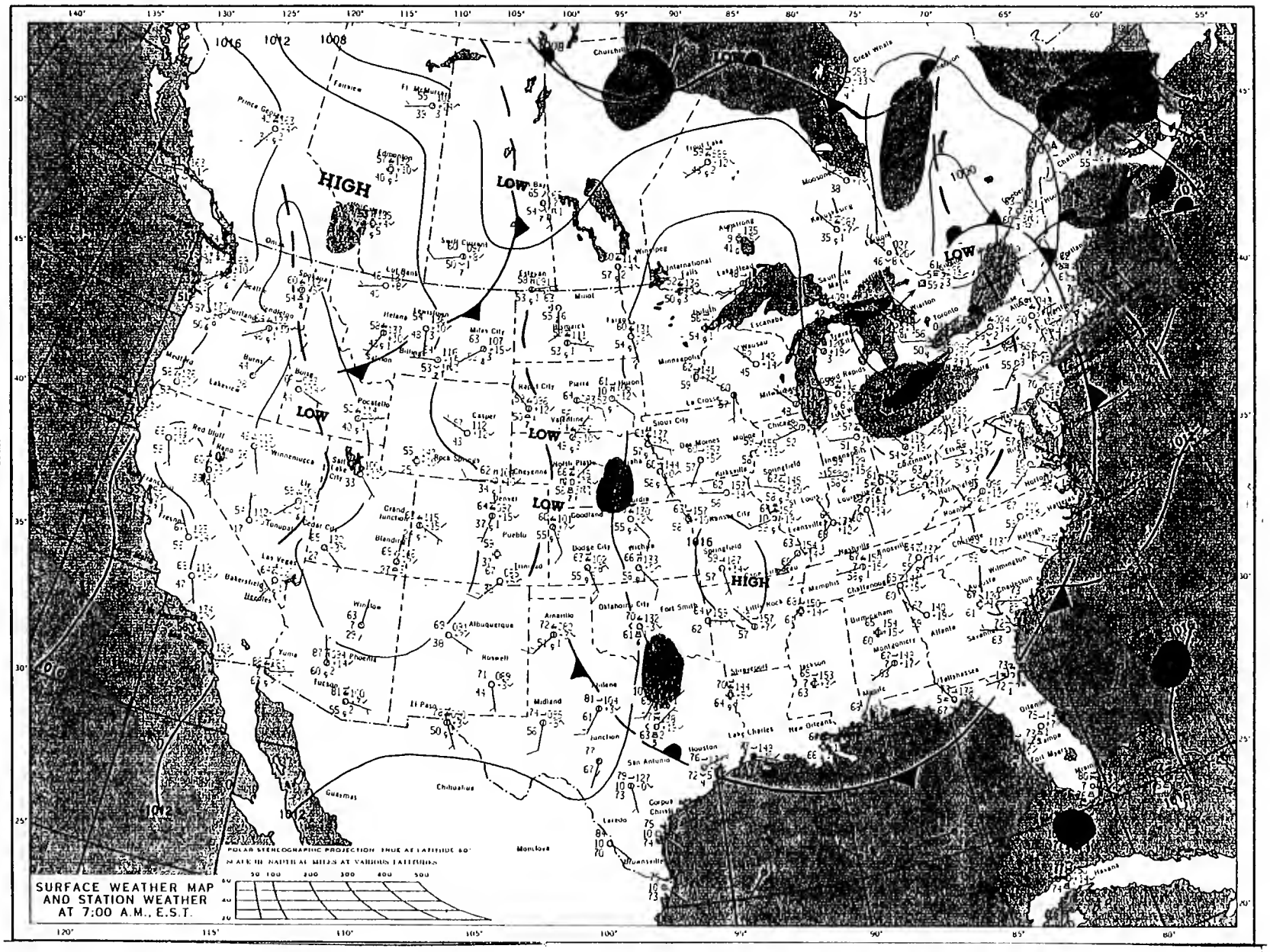

MONDAY, JUNE 25, 1990

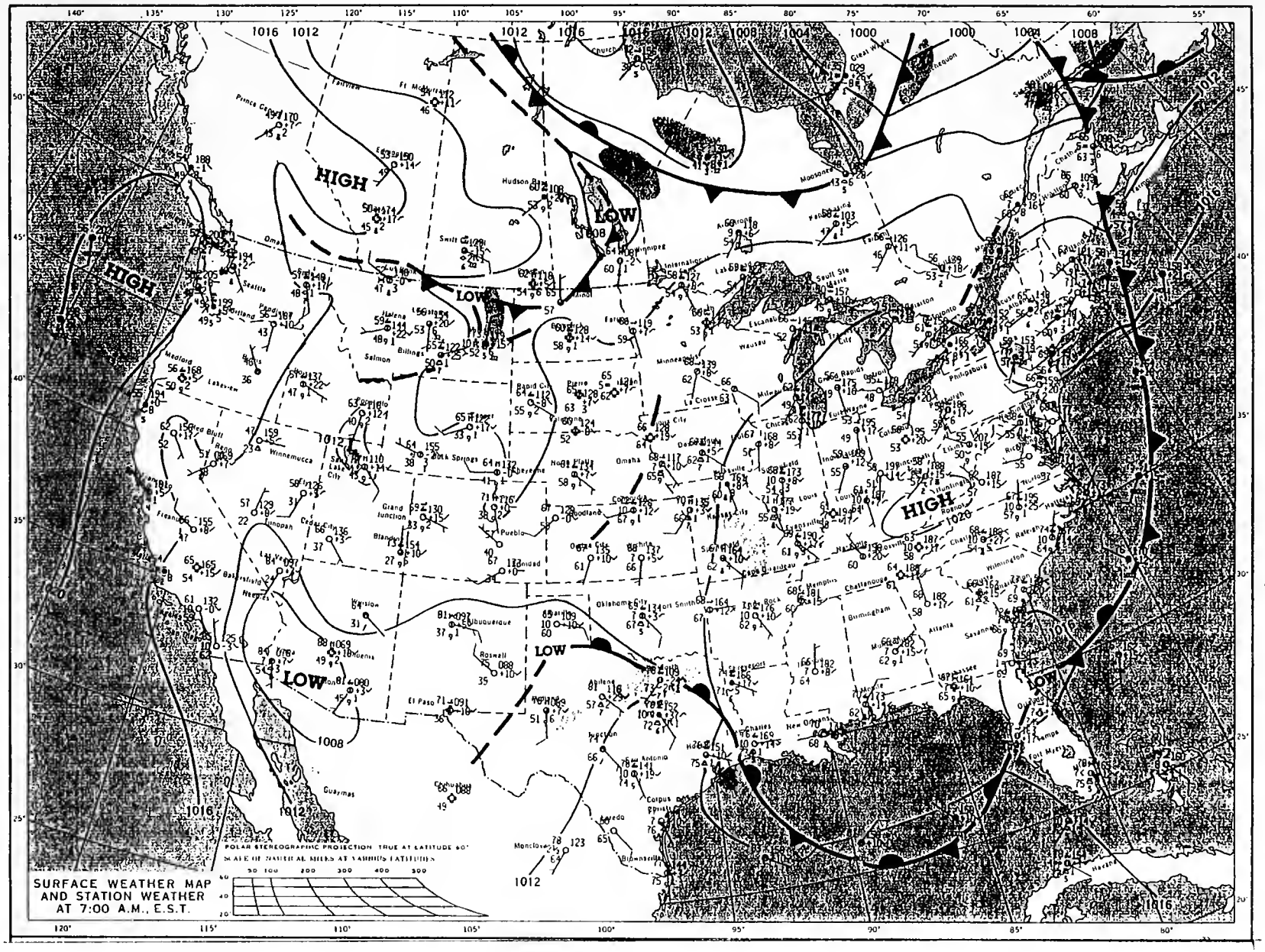

TUESDAY, JUNE 26, 1990

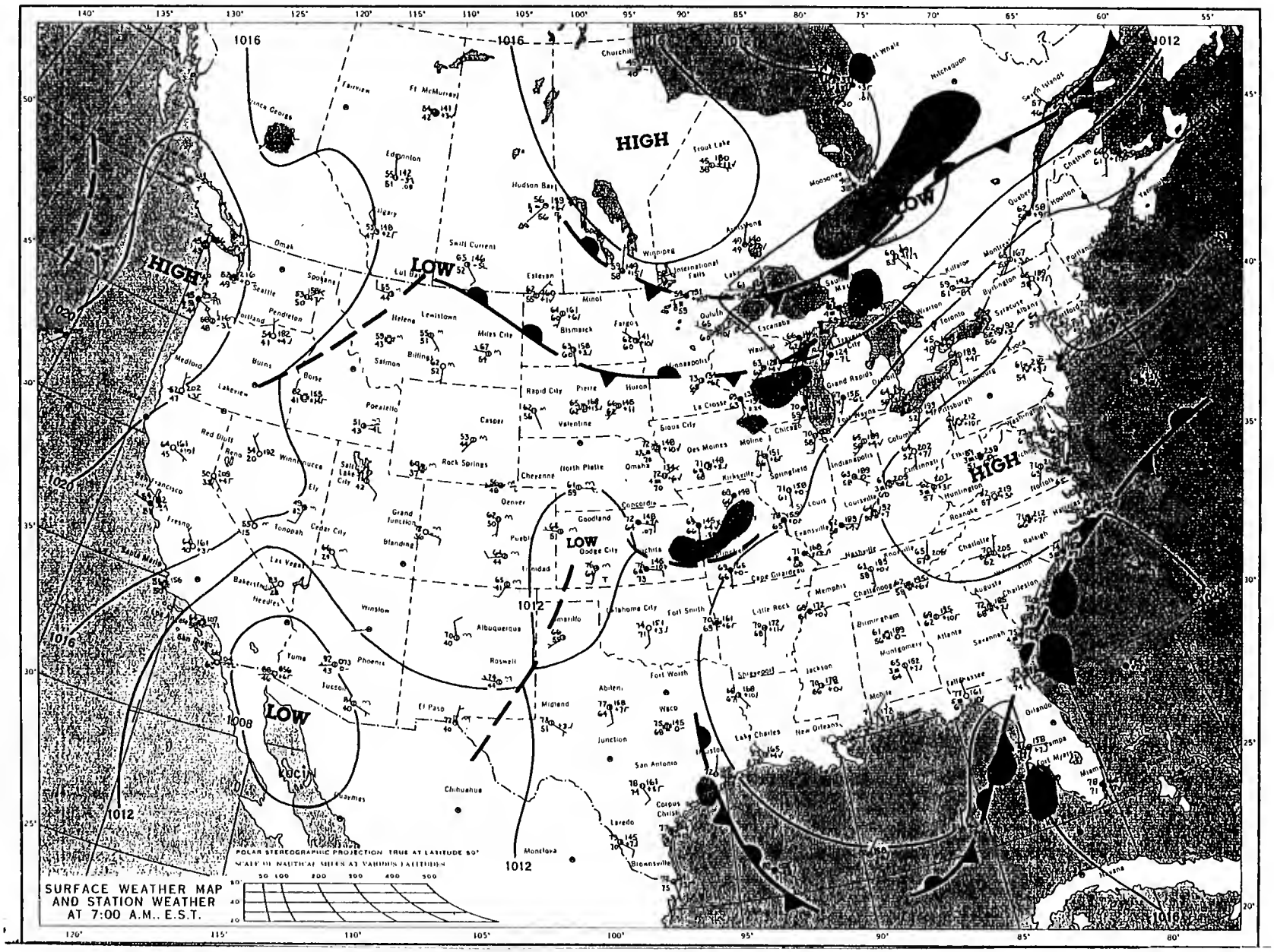

WEDNESDAY, JUNE 27, 1990

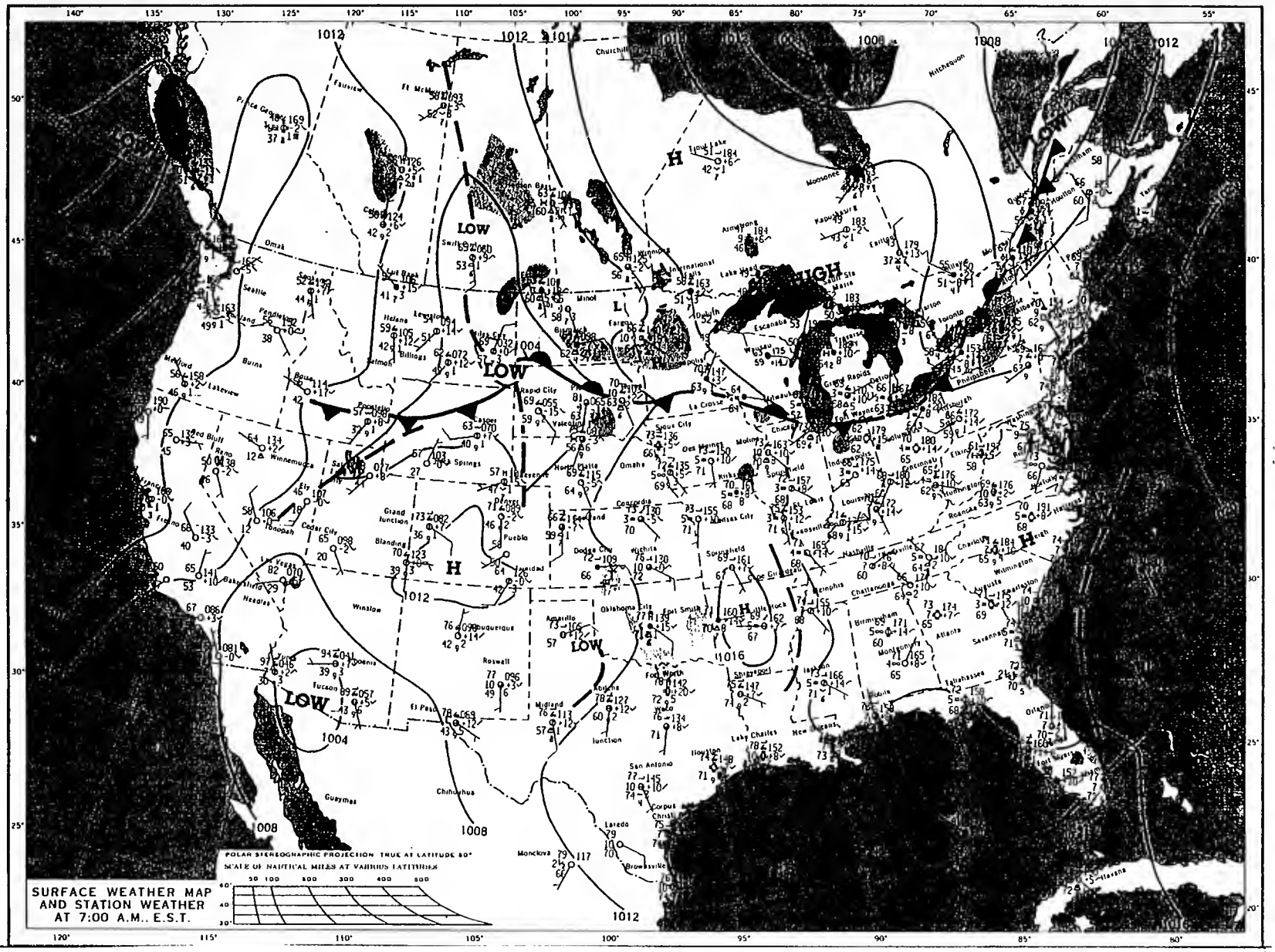

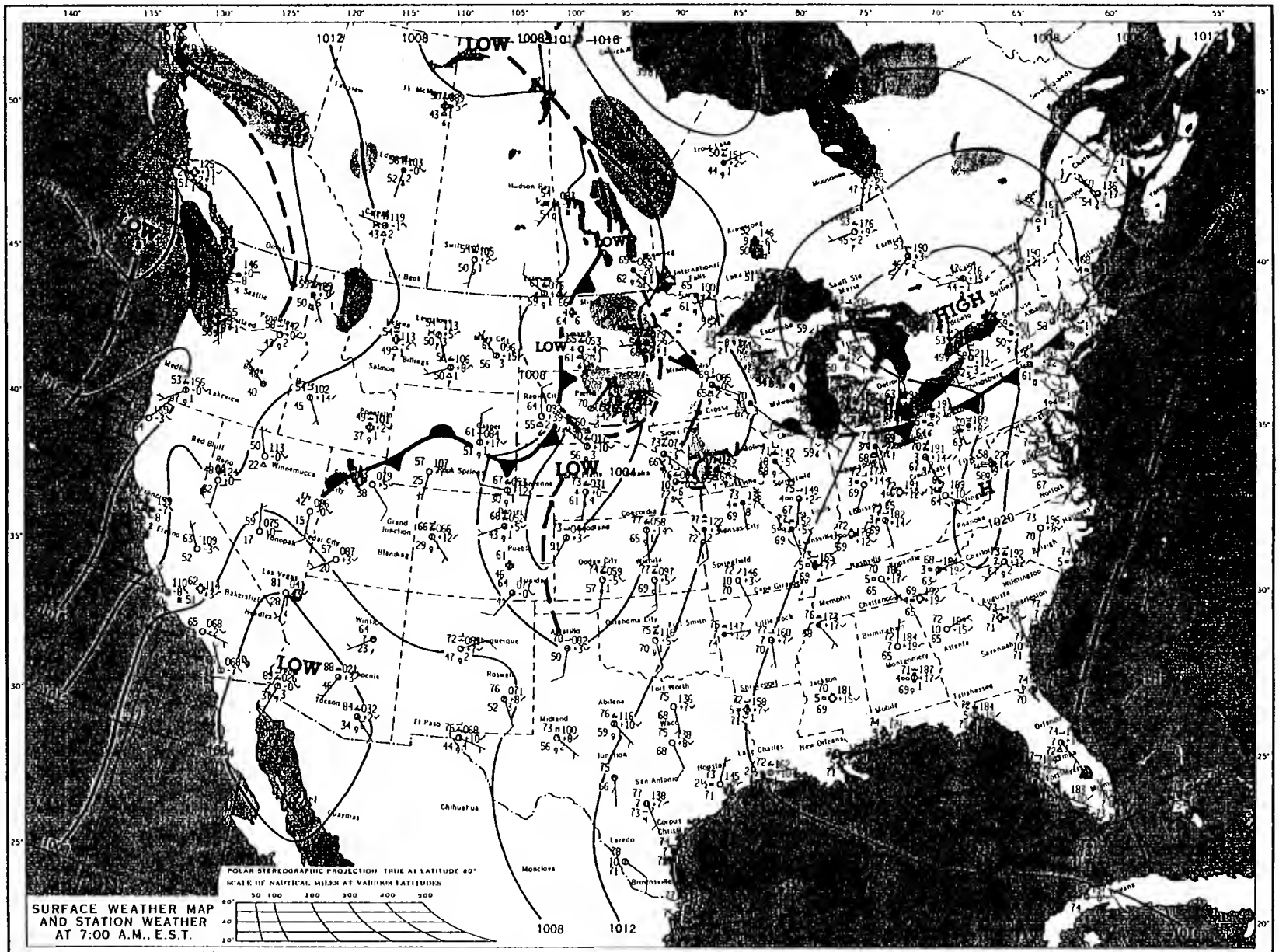
LOW
LOW
LOW
LOW
HIGH
HIGH
1012
1008
1004
1020
POLAR STEREOGRAPHIC PROJECTION TRUE AT LATITUDE 60°
SCALE OF NAUTICAL MILES AT VARIOUS LATITUDES
50 100 200 300 400 500
SURFACE WEATHER MAP
AND STATION WEATHER
AT 7:00 A.M., E.S.T.

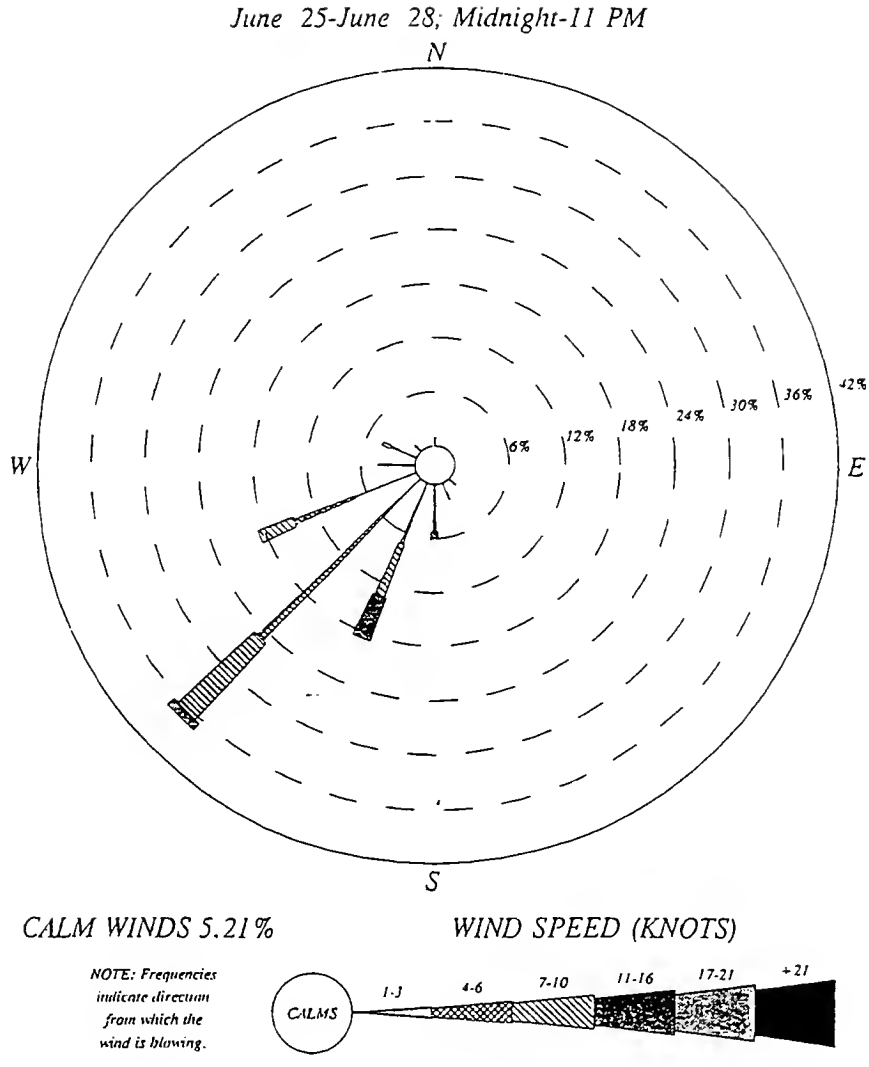

Figure 2.5. Wind rose plot of the Indianapolis international airport weather report on June 25-28, 1990.

2.5.2. Air Quality Overview of the June 25-28, 1990 Episode

The meteorological pattern developed during this episode led to a warming trend with relatively clear skies, light wind from the southwest, and increasing humidity. This allowed conditions in the domain to develop to ozone episode characteristics in which emissions could be transported from neighboring regions. These emissions along with those emitted from within the domain led to relatively high ozone concentrations that lasted for three consecutive days. On the primary modeling day, June 28, 1990, the maximum hourly average ozone concentrations were between 0.090 and 0.119 ppm for all the sites and the times of their occurrence were between 1:00 P.M. and 4:00 P.M. local standard time (LST) (Table 2.8).

Table 2.8. One-hour average ozone concentration daily maximum on June 13,28, 1990.

Site Number	County	Latitude	Longitude	06/13 Max (ppm)	Time (LST)	06/28 Max (ppm)	Time (LST)
18-005-0004	Bartholomew	39/15/38	86/00/24	0.101	1800	0.119	1500
18-109-0003	Morgan	39/23/47	86/34/02	0.096	1600	0.102	1300
18-097-0042	Marion	39/38/46	86/14/55	0.091	1600	0.103	1400
18-097-0057	Marion	39/44/56	86/11/11	0.086	1500	0.097	1400
18-097-0073	Marion	39/47/21	86/03/39	0.084	1500	0.090	1400
18-097-0050	Marion	39/51/30	86/01/13	0.099	1400	0.112	1500
18-059-0003	Hancock	39/56/05	85/50/27	0.101	1400	0.106	1400
18-057-1001	Hamilton	40/03/21	86/00/04	0.104	1600	0.106	1600

2.6. Summary of the Base Case UAM-IV Input Preparation

The thirteen input files required by the UAM-IV must be prepared in a consistent and objective form in order to best represent the emissions, meteorology, air quality and other physical aspects of the modeling episode and domain. In this research study, the UAM-IV preprocessors for input files preparation were used as much as possible. All the available raw data were analyzed and processed for goodness and completeness before the input files development.

2.6.1. Meteorological Input Files

To obtain the DIFFBREAK input file, a three-step process was used. The twice daily upper air sounding and surface meteorological data from the National Weather

Service (NWS) stations chosen for this study were fed into the preprocessor MIXHT to determine the morning minimum and evening maximum mixing heights from interpolation between the potential temperature at the surface and the potential temperature at heights above the surface. These minimum and maximum mixing heights were then used by the preprocessor RAMMET which interpolated between the two mixing heights to determine the hourly mixing heights for a given station. The interpolation scheme is detailed in USEPA, 1990b. Finally, the hourly mixing heights were gridded out by the preprocessor DFSNBK using the inverse-distance spatial interpolation scheme. The mixing heights obtained from these processes varied from a nightly low of 100 m to an afternoon high of 1900 m throughout the study domain during the modeling episode. As part of this project a new mixing height model was developed in order to provide better estimates of this important diffusion parameter. The results of this new model provided a much better prediction of one-hour average ozone concentration (see Fatogoma, 1996). The height of the top of the region was set to 2000 m regardless of time of the day and location in the REGIONTOP input file. This represents the maximum height of the mixing height plus 100 m. In the METSCALARS input file, the hourly average concentration of water was obtained from the surface relative humidity and dew point temperature data. The hourly atmospheric pressure reduced at ground level, was obtained from the surface pressures data. The hourly vertical temperature gradient above and below the diffusion break were estimated by interpolation of the twice-daily upper air temperature profiles. Photolysis rates for other species calculated by the CB-IV mechanism are a function of the NO_2 photolysis rate constant. Its region-wide hourly values were determined by the preprocessor SUNFUNC given a representative radiation database with the clear sky assumption. The exposure class or the measure of near ground level stability due to heating and cooling was calculated from empirical stability relationships based on total cloud cover and solar zenith angle data. To obtain the TEMPERATUR input file, the hourly surface temperatures of the weather stations within the domain were spatially interpolated. The hourly and gridded horizontal wind components for each of the vertical layers contained in the wind input file (WIND) were estimated using the DWM and the preprocessor UAMWND.

2.6.2. Initial and Boundary Conditions Input Files

The gridded surface roughness lengths and deposition factors contained in the TERRAIN input file were determined from the 1:250000 scale United States Geological Survey (USGS) maps and land use data. In the AIRQUALITY input file the gridded concentrations of ozone, CO, and NO_2 at the beginning of the modeling period were obtained from spatial interpolation of the observations at the existing monitoring stations. The remaining UAM-IV chemical species concentrations were estimated based on values from the literature. In the BOUNDARY input file, the lateral boundary cells were set at the last row and column of each boundary; thus reducing the study domain to 27 by 27 grids. The time-varying matrix of ozone concentration in each boundary (south, east, north, west) cell were obtained from interpolations of observed ozone concentrations at the monitoring sites BAR0004 and MOR0003 and from the database of the ozone monitoring study performed by Dr. R. B. Jacko for the Lake Michigan Ozone Study (LMOS). The concentrations of the other chemicals were set to their default values (USEPA, 1991). In this research study, it was assumed that the top of the region is relatively clean. Therefore, in the TOPCONC input file, background values from the literature were used to determine the time-varying matrices of the UAM-IV chemical concentrations at the top of the region.

2.6.3. Emission Input files

Two files (EMISSIONS, and PTSOURCE) describe the emissions inputs to the UAM-IV. The EMISSIONS input file contains low-level emissions which are from area, mobile, biogenic, and low-level point sources. The PTSOURCE input file contains the elevated point source emissions. All the point sources with effective plume height greater than 25 m were included in this file. These two files are produced by the Emission Preprocessor System (EPS) (USEPA, 1990e). The EPS processes annually-average county-wide total emissions to create episode-specific estimates based on ambient conditions. It consists of six programs which are executed sequentially to prepare the emissions files. PREPNT reformats the point source emissions inventory and prepares it for hydrocarbon speciation. PREGRD reformats the area and mobile source emissions inventory and prepares it for gridding. GREMS allocates the area

and mobile source emissions prepared by PREGRD to the modeling region cells. CENTEMS, the central program of the EPS, allocates emissions for each cell in the modeling region across time and splits THC and NO_x organic compounds into the chemical species of the UAM-IV. POSTEMS merges ground-level emissions files to create one input file for the UAM-IV. MRGEMS merges the biogenic emissions file with the anthropogenic emissions file to obtain the EMISSIONS input file. Moreover, the UAM-IV preprocessor PTSOURCE is used to process the elevated point source file created by CENTEMS to obtain the PTSOURCE input file. Before the EPS can be used, an emission inventory for UAM-IV application must be prepared. In this study, the area and mobile emissions inventories consisted of the total summertime-average county-wide emissions of VOCs, NO_x, and CO described in section 2.2. The point source emissions inventory included all sources emitting at least 10 tons/year for VOC and 100 tons/year for NOx as recommended by USEPA. All sources and emissions of TSP and SO_x were also included in the inventory. The gridded episode-specific biogenic emissions of VOCs were determined following execution of the Biogenic Emission Inventory System (BEIS). On-road mobile source emissions were estimated by multiplying the Mobile5a emission factors by the activity level (VMT) for each vehicle and road class.

2.6.4. Chemistry Parameters and Simulation Control Input Files

The CB-IV database containing the UAM-IV chemical species characteristics, reaction properties, and stochiometric coefficients was used to develop the CHEMPARAM input file. The simulation option flags and simulation times were set in the SIMCONTROL input file.

3. Modeling Results and Discussion

3.1. Model Performance Evaluation

Using the base case inputs, the UAM-IV was operated over the study domain for the June 25-28, 1990 episode to predict near surface one-hour average ozone concentrations. In order to use the UAM-IV for further studies, it should perform well. The performance of the model was assessed by determining the biases and correlations between observations and predictions. This was done using visual inspections and statistical methods. The visual inspections included contour maps of predicted domain-wide one-hour average ozone concentration peaks, time series of predicted and observed hourly ozone concentrations at selected monitoring stations, scatter plots of predicted versus observed hourly ozone concentrations, and residual plots. Statistical methods included the unpaired highest prediction accuracies, the station peak prediction accuracies, and the normalized biases from all hourly prediction-observation pairs. The average normalized bias is defined as

$$\overline{(C_p - C_o)/C_o} \tag{16}$$

and the average normalized absolute bias is

$$\overline{|C_p - C_o|/C_o} \tag{17}$$

C_p and C_o are the predicted and observed ozone concentrations respectively and — represents the average. The analyses also used three other measures: the fractional bias of the mean

$$FB = (\overline{C_o} - \overline{C_p}) / (0.5(\overline{C_o} + \overline{C_p})) \tag{18}$$

the normalized mean square error

$$NMSE = \overline{(C_o - C_p)^2} / \overline{C_o C_p} \tag{19}$$

and the correlation coefficient

$$R = \overline{(C_o - \overline{C_o})(C_p - \overline{C_p})} / \sigma_o \sigma_p \tag{20}$$

σ_p and σ_o are the predicted and observed ozone concentration standard deviations respectively. As recommended by USEPA, the performance measures should apply to the second day of the episode to avoid the effects of initial conditions, that is from June 26 to 28, 1990.

3.1.1. Statistical Methods

3.1.1.1. Unpaired Highest Prediction Accuracy

This measure quantifies the difference between the magnitude of the highest one-hour average observed ozone concentration over all hours and monitoring stations and the highest one-hour average predicted ozone concentration over all hours and surface grid squares. USEPA recommends that the average absolute bias or accuracy be less than 20%. Table 3.1 presents the observed and predicted one-hour average peak ozone concentrations anywhere in the modeling domain for each day of the episode. The biases are also given.

Table 3.1. Predicted and observed domain-wide one-hour average ozone concentration daily maximum biases.

Date	Observed ozone (ppm)	Predicted Ozone (ppm)	Bias (%)	Absolute Bias (%)
06/26/90	0.082	0.104	26.8	26.8
06/27/90	0.104	0.129	24.0	24.0
06/28/90	0.112	0.123	9.8	9.8
Mean	0.099	0.119	20.2	20.2

On average, the model overpredicts the unpaired one-hour average ozone concentration daily peaks by 20%. However, the accuracies are different from one day to another. The lowest accuracy is 9.8% on June 28, 1990 and the highest is 26.8% on June 26, 1990. These accuracies would improve if the spatial coverage of ozone monitoring sites were denser, especially, in the northeastern part of the study domain where the highest predicted one-hour average ozone daily peaks were simulated by the UAM-IV.

3.1.1.2. Average Station Peak Prediction Accuracy

This measure represents the paired peak prediction accuracy averaged over all monitoring stations. It quantifies the difference between the magnitude of the peak one-hour average observed ozone concentration at a monitoring station and the predicted one-hour average ozone concentration at the same monitoring station and time of observed peak. Thus, the prediction and observations are matched in space and time. USEPA recommends that the

average absolute bias or accuracy be less than 20%. Table 3.2.a to 3.2.c presents the observed and predicted one-hour average peak ozone concentration at each monitoring site in the modeling domain (except at BAR0004 and MOR0003 which were used for boundary conditions determination) for each day of the episode. The biases are also given. As it can be seen, the average absolute biases or absolute errors are consistently within the USEPA-recommended 20% for each day. The model overpredicts the mean station maximum by 0.8% on June 26, underpredicts by 2.3% on June 27, and underpredicts by 7.0% on June 28, 1990.

Table 3.2.a. Average station one-hour average ozone concentration peak estimation accuracies at selected sites on June 26, 1990.

Station	Observed Ozone (ppm)	Predicted Ozone (ppm)	Bias (%)	Absolute Bias (%)
HAM1001	0.080	0.082	2.5	2.5
HAN0003	0.082	0.088	7.3	7.3
MAR0042	0.075	0.066	-12.0	12.0
MAR0050	0.081	0.081	0.0	0.0
MAR0057	0.070	0.068	-2.9	2.9
MAR0073	0.072	0.076	5.6	5.6
Mean			0.08	5.0

Table 3.2.b. Average station one-hour average ozone concentration peak estimation accuracies at selected sites on June 27, 1990.

Station	Observed Ozone (ppm)	Predicted Ozone (ppm)	Bias (%)	Absolute Bias (%)
HAM1001	0.094	0.074	-21.3	21.3
HAN0003	0.104	0.112	7.7	7.7
MAR0042	0.082	0.060	-26.8	26.8
MAR0050	0.094	0.093	-1.1	1.1
MAR0057	0.077	0.075	-2.6	2.6
MAR0073	0.074	0.096	29.7	29.7
Mean			-2.3	14.9

Table 3.2.c. Average station one-hour average ozone concentration peak estimation accuracies at selected sites on June 28, 1990.

Station	Observed Ozone (ppm)	Predicted Ozone (ppm)	Bias (%)	Absolute Bias (%)
HAM1001	0.106	0.096	-9.4	9.4
HAN0003	0.106	0.104	-1.9	1.9
MAR0042	0.103	0.089	-13.6	13.6
MAR0050	0.112	0.097	-13.4	13.4
MAR0057	0.097	0.089	-8.2	8.2
MAR0073	0.090	0.094	4.4	4.4
Mean			-7.0	8.5

3.1.1.3. Analysis of Ozone Concentrations at all Stations and Hours

When the analysis is extended to all ozone monitoring sites and all hours of the episode, USEPA recommends that the average normalized bias and the average normalized absolute bias be less than 15% and 35% respectively for hourly ozone concentrations paired in space and time. Consistent with USEPA recommendations for UAM evaluation, a minimum cutoff level was imposed to the observed hourly ozone concentrations in order to eliminate the low background ozone concentrations in the analysis. Table 3.3. summarizes the results for a chosen cutoff level of 40 ppb. As it can be seen, the mean of the predicted hourly average ozone concentrations for the cutoff level of 40 ppb departs from the observation by only 4.9% for the episode. The average normalized bias varies from 1.7% to 9.1% with an episodic mean of 6.6% and the average normalized absolute bias varies from 16.4% to 23.1% with an episodic mean of 20%. They are therefore less than the USEPA-recommended 15% and 35% respectively for each day of the episode. Using these paired hourly average ozone concentrations, the fractional bias of the mean, the normalized mean square error, and the correlation coefficient for the entire episode were calculated. Their values are also presented in Table 3.3. The model presents a relatively high correlation and low normalized mean square error. Moreover the magnitude and sign of the fractional bias indicate that the model is only slightly overpredicting the mean hourly average ozone concentration.

Table 3.3. Average normalized bias, average absolute gross error, fractional bias, normalized mean square error, and correlation for hourly average ozone concentration over all hours and sites and for a cutoff level of 40 ppb in observations.

Date	Average Observed Hourly Ozone (ppm)	Average Predicted Hourly Ozone (ppm)	Accuracy of the Average Hourly Ozone (%)	Average Normalized Bias (%)	Average Normalized Absolute Bias (%)
06/26/90	0.062	0.063	1.2	1.7	20.9
06/27/90	0.072	0.077	7.1	8.9	23.1
06/28/90	0.076	0.081	6.6	9.1	16.4
Mean			4.9	6.6	20.1
	FB				-0.05
Episode	NMSE				0.04
	R				0.66

3.1.2. Visual Inspections

3.1.2.1. Scatter and Residual plots

Paired predicted and observed hourly average ozone concentration for all the sites and hours of the episode were plotted against each other. Figures 3.1.a to 3.1.c present these plots. The model shows a good skill in predicting hourly average ozone concentrations since the points tend to cluster along the 45° line representing perfect agreement. However, the scatters are higher on June 27, 1990 than the other days. This may be due to many factors such as the shift in the wind field to the west on that day, the advent of a light shower that increased the humidity thus affecting ozone overall chemistry, or the boundary conditions. The residuals of paired predicted and observed hourly average ozone concentrations for all the sites and hours were also plotted against time of the day on Figures 3.2.a to 3.2.c and ozone monitoring sites on Figures 3.3.a to 3.3.c. It can be seen again that the model shows a good skill in predicting hourly average ozone concentration with respect to time and site since the residuals are fairly equally distributed along the zero residual line with the exception of June 27, 1990 which shows the highest overprediction.

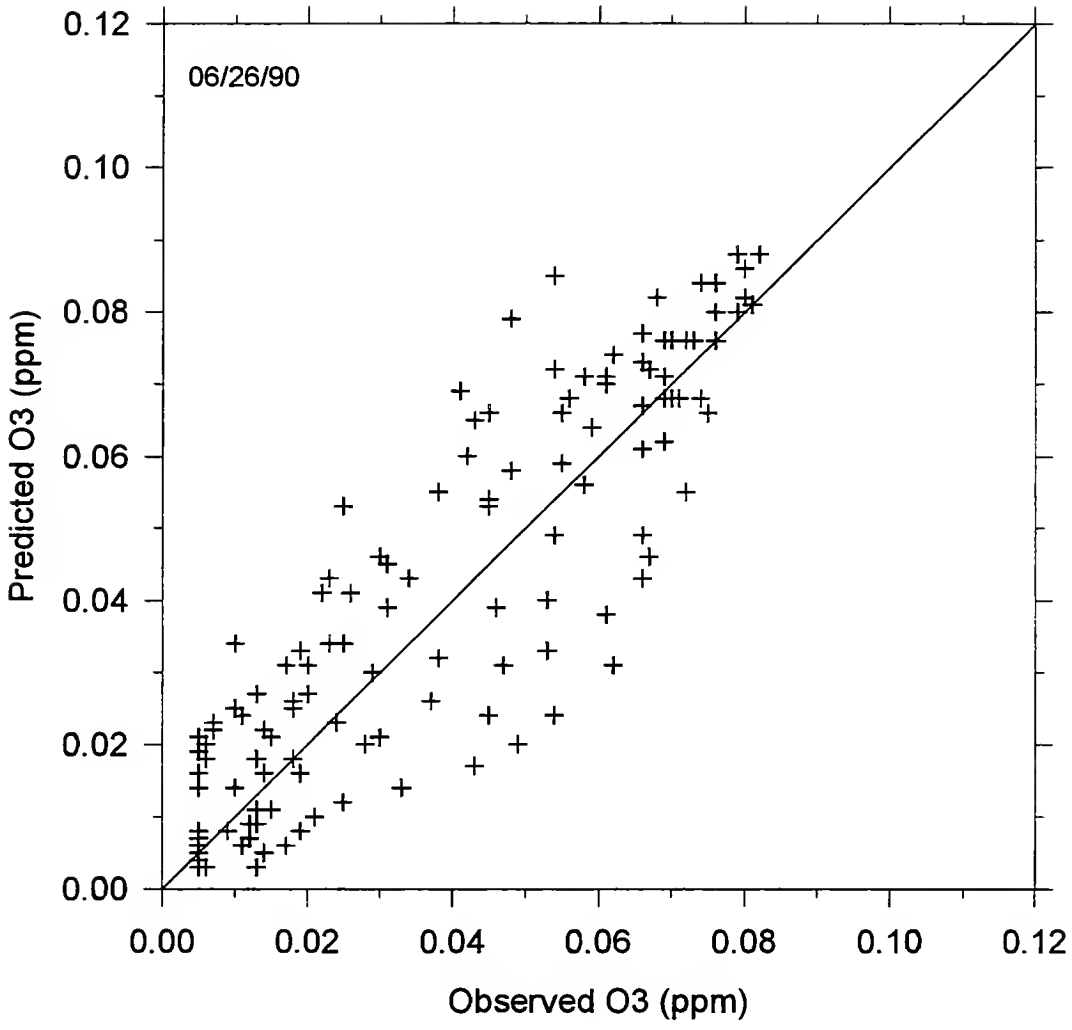

Figure 3.1.a. Predicted versus observed hourly average ozone concentration over all hours and sites on June 26,1990.

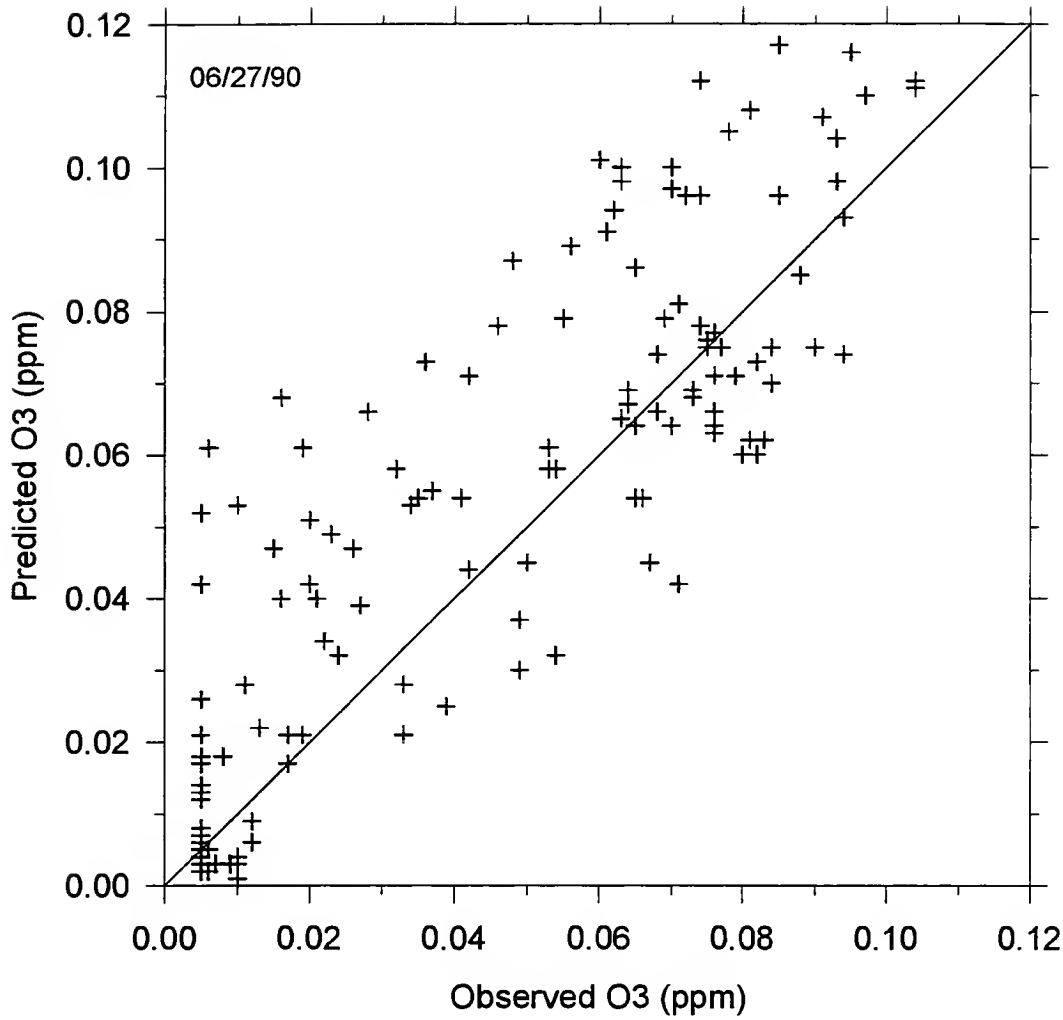

Figure 3.1.b. Predicted versus observed hourly average ozone concentration over all hours and sites on June 27, 1990.

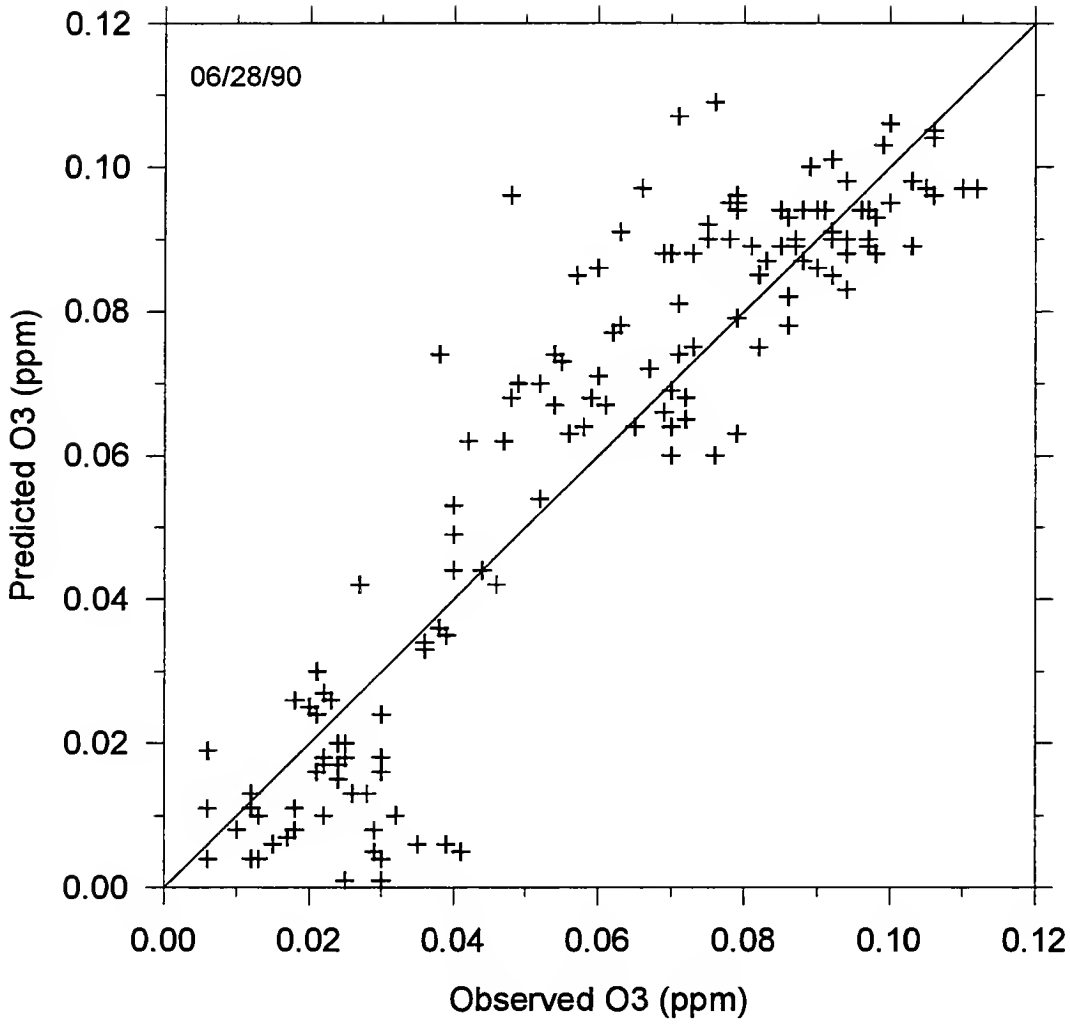

Figure 3.1.c. Predicted versus observed hourly average ozone concentration over all hours and sites on June 28, 1990.

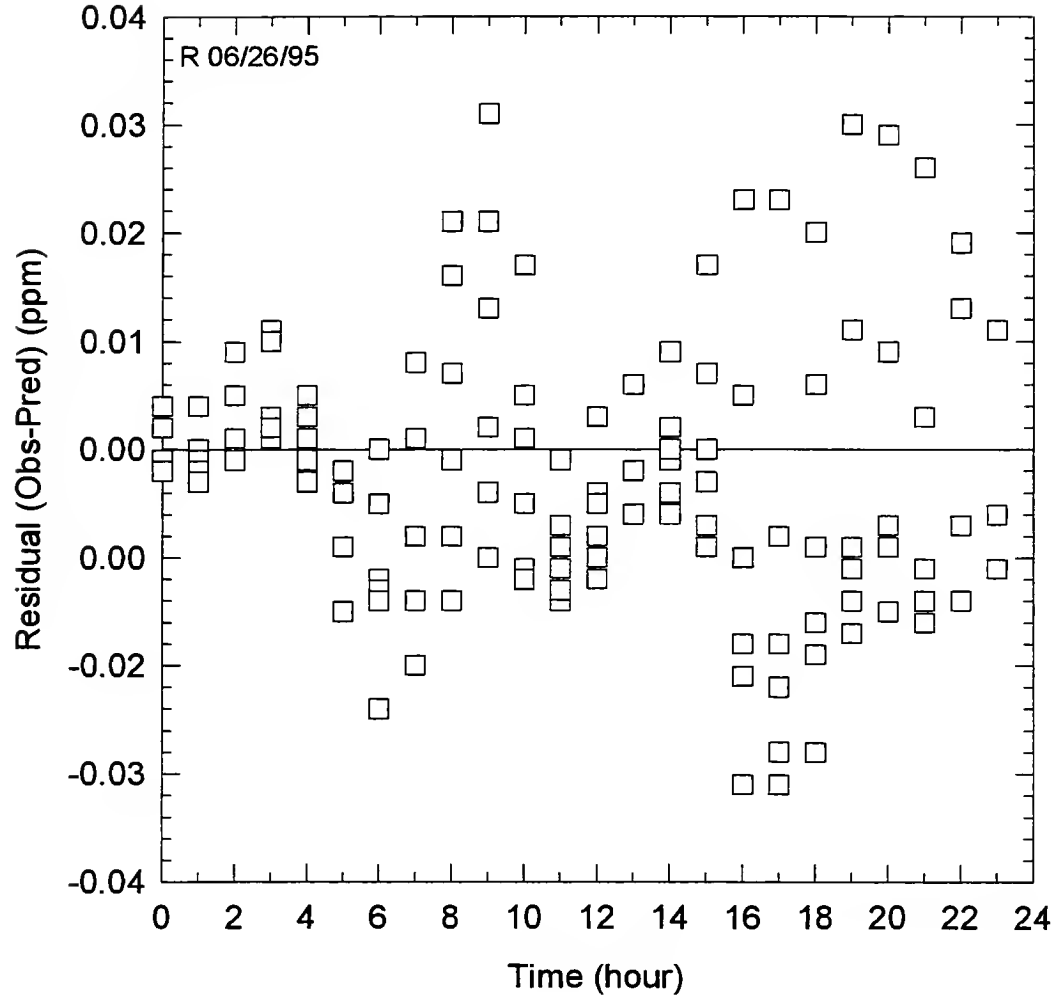

Figure 3.2.a. Paired predicted and observed hourly ozone concentration residuals versus time on June 26, 1990.

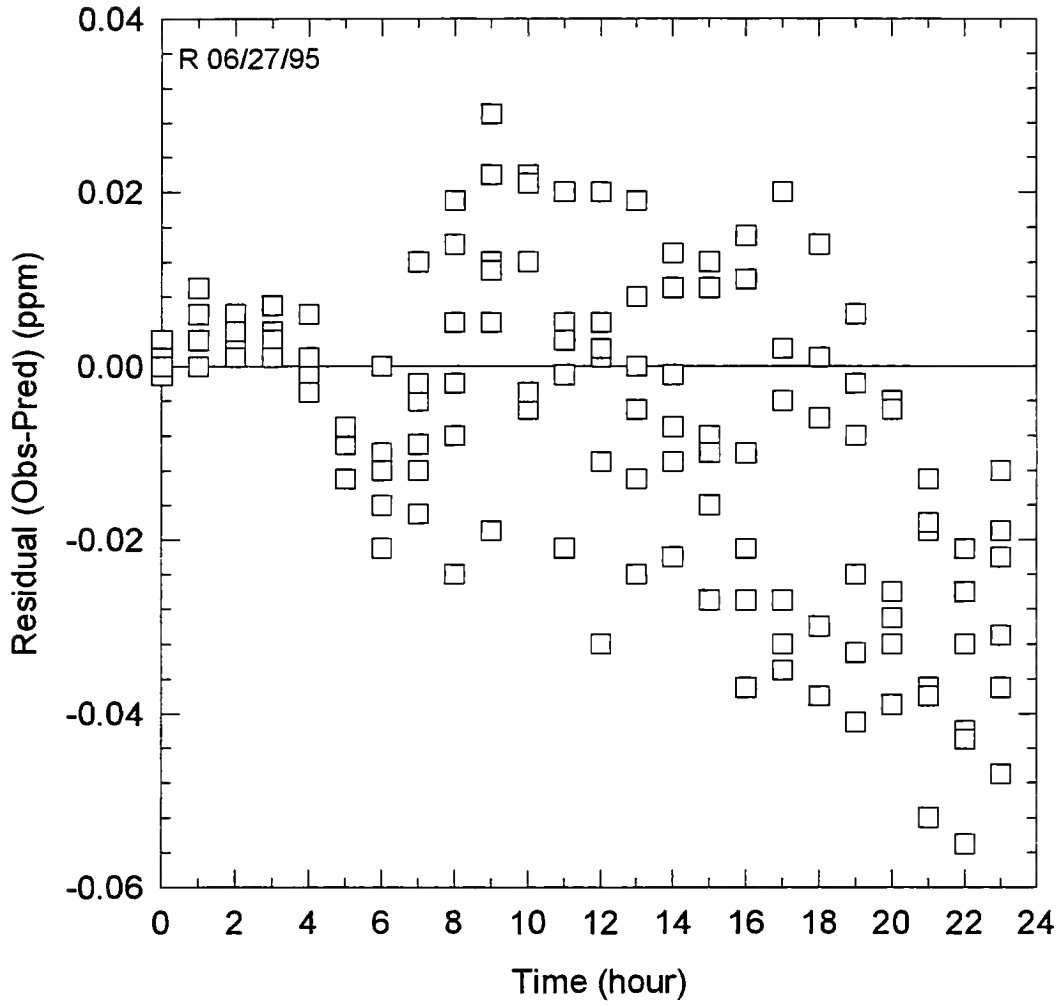

Figure 3.2.b. Paired predicted and observed hourly ozone concentration residuals versus time on June 27, 1990.

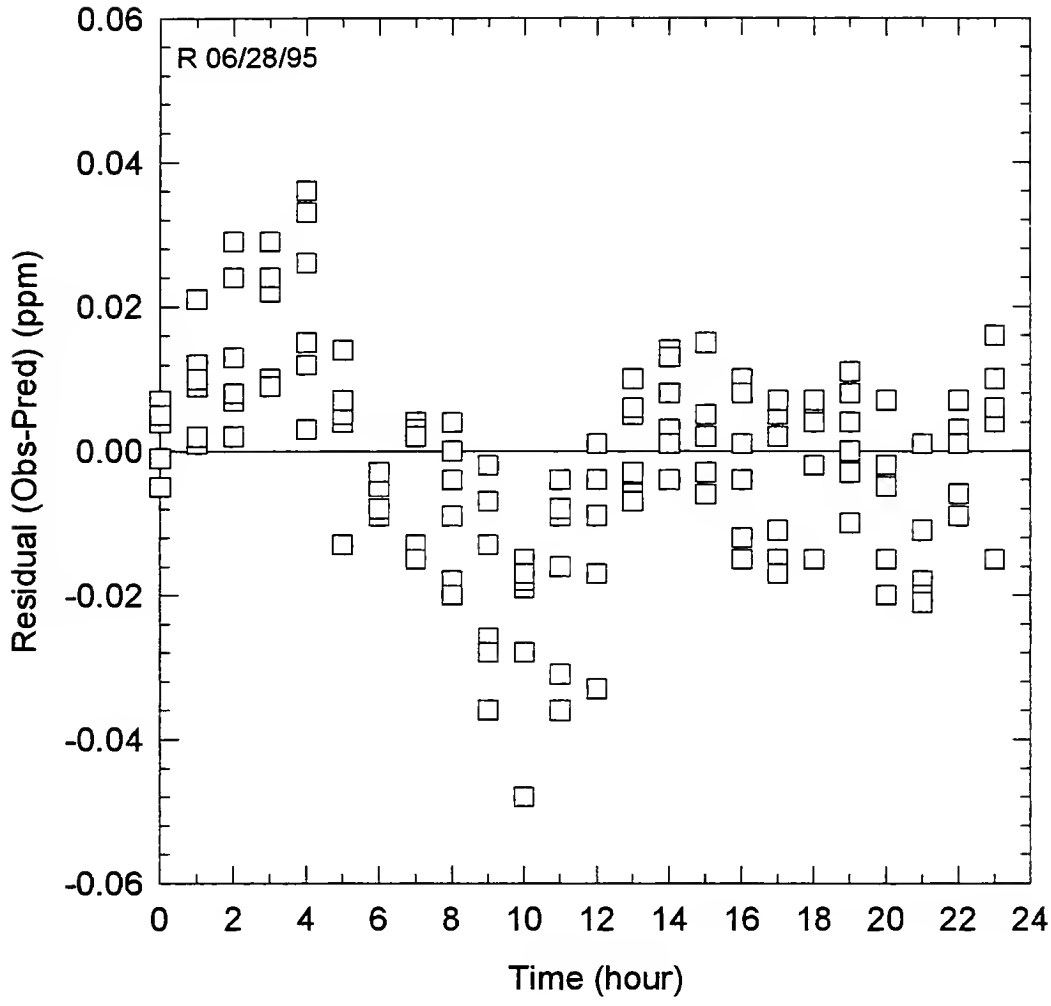

Figure 3.2.c. Paired predicted and observed hourly ozone concentration residuals versus time on June 28, 1990.

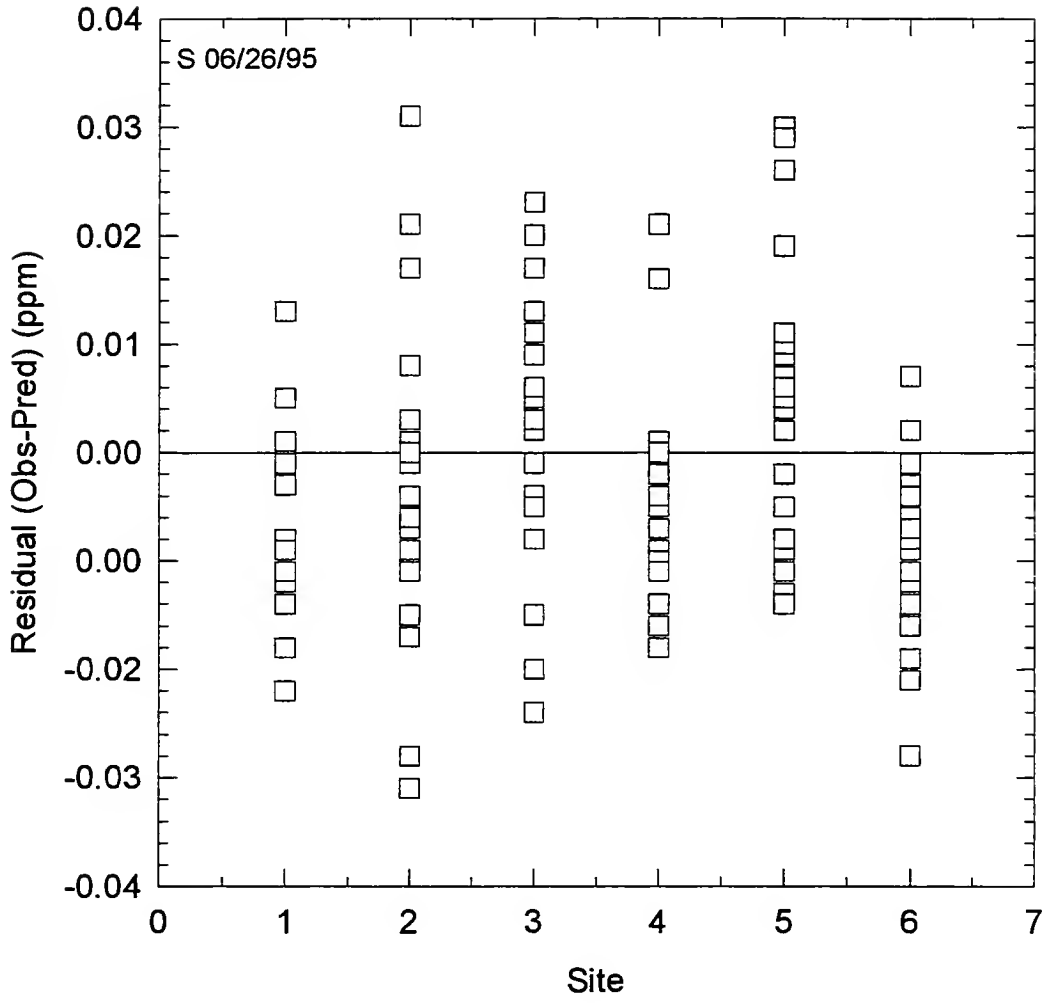

Figure 3.3.a. Paired predicted and observed hourly ozone concentration residuals versus site on June 26, 1990 (1=HAM1001, 2=HAN0003, 3=MAR0042, 4=MAR0050, 5=MAR0057, 6=MAR0073).

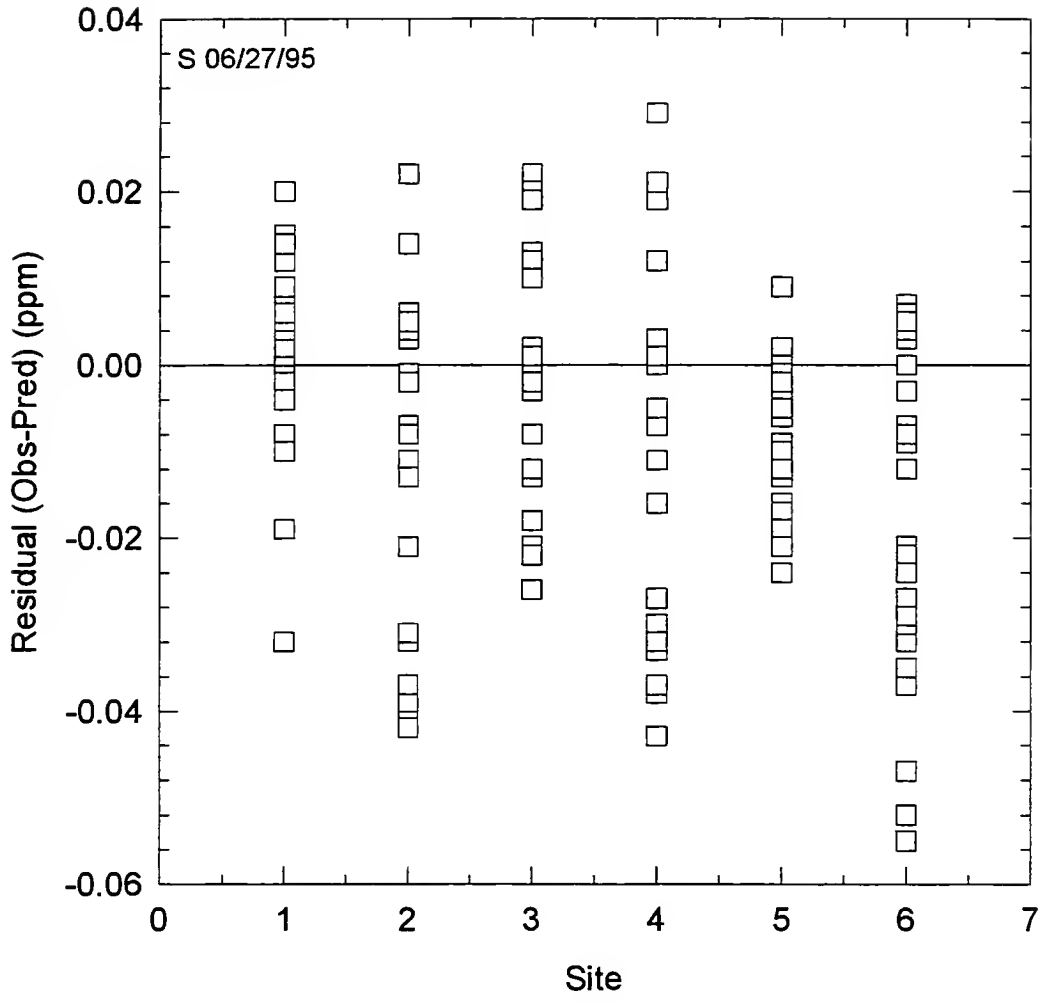

Figure 3.3.b. Paired predicted and observed hourly ozone concentration residuals versus site on June 27, 1990 (1=HAM1001, 2=HAN0003, 3=MAR0042, 4=MAR0050, 5=MAR0057, 6=MAR0073).

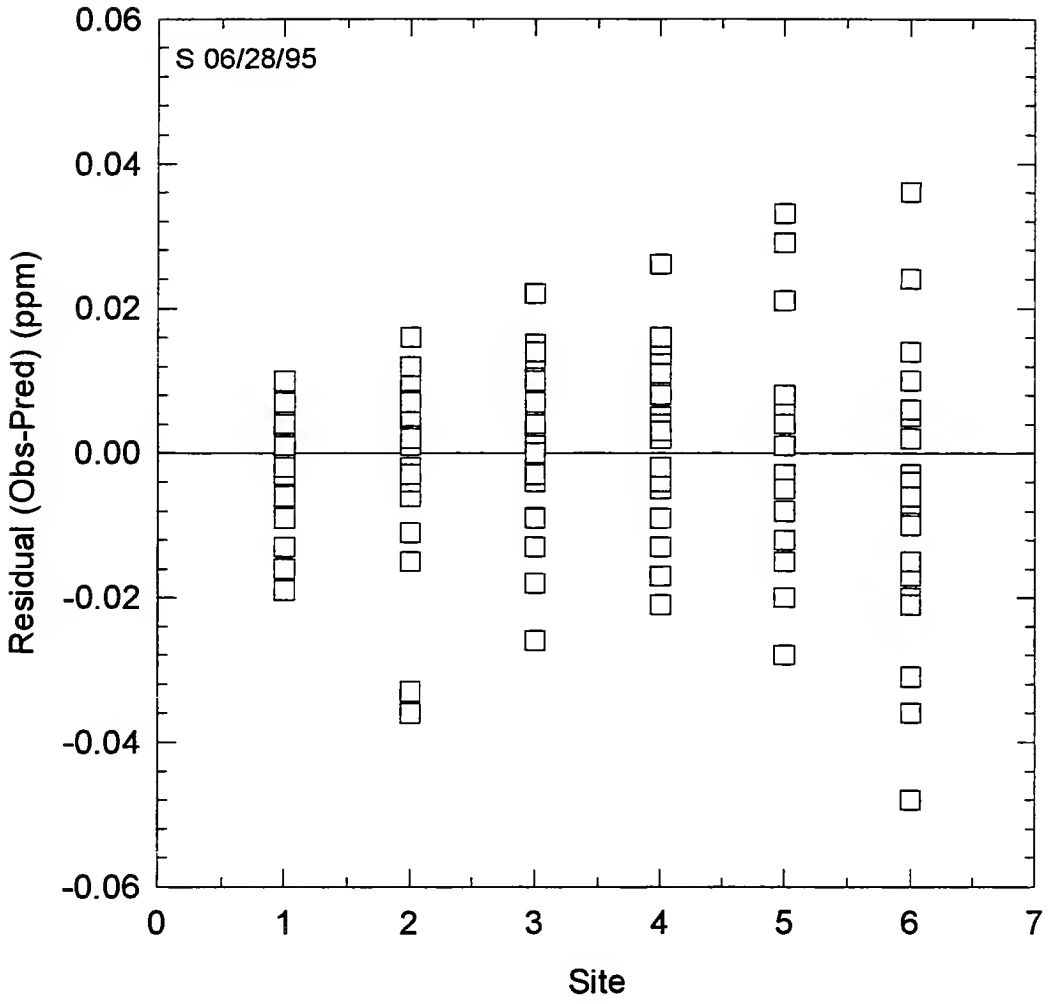

Figure 3.3.c. Paired predicted and observed hourly ozone concentration residuals versus site on June 28, 1990 (1=HAM1001, 2=HAN0003, 3=MAR0042, 4=MAR0050, 5=MAR0057, 6=MAR0073).

3.1.2.2. Daily Ozone Peak Contour Maps

Figures 3.4.a to 3.4.c show the contour maps of the predicted one-hour average ozone concentration daily peaks, plotted with contour intervals of 5 or 10 ppb. Likewise Figures 3.4.d to 3.4.f show the observed one-hour average ozone concentration daily peaks plotted next to the solid squares representing the ozone monitoring sites. Even though the spatial coverage of monitoring stations is not sufficiently dense in the domain, Figures 3.4.a to 3.4.f show that there is a good agreement between observed and predicted one-hour average ozone concentration daily peaks. The spatial pattern of the predicted peaks and the few observed peaks show that the areas of highest one-hour average ozone concentration daily peaks are mostly located downstream of the source area (Indianapolis) in the northeastern quadrant of the study domain. Unfortunately, observation sites seldom exist in that area. However, the database from the ozone monitoring study conducted in the summers of 1994 and 1995 by Dr. R. B. Jacko for LMOS confirms this finding.

3.1.2.3. Station Time Series Plots

The observed and predicted hourly average ozone concentration time series for the six selected monitoring stations and for the entire episode were plotted in Figures 3.5.a to 3.5.f. On June 26, 1990, the model overpredicts the observed one-hour average ozone concentration peaks of the station downstream of the source area. The maximum overprediction is 4 ppb and the timing of the predicted peaks occur within 0 to 2 hours earlier. The station located upstream (MAR0042) observed one-hour average ozone concentration peak is underestimated by 13 ppb and the timing of the predicted peak occurs 2 hours earlier. On June 27, 1990, when the winds shifted to the west no definite pattern is discernible. However, the peak ozone concentration is overpredicted in some stations by as much as 26 ppb (MAR0073) and underestimated in others by as much as 19 ppb (HAM1001). The timing of the predicted peaks occur within -4 to +4 hours. The June 28, 1990 pattern is similar to June 27, 1990. The peak one-hour average ozone concentration is overpredicted in some stations by as much as 7 ppb (MAR0073) and underestimated in others by as much as 12 ppb (MAR0042). The timing of the predicted peaks occur within -4 to +2 hours.

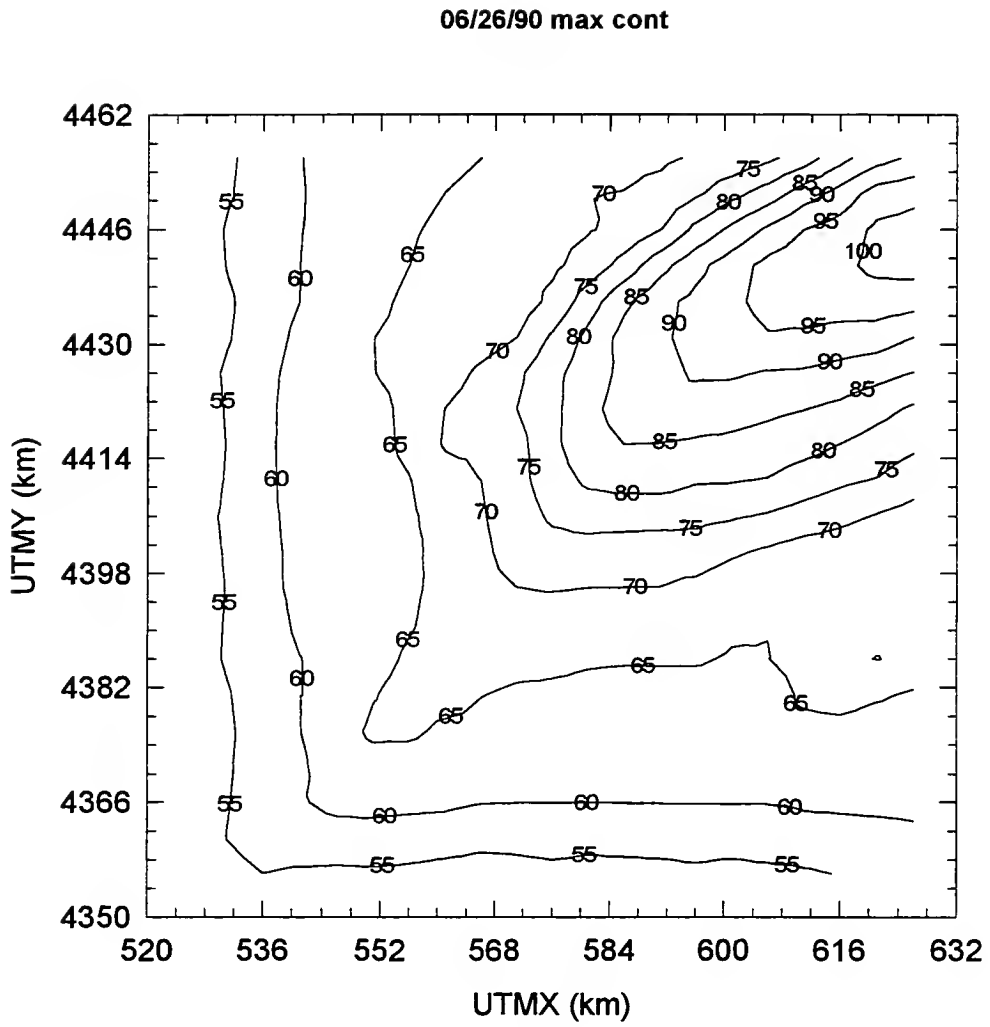

Figure 3.4.a. Predicted one-hour average ozone concentration daily peak (ppb) contour map on June 26, 1990.

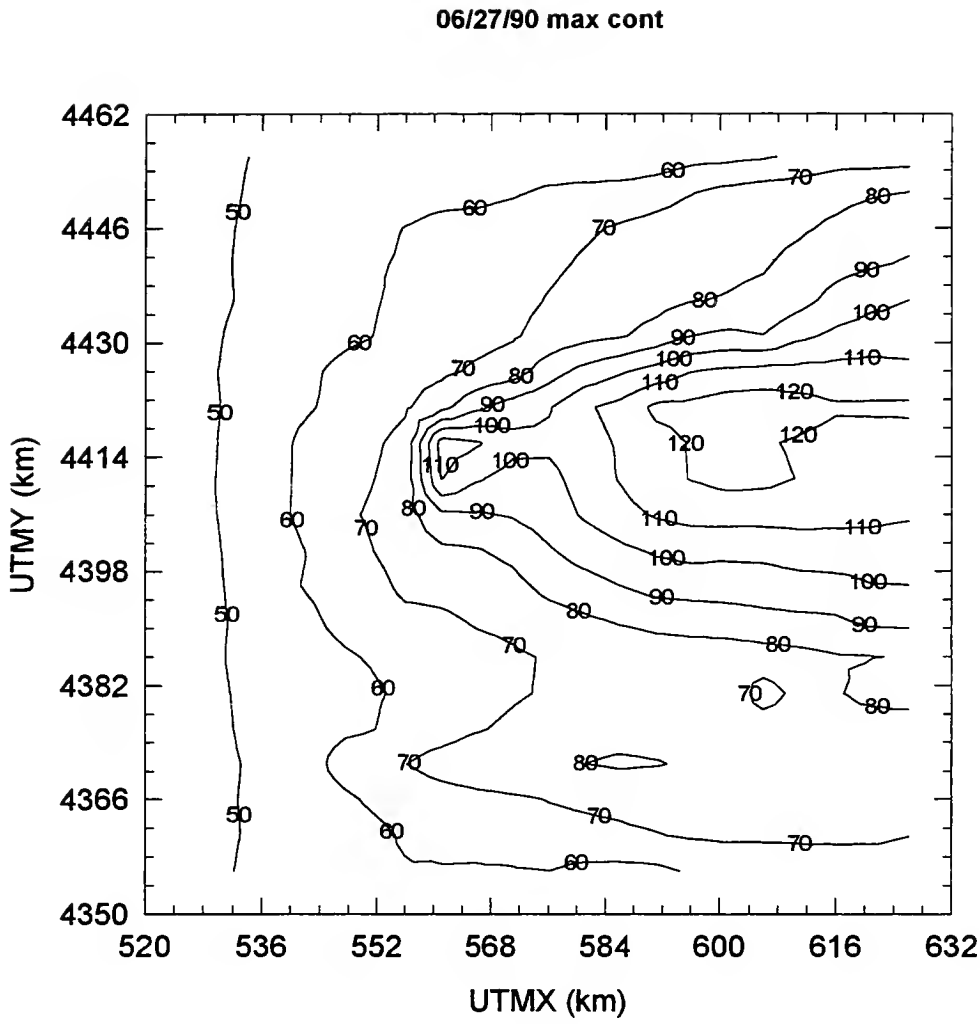

Figure 3.4.b. Predicted one-hour average ozone concentration daily peak (ppb) contour map on June 27, 1990.

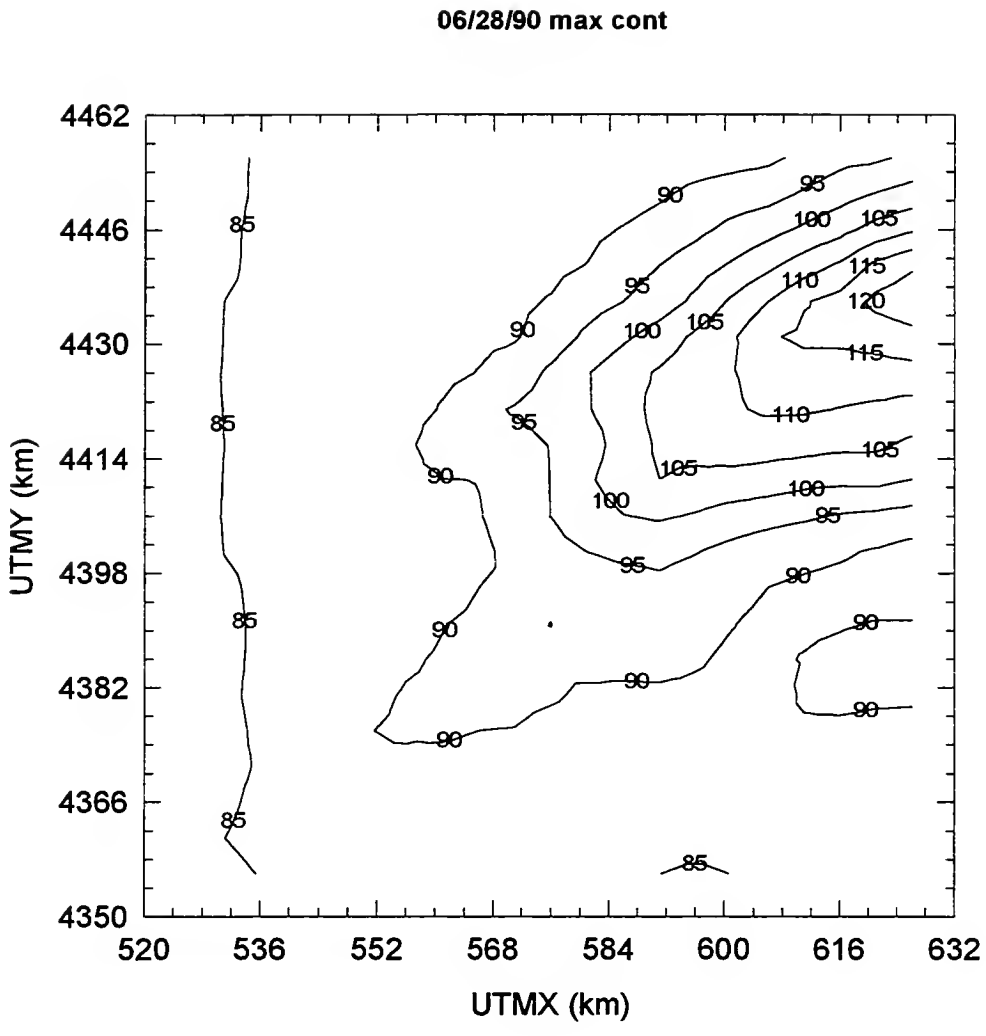

Figure 3.4.c. Predicted one-hour average ozone concentration daily peak (ppb) contour map on June 28, 1990

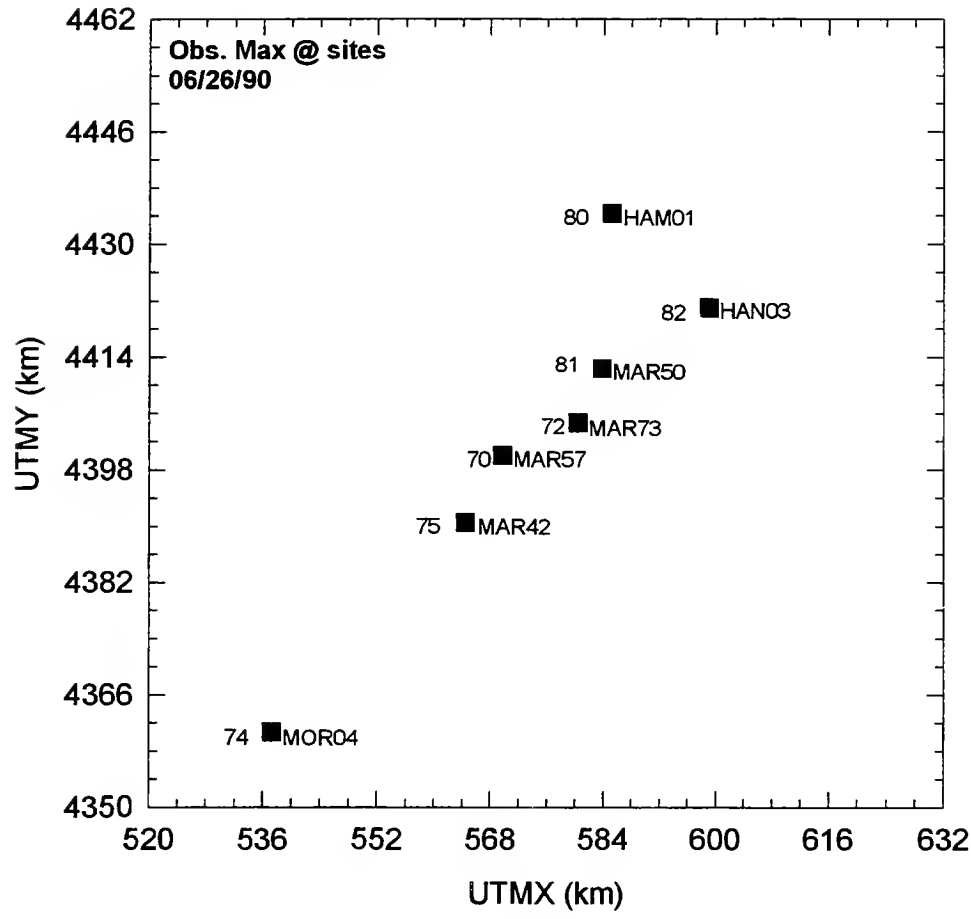

Figure 3.4.d. Observed one-hour average ozone concentration daily peaks (ppb) at each ozone monitoring site on June 26, 1990.

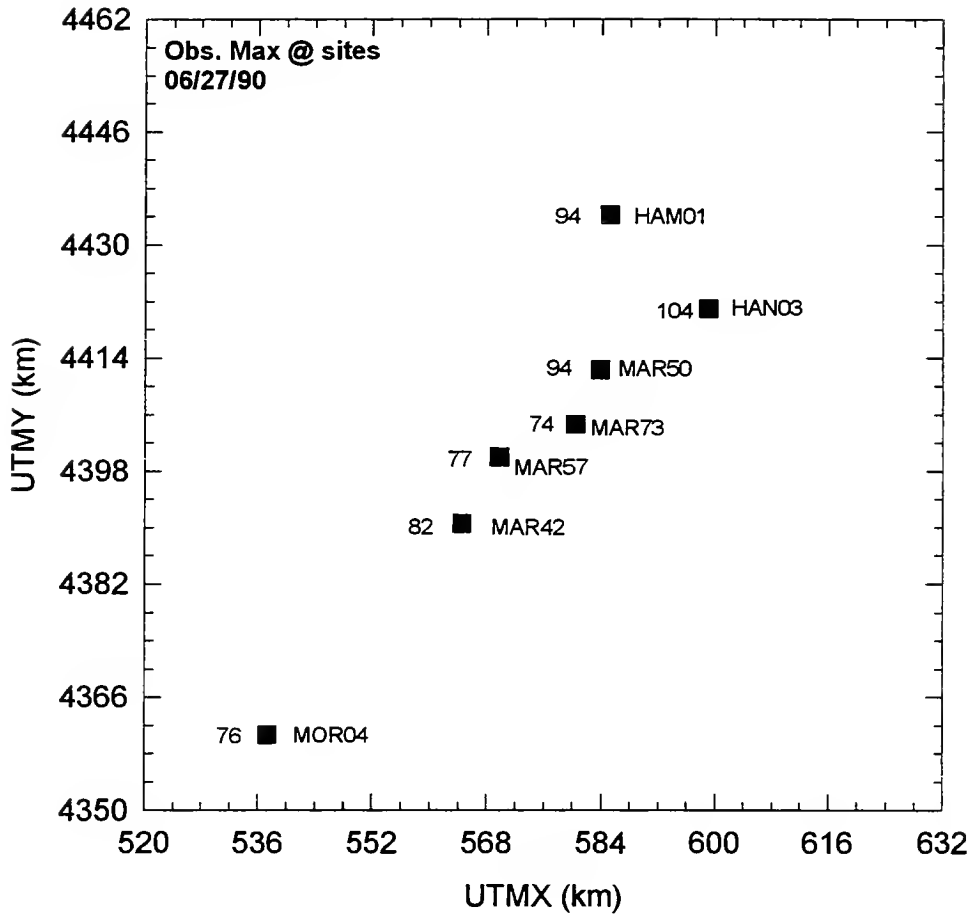

Figure 3.4.e. Observed one-hour average ozone concentration daily peaks (ppb) at each ozone monitoring site on June 27, 1990.

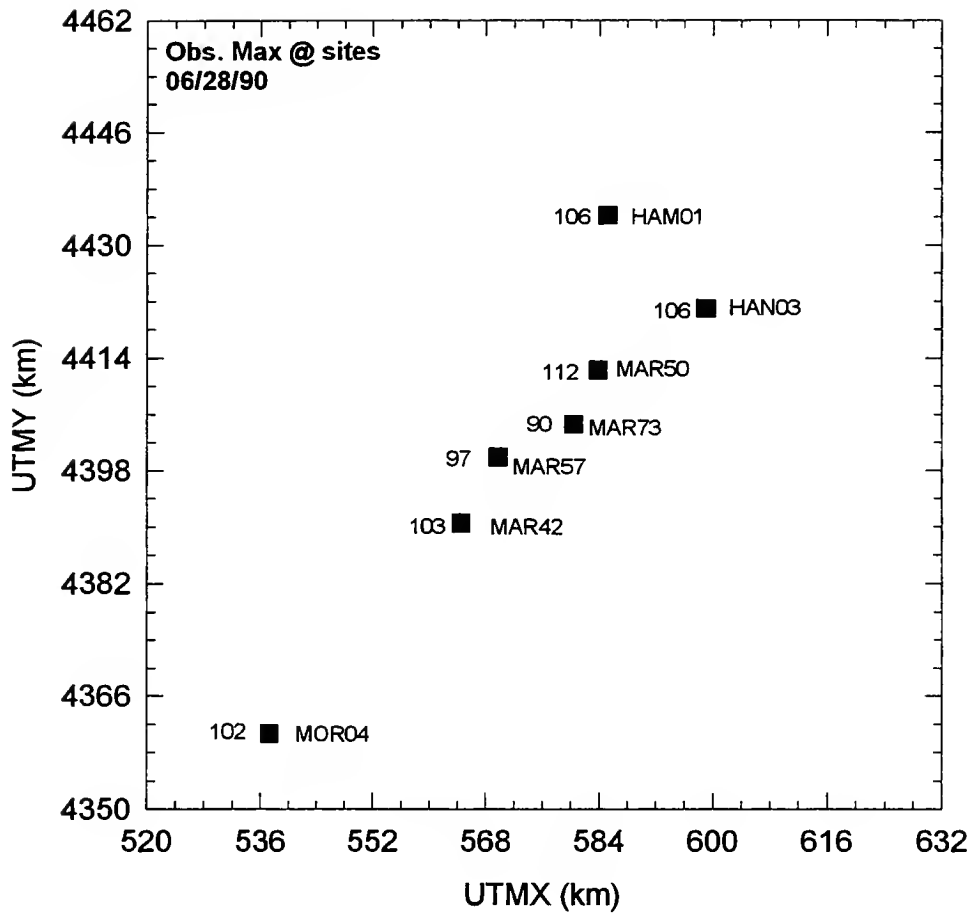

Figure 3.4.f. Observed one-hour average ozone concentration daily peak (ppb) at each ozone monitoring site on June 28, 1990.

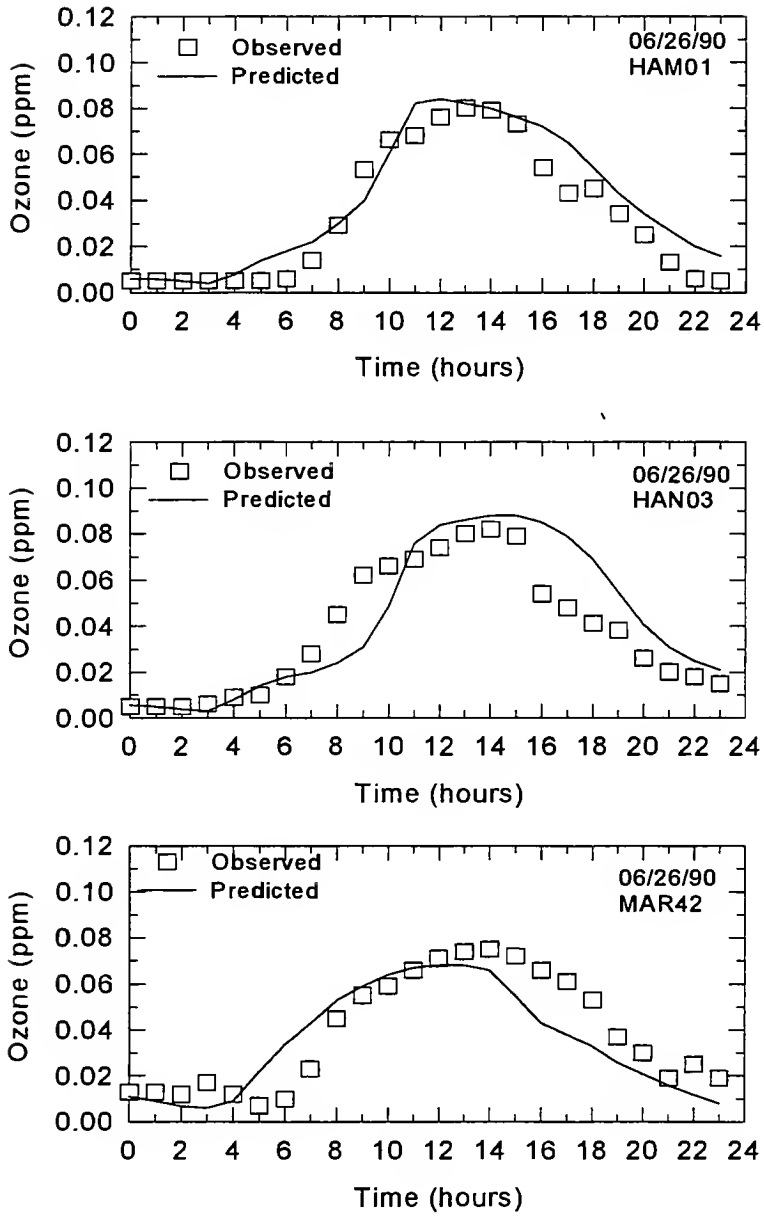

Figure 3.5.a. Hourly average ozone concentration time evolution on June 26, 1990 for sites HAM01 (above), HAN03 (center), and MAR42 (below).

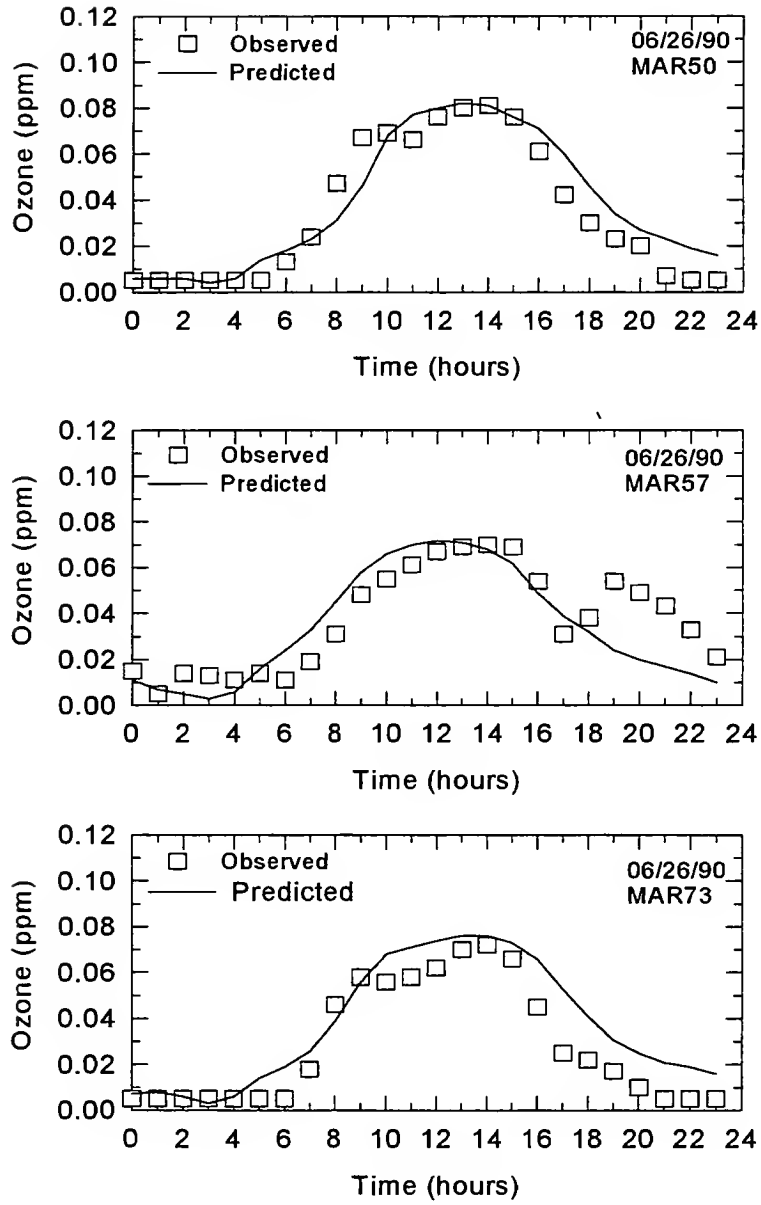

Figure 3.5.b. Hourly average ozone concentration time evolution on June 26, 1990 for sites MAR50 (above), MAR57 (center), and MAR73 (below).

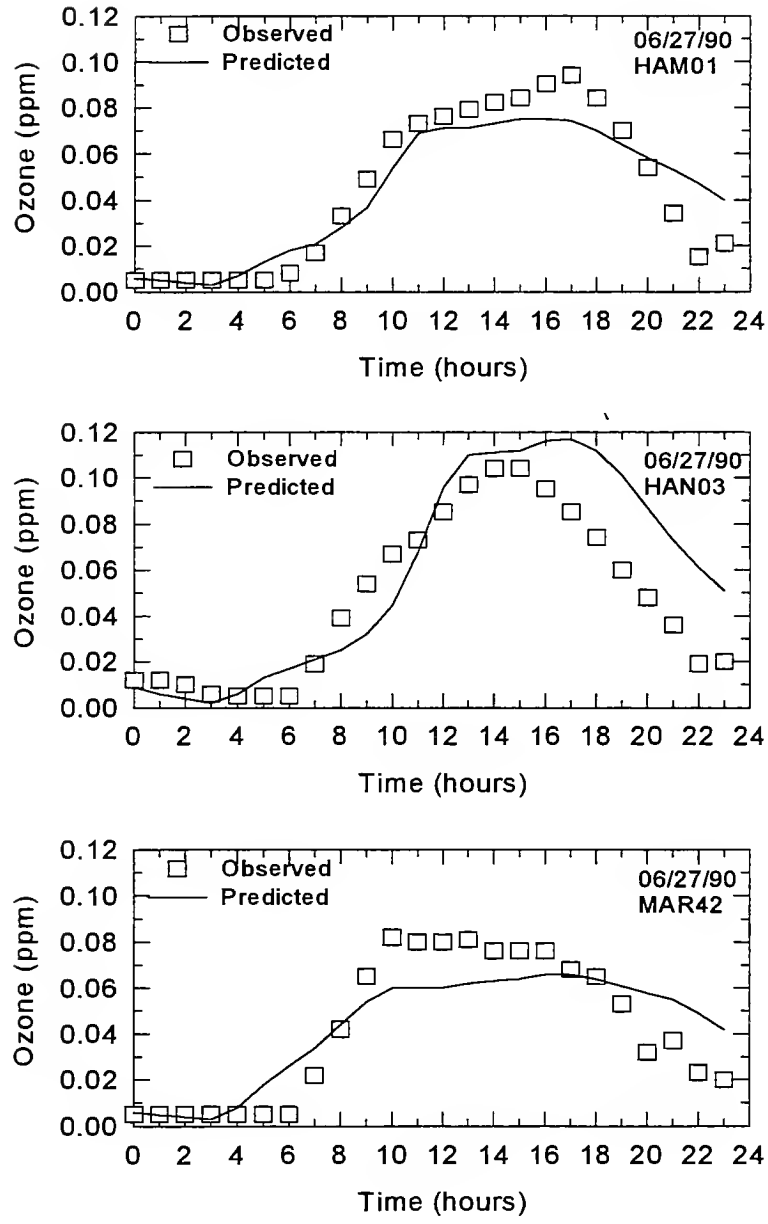

Figure 3.5.c. Hourly average ozone concentration time evolution on June 27, 1990 for sites HAM01 (above), HAN03 (center), and MAR42 (below).

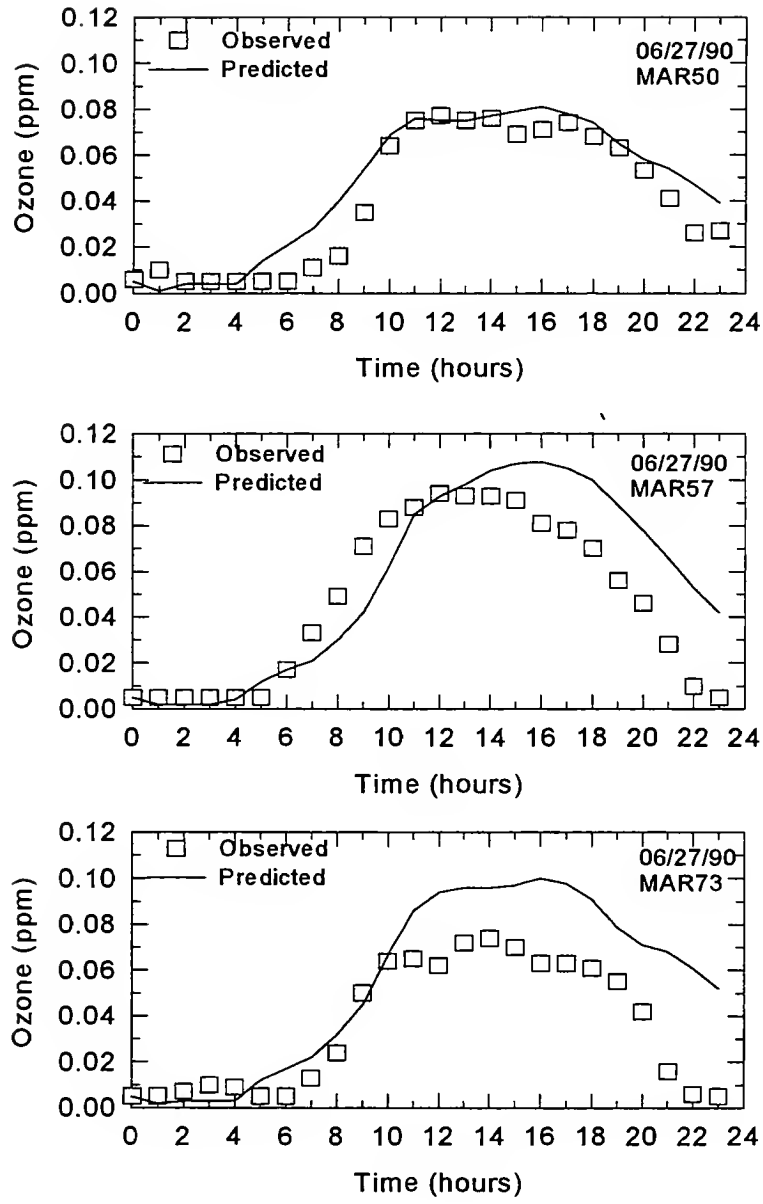

Figure 3.5.d. Hourly average ozone concentration time evolution on June 27, 1990 for sites MAR50 (above), MAR57 (center), and MAR73 (below).

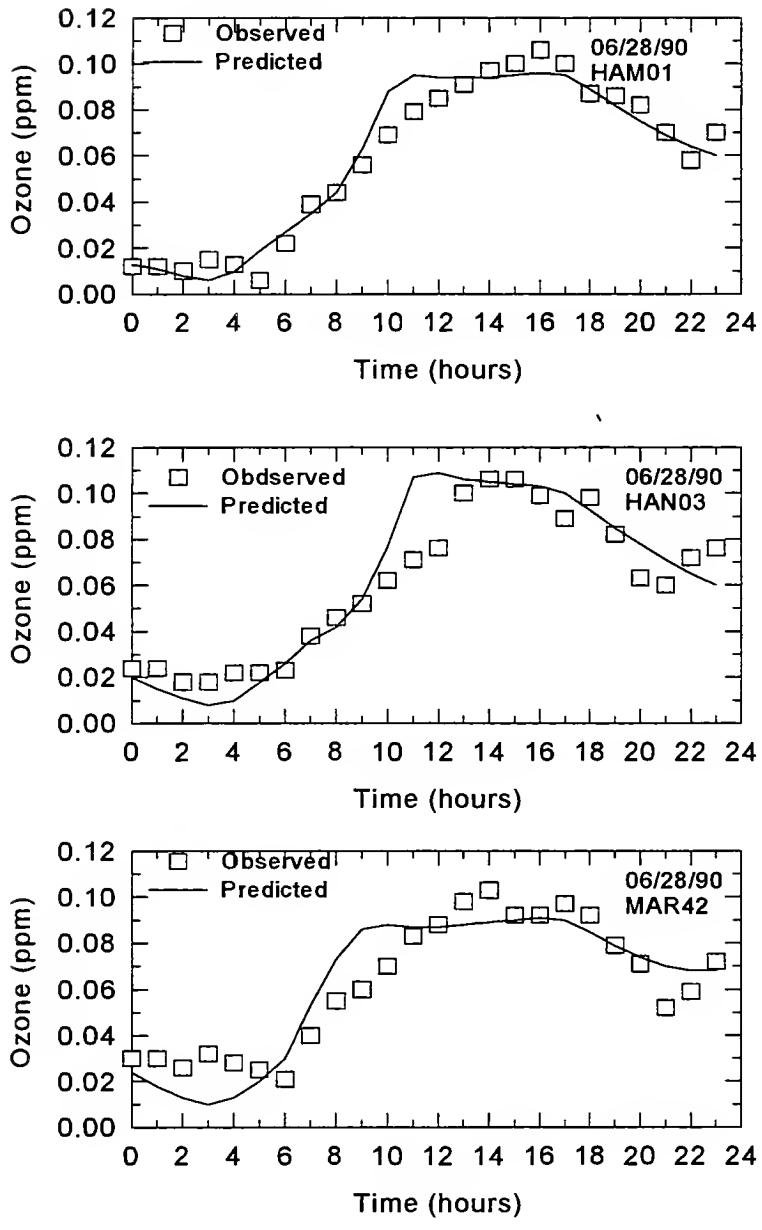

Figure 3.5.e. Hourly average ozone concentration time evolution on June 28, 1990 for sites HAM01 (above), HAN03 (center), and MAR42 (below).

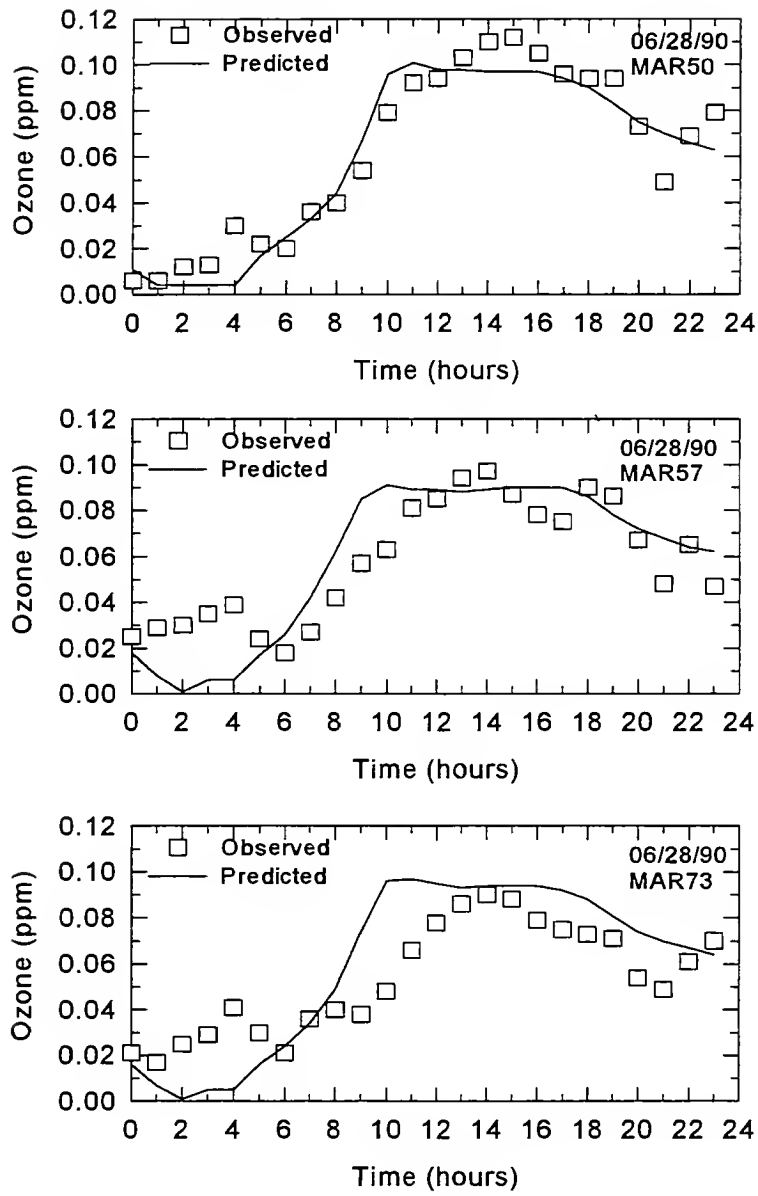

Figure 3.5.f. Hourly average ozone concentration time evolution on June 28, 1990 for sites MAR50 (above), MAR57 (center), and MAR73 (below).

Based on all the results of the performance evaluation shown in this section, it was concluded that the UAM-IV model performs well in the Indianapolis MSA for the episode chosen. Therefore, the UAM-IV as calibrated in this research project can be used for further studies especially, the emission control sensitivity analyses and ozone projection studies in the Indianapolis MSA.

3.2. Emission Reduction Sensitivity Analyses

Ten sets of emission reduction sensitivity runs were performed in order to analyze the magnitudes and directions of changes in the predicted one-hour average near-surface ozone concentrations. The hypothetical cases in which the total low-level emissions (including all the emissions of VOCs, NO_x, CO, SO_2, and TSP inventoried from area, mobile, low-level point, and biogenic sources) and the total elevated point source (stack height > 25 m) emissions were independently set to zero across the study domain were studied. The effects of VOCs and NO_x emissions on the domain-wide ground-level one-hour average ozone concentration daily peaks were analyzed from the uniform and independent reductions of these emissions by 25%, 50%, 75%, and 100% respectively across the modeling domain. The spatial patterns of the predicted one-hour average ozone concentration daily peaks were also analyzed.

3.2.1. Zero Low-level Emissions and Elevated Point Source Emissions

When the total low level emissions were uniformly set to zero across the study domain and the total elevated point source emissions unchanged, the domain-wide one-hour average near-surface ozone concentration daily peak decreased by 35.6% on June 26, 43.4% on June 27, and 27.6% on June 28. The episodic mean decrease was 35.5% (Table 3.4). The spatial patterns of the predicted one-hour average ozone concentration daily peaks were reduced tremendously. In fact, the highest one-hour average ozone concentration daily peaks (i.e. $\geq$ 90 ppb) disappeared completely from the contour plots (Figure 3.6.a to 3.6.c). On the other hand, when the total elevated point source emissions were uniformly set to zero across the study domain and the total low level emissions unchanged, the magnitudes of the changes in the domain-wide one-hour average near-surface ozone daily peaks were very small. In fact, the mean episodic decrease was only 1.8% (Table 3.4). Moreover, the spatial pattern of the

Table 3.4. Changes in the predicted domain-wide one-hour average ozone concentration daily peaks following various emission reduction scenarios. ( ) = % reduction, LLE = low-level emissions, EPSE = elevated point source emissions.

	Mobile Source Emission Reductions (%)	Episodic Mean Predicted Ozone Peak Change due to Mobile Sources (%)	Predicted Ozone Peak Change (ppb) 06/26/90	Predicted Ozone Peak Change (ppb) 06/27/90	Predicted Ozone Peak Change (ppb) 06/28/90	Predicted Ozone Peak Change (ppb) Episode mean
Base Case			104	129	123	118.67
0 LLE			67 (-35.6)	73 (-43.4)	89 (-27.6)	76.3 (-35.5)
0 EPSE			101 (-2.9)	128 (-0.8)	121 (-1.6)	116.7 (-1.8)
Total VOCs Reductions (%)						
25	11.5	-1.6	100 (-3.8)	125 (-3.1)	119 (-3.2)	114.7 (-3.4)
50	23.0	-3.5	95 (-8.6)	120 (-6.9)	114 (-7.3)	109.7 (-7.6)
75	34.5	-5.2	93 (-10.6)	111 (-13.9)	111 (-9.8)	105.0 (-11.4)
100	46.0	-7.2	91 (-12.5)	100 (-22.5)	108 (-12.2)	99.7 (-15.7)
Total NO_x Reductions (%)						
25	10.0	-2.4	100 (-3.8)	117 (-9.3)	117 (-4.9)	111.3 (-6.0)
50	20.0	-4.8	97 (-6.7)	102 (-20.9)	113 (-8.13)	104.0 (-11.9)
75	30.0	-7.2	92 (-11.5)	91 (-29.5)	107 (-13.0)	96.7 (-18.0)
100	40.0	-9.7	86 (-17.3)	83 (-35.6)	99 (-19.5)	89.3 (-24.2)

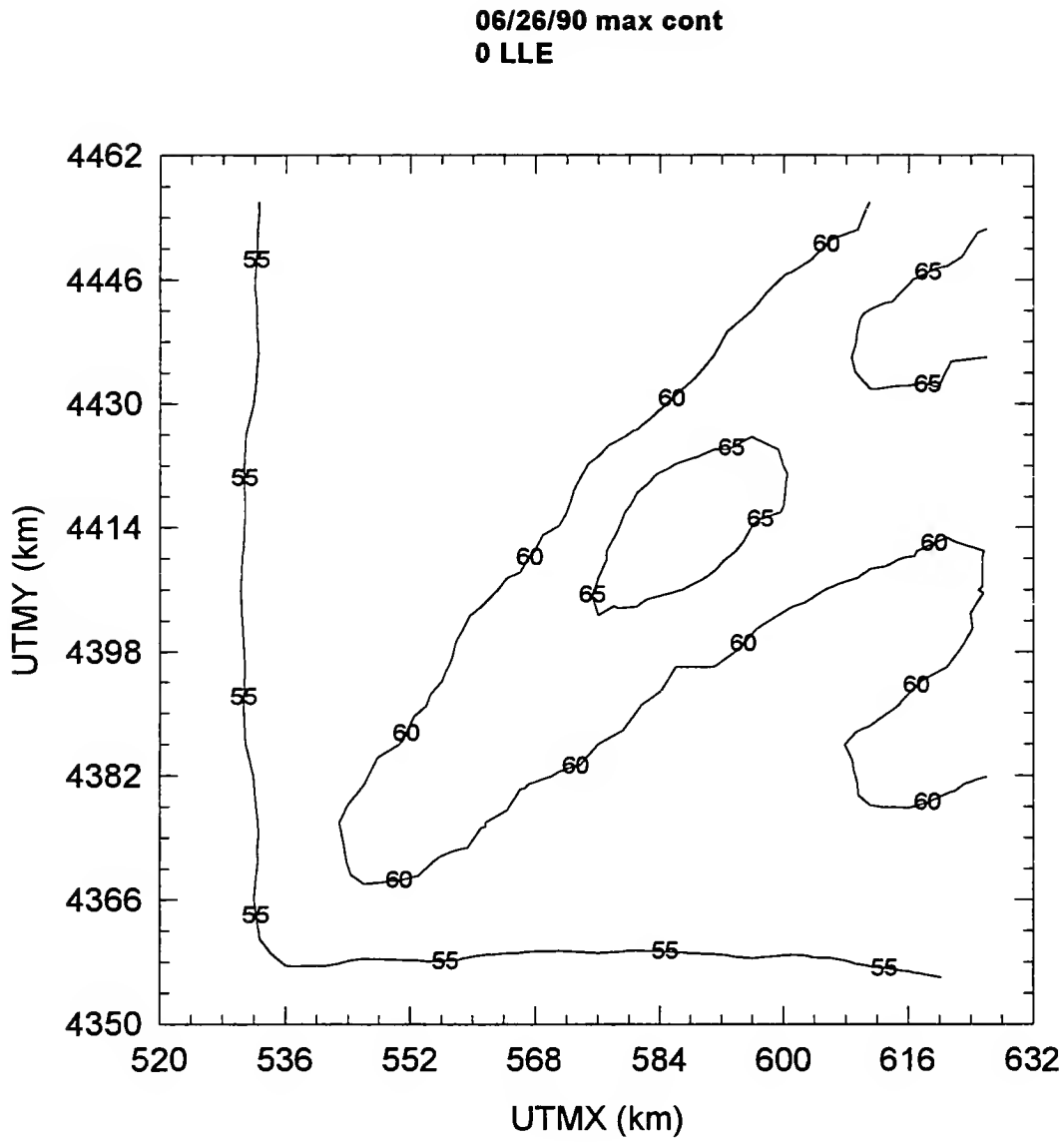

Figure 3.6.a. Predicted one-hour average ozone concentration peaks (ppb) contour map for zero low-level emissions on June 26, 1990.

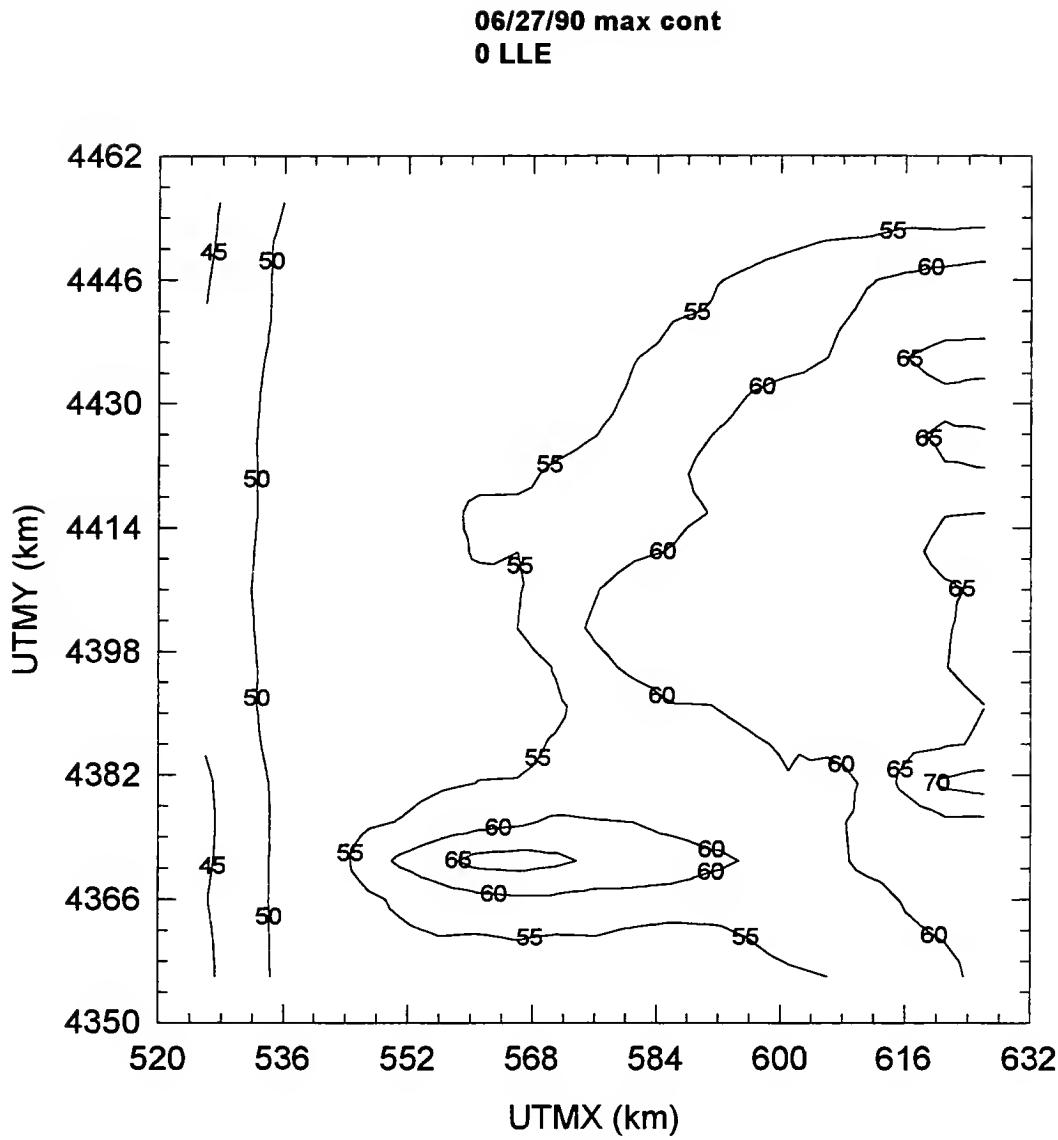

Figure 3.6.b. Predicted one-hour average ozone concentration peaks (ppb) contour map for zero low-level emissions on June 27, 1990.

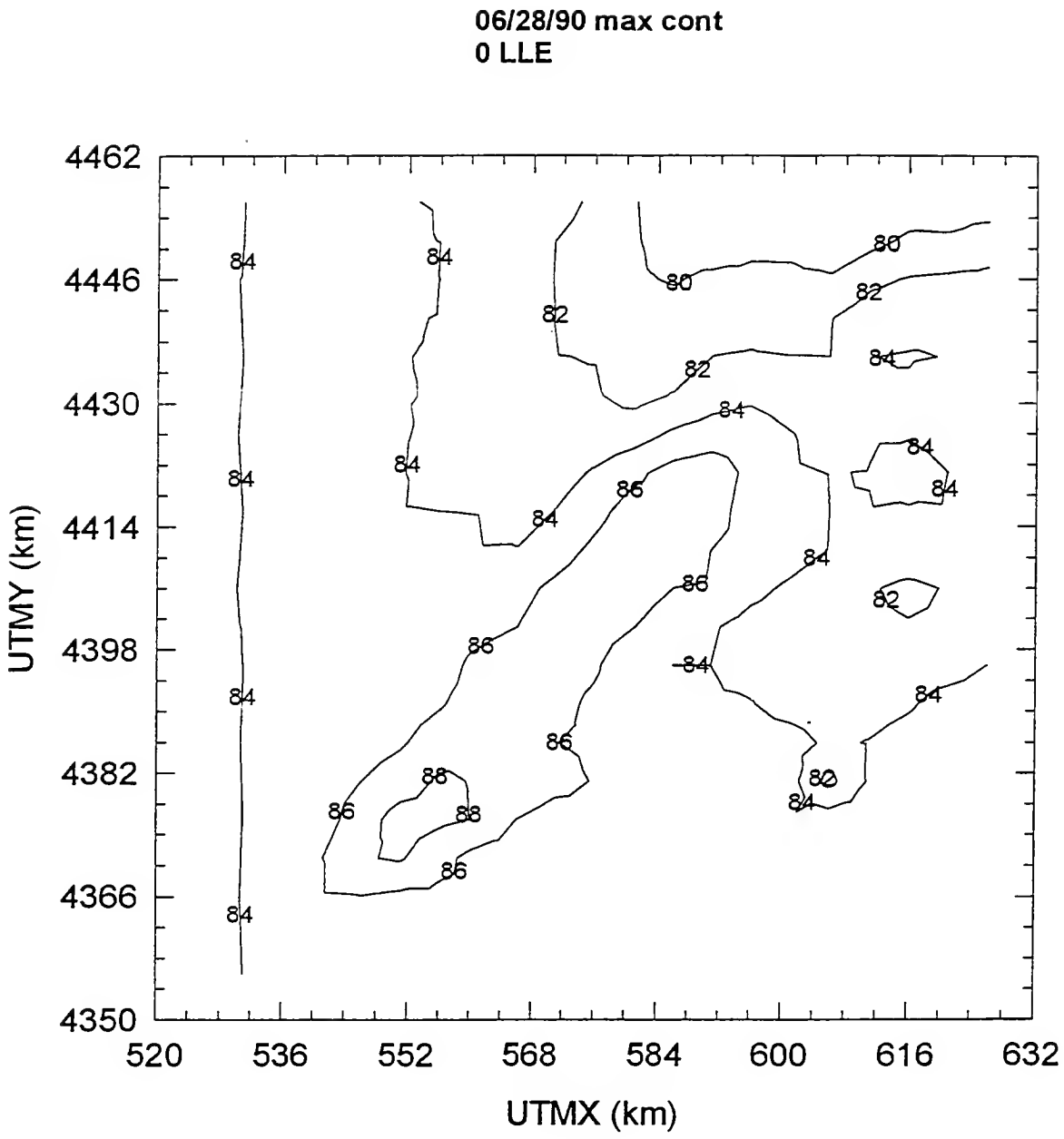

Figure 3.6.c. Predicted one-hour average ozone concentration peaks (ppb) contour map for zero low-level emissions on June 28, 1990.

predicted one-hour average ozone concentration daily peaks barely changed (Figure 3.7.a to 3.7.c). This infers that the elevated point source emissions originated from the study domain do not influence the generation of ground level ozone as much as does the low-level emissions. This might be a consequence of the relatively small size of the modeling domain in which the ground level impact of stationary sources plume may be minimal. Nonetheless, a 100% reduction in emissions is unrealistic. Furthermore, it is not possible to pinpoint the effects of VOCs nor NO_x emissions from this type of general emissions reduction sensibility analysis.

3.2.2. Anthropogenic VOCs Emissions Reductions

The domain-wide one-hour average near-surface ozone concentration peaks decreased as seen in Table 3.4 and Figure 3.8.a to 3.8.d following the uniform reductions of anthropogenic VOCs emissions across the study domain when the NO_x emissions remained unchanged. The decreases are almost linearly proportional to VOCs emissions reductions. On average, a 50% reduction in anthropogenic VOCs emissions caused a 7.6% or 9.0 ppb decrease in the domain-wide one-hour average ozone concentration daily peak. The spatial coverage of the highest one-hour average ozone concentration daily peaks reduced considerably on the contour maps (Figure 3.10.a to 3.10.l) and vanished completely when VOCs emissions were further reduced. However, the positioning of the centroid of the peaks did not move geographically. Furthermore, it can be seen from the ozone concentration daily peaks contour maps that the changes occur mostly downwind of the source region. As indicated in section 2, mobile source emissions of VOCs account for 46% of the total anthropogenic VOCs emissions in the study domain. Therefore, from a proportionality study, the contribution of mobile sources in emissions reduction may be assessed (Table 3.4) assuming that the VOCs speciation profiles of the emissions remain constant. For example, a uniform reduction of 50% in total anthropogenic VOCs emissions would correspond to a 23% reduction in mobile source VOCs emissions. The contribution of mobile sources in the domain-wide one-hour average ozone concentration daily peak changes may be assessed in a similar way (Table 3.4). Consequently, the average decrease in the domain-wide one-hour average ozone concentration daily peak due to mobile source emissions of VOCs when the total anthropogenic VOCs emissions are reduced by 50% is 3.5%.

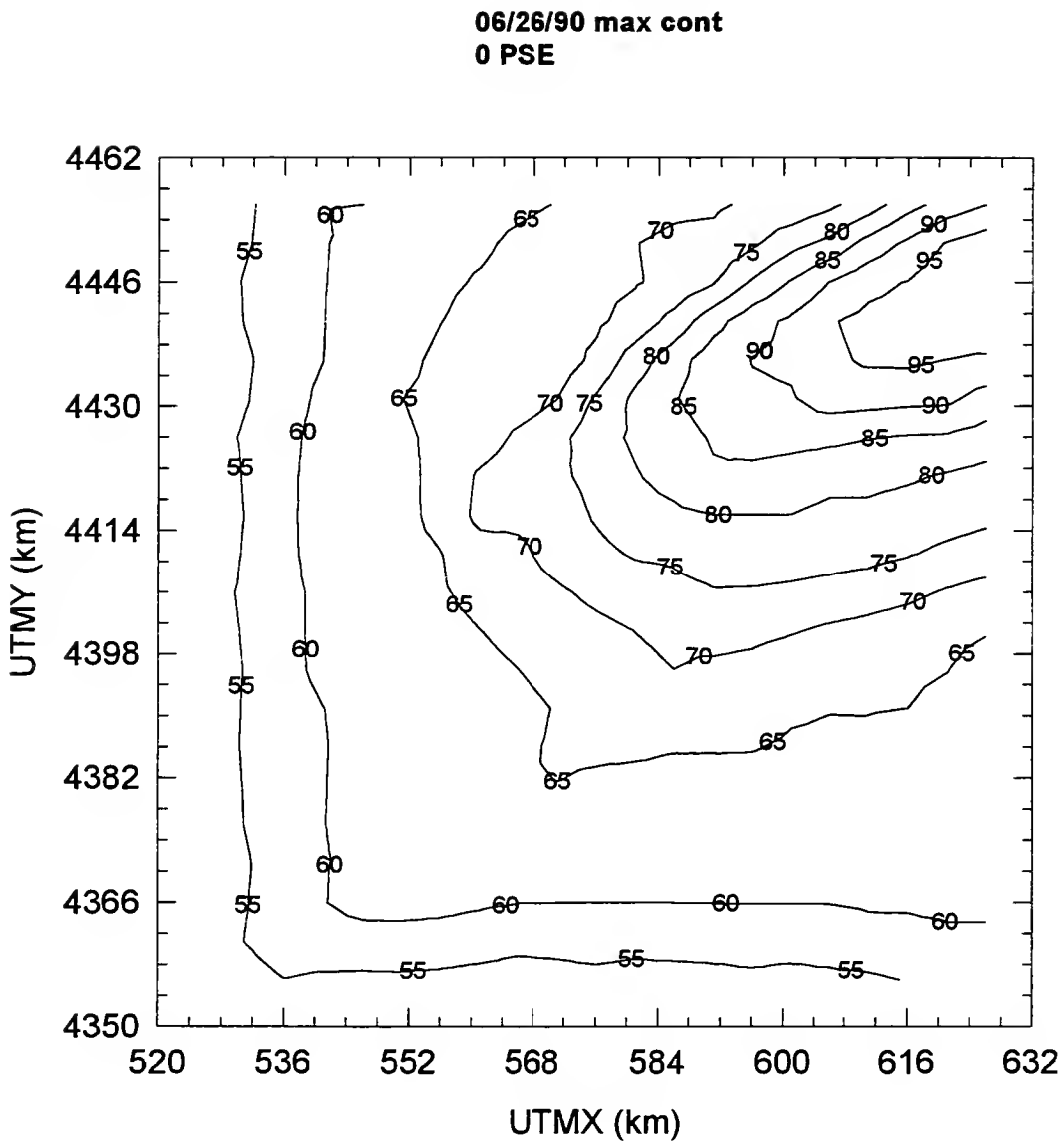

Figure 3.7.a. Predicted one-hour average ozone concentration daily peak (ppb) contour map for zero elevated point source emissions on June 26, 1990.

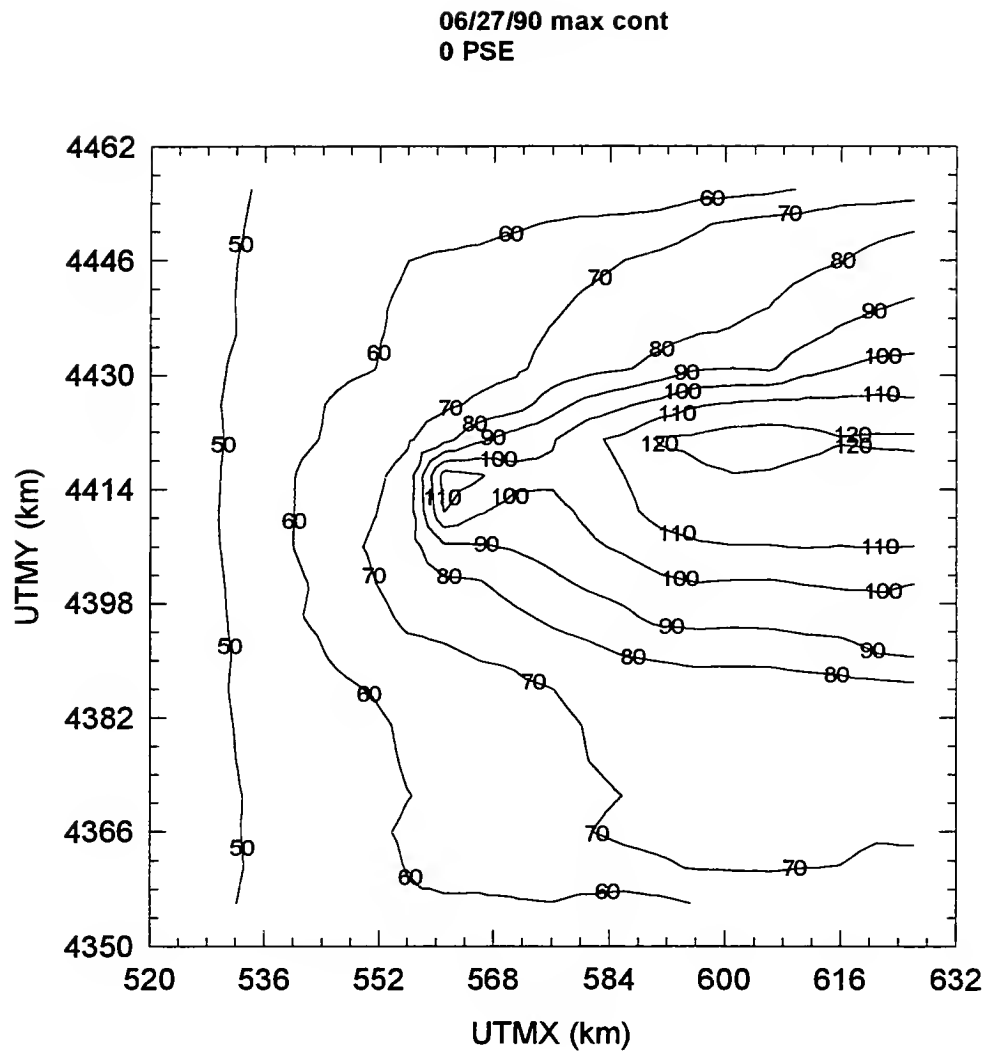

Figure 3.7.b. Predicted one-hour average ozone concentration daily peak (ppb) contour map for zero elevated point source emissions on June 27, 1990.

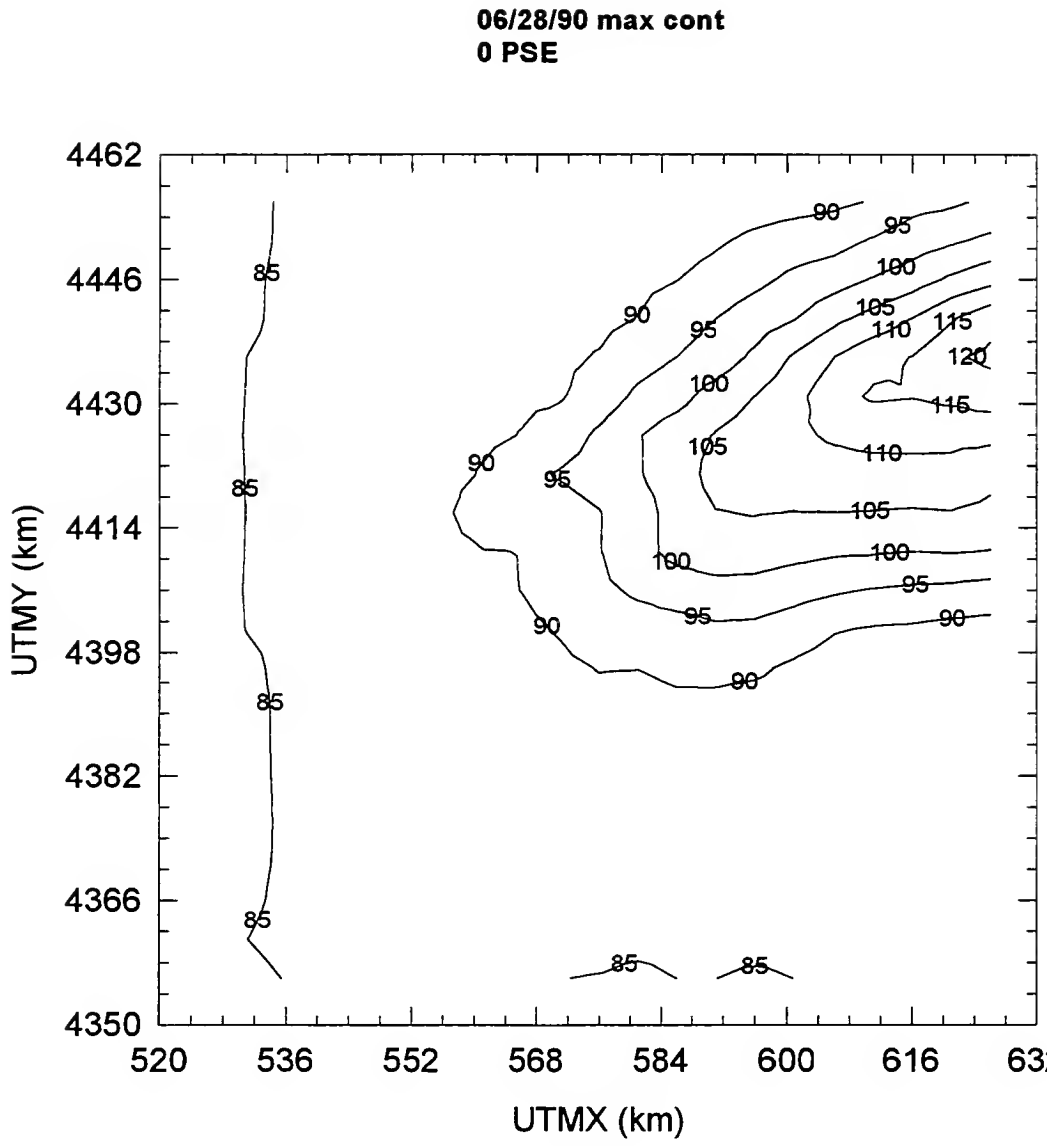

Figure 3.7.c. Predicted one-hour average ozone concentration daily peak (ppb) contour map for zero elevated point source emissions on June 28, 1990.

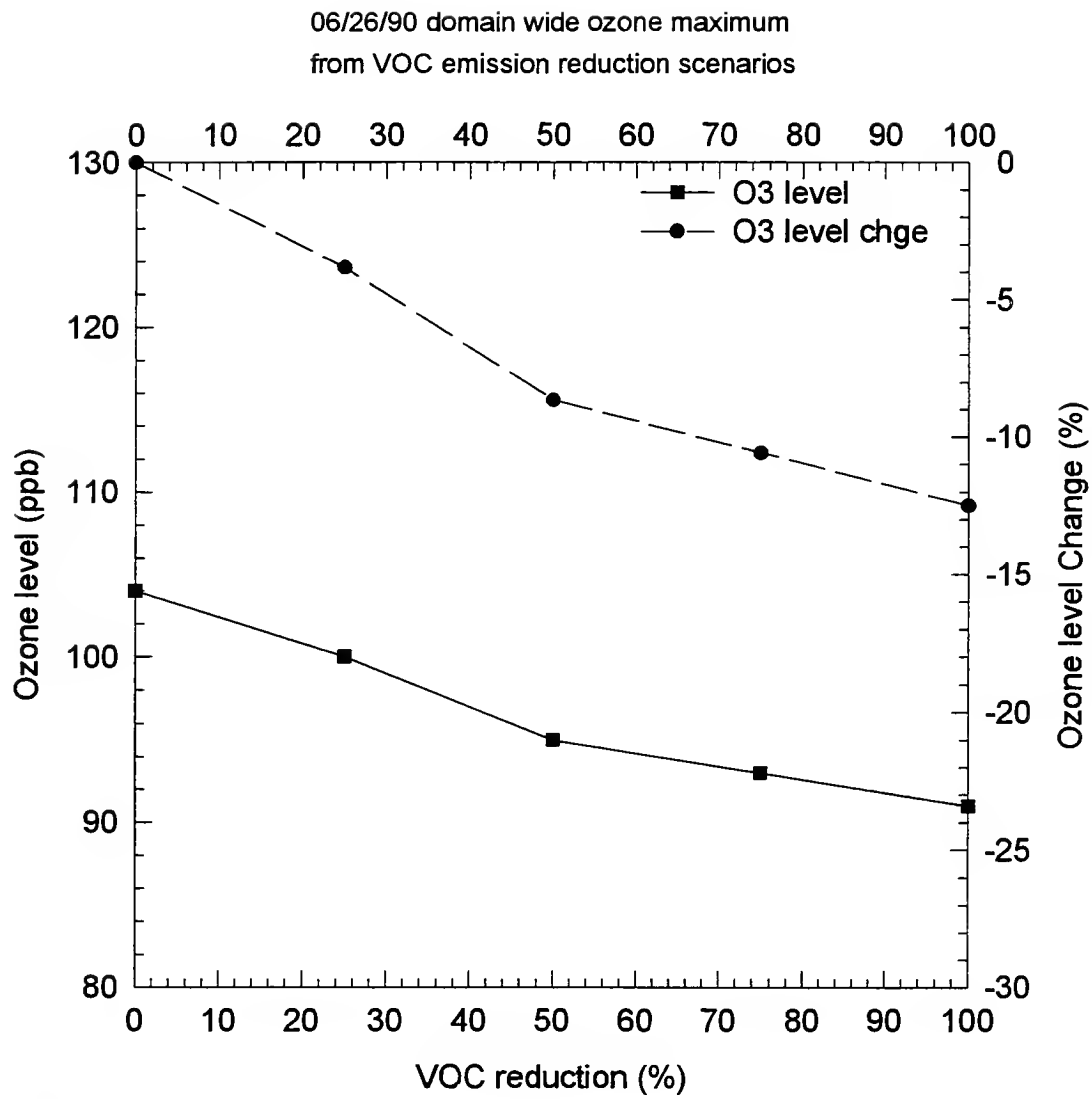

Figure 3.8.a. Changes in predicted domain-wide one-hour average ozone concentration daily peak (ppb) following VOCs emissions reduction scenarios on June 26, 1990.

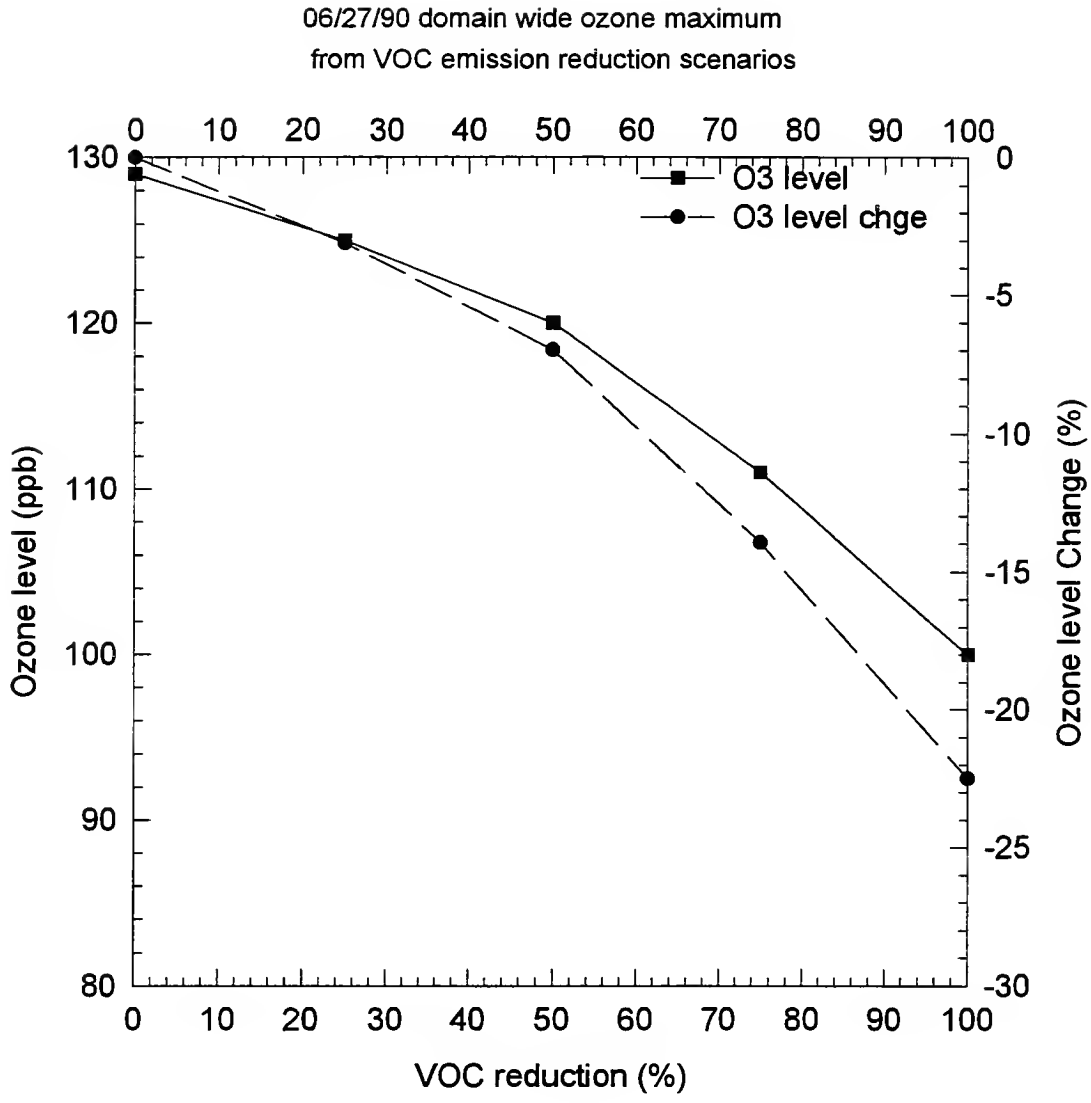

Figure 3.8.b. Changes in predicted domain-wide one-hour average ozone concentration daily peak (ppb) following VOCs emissions reduction scenarios on June 27, 1990.

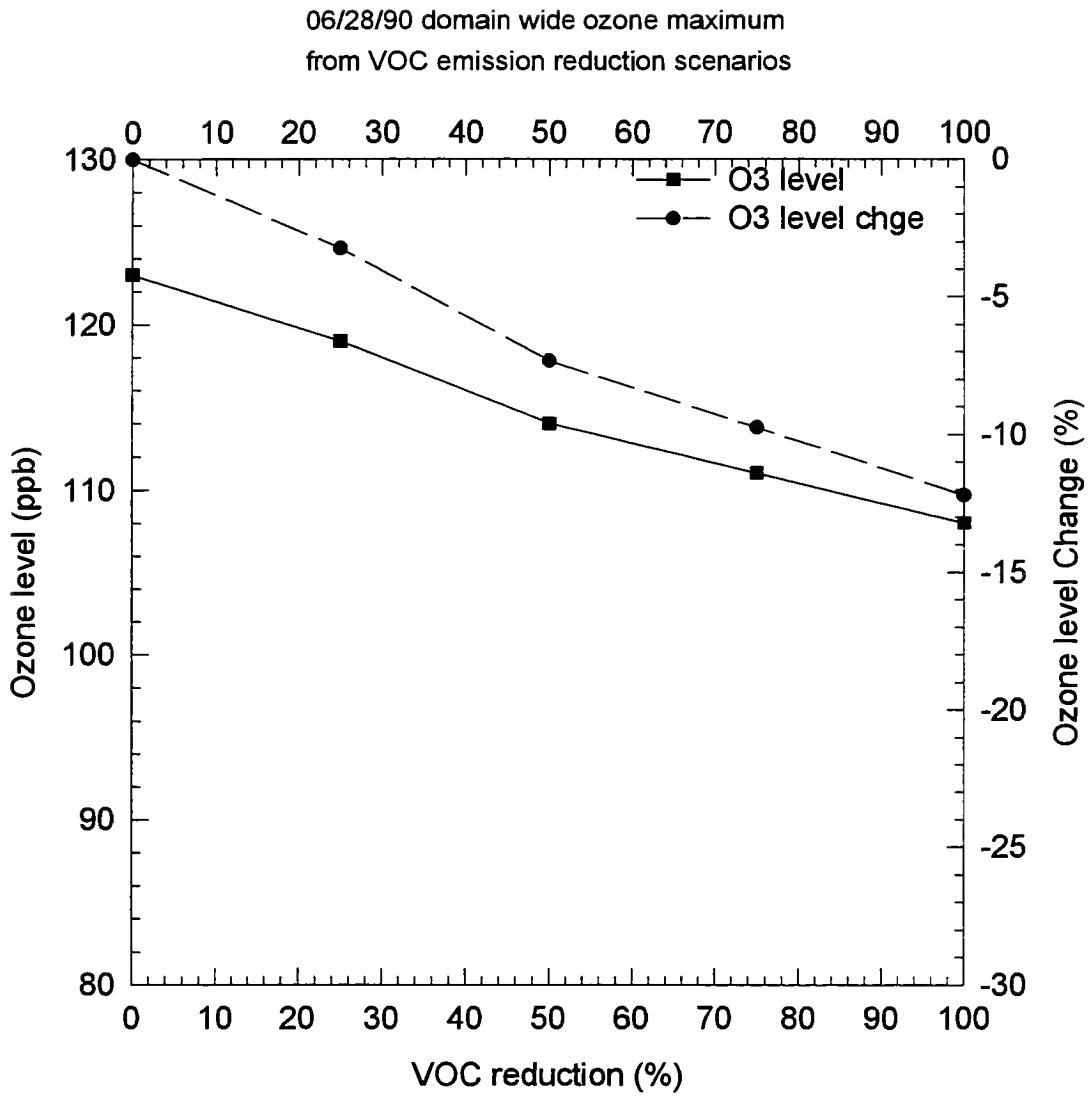

Figure 3.8.c. Changes in predicted domain-wide one-hour average ozone concentration daily peak (ppb) following VOCs emissions reduction scenarios on June 28, 1990.

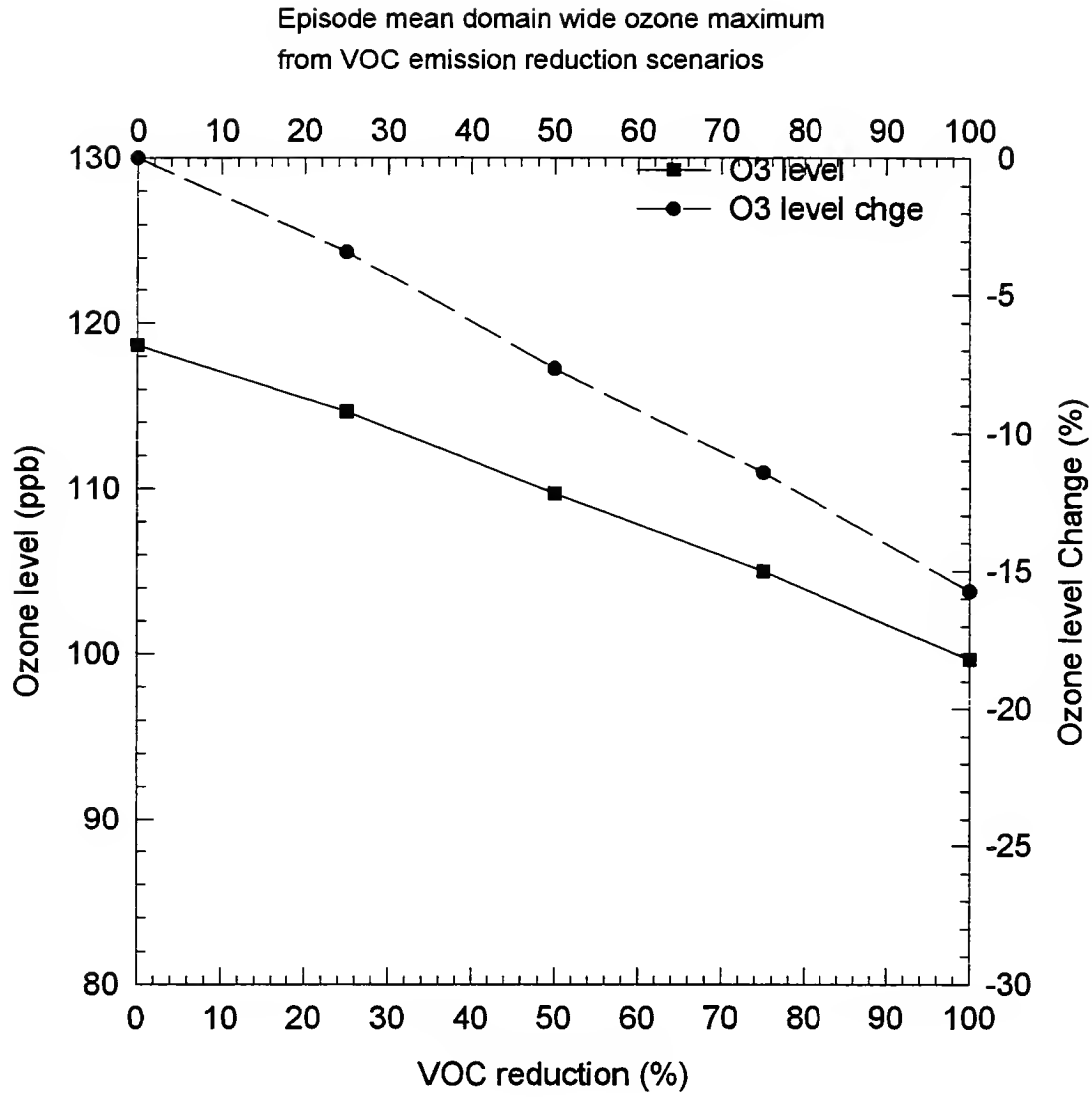

Figure 3.8.d. Episodic mean changes in predicted domain-wide one-hour average ozone concentration daily peak (ppb) following VOCs emissions reduction scenarios.

3.2.3. Anthropogenic NOx Emissions Reductions

Like the VOCs emissions reduction scenarios, the domain-wide one-hour average near-surface ozone concentration daily peaks decreased following the uniform reductions of anthropogenic NO_x emissions across the study domain when the VOCs emissions remained unchanged (Table 3.4 and Figures 3.9.a to 3.9.d). The decreases are linearly proportional to NO_x emissions reductions and greater than that caused by VOCs emissions reductions. On average, a 50% reduction in anthropogenic NO_x emissions caused an 11.9% or 14.67 ppb decrease in the domain-wide one-hour average ozone concentration daily peak. The spatial coverage of the highest one-hour average ozone concentration daily peaks reduced considerably on the contour maps (Figure 3.11.a to 3.11.l) and vanished completely when NO_x emissions were further reduced and the positioning of the centroid of the peaks did not move geographically. Furthermore, it can also be seen from the ozone concentration daily peaks contour maps that the changes occur mostly downwind of the source region. Mobile source emissions of NO_x account for 40% of the total anthropogenic VOCs and NO_x emissions in the study domain. Therefore, a uniform reduction of 50% in total anthropogenic NO_x emissions would correspond to a 20% reduction in mobile source NO_x emissions. Consequently, the average decrease in the domain-wide one-hour average ozone concentration daily peak due to mobile source emissions NO_x when the total anthropogenic NO_x emissions are reduced by 50% is 4.8%. One would expect the domain wide one-hour average ozone concentration daily peak to increase when anthropogenic NO_x emissions were reduced because the amount of ozone titration reduces and consequently the efficiency of ozone production increases. However, it was not the case in this study and the results agreed with the study of Milford et al (1989) who found increases in ozone concentrations with NO_x emissions reductions for locations within the high emissions areas of the Los Angeles airshed but found that basin-wide NO_x controls were more effective at sites located farther downwind. Similar results were obtained in the rural areas far downwind of the NO_x sources areas (Chicago and Milwaukee) in the LMOS study. The study of the spatial coverage of the ambient VOC-to-NO_x ratio in the study domain would be beneficial in order to further investigate this finding. Unfortunately, there was no ambient VOCs data for the modeling domain at the time of the study.

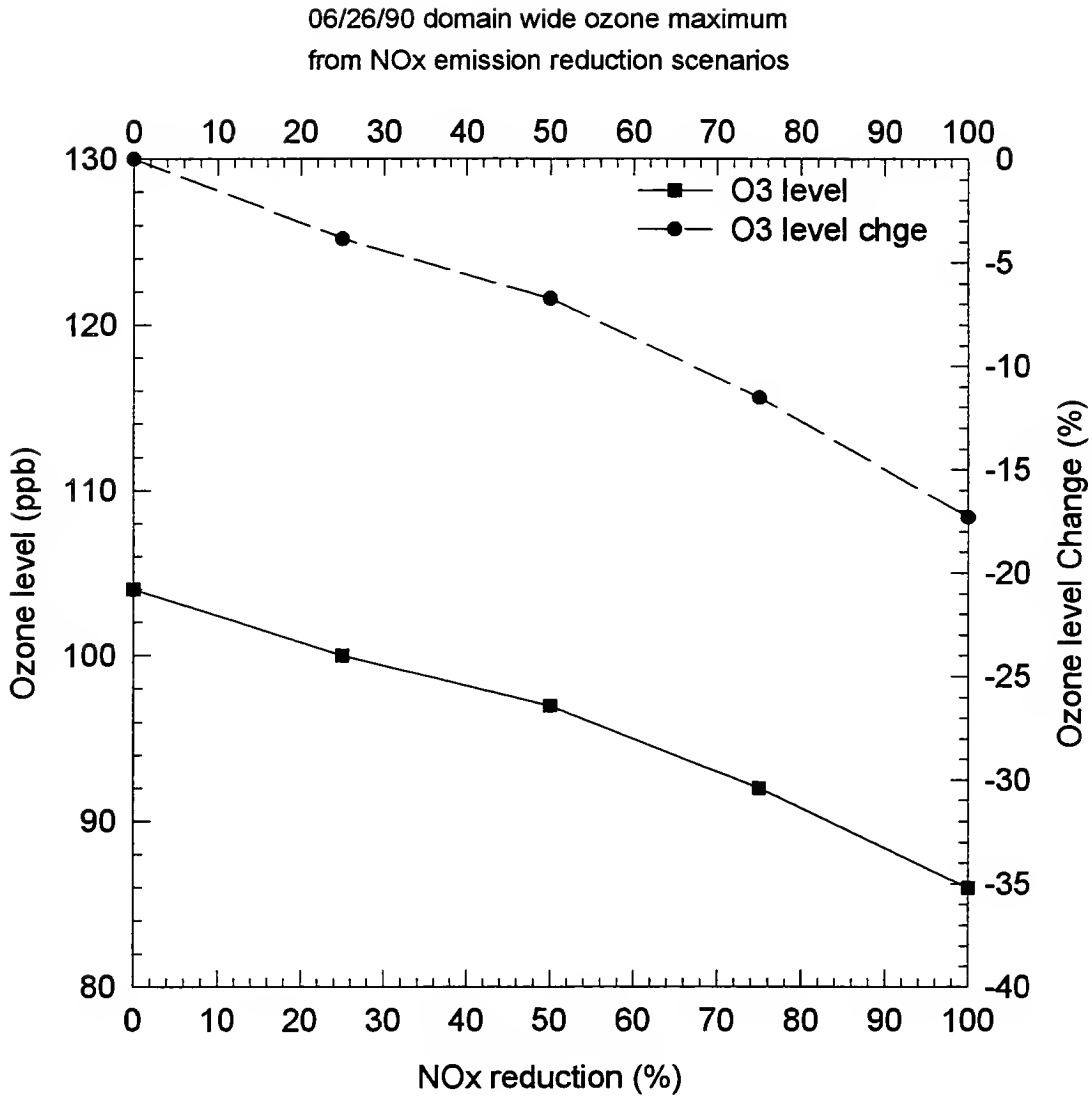

Figure 3.9.a. Changes in predicted domain-wide one-hour average ozone concentration daily peak (ppb) following NO_x emissions reduction scenarios on June 26, 1990.

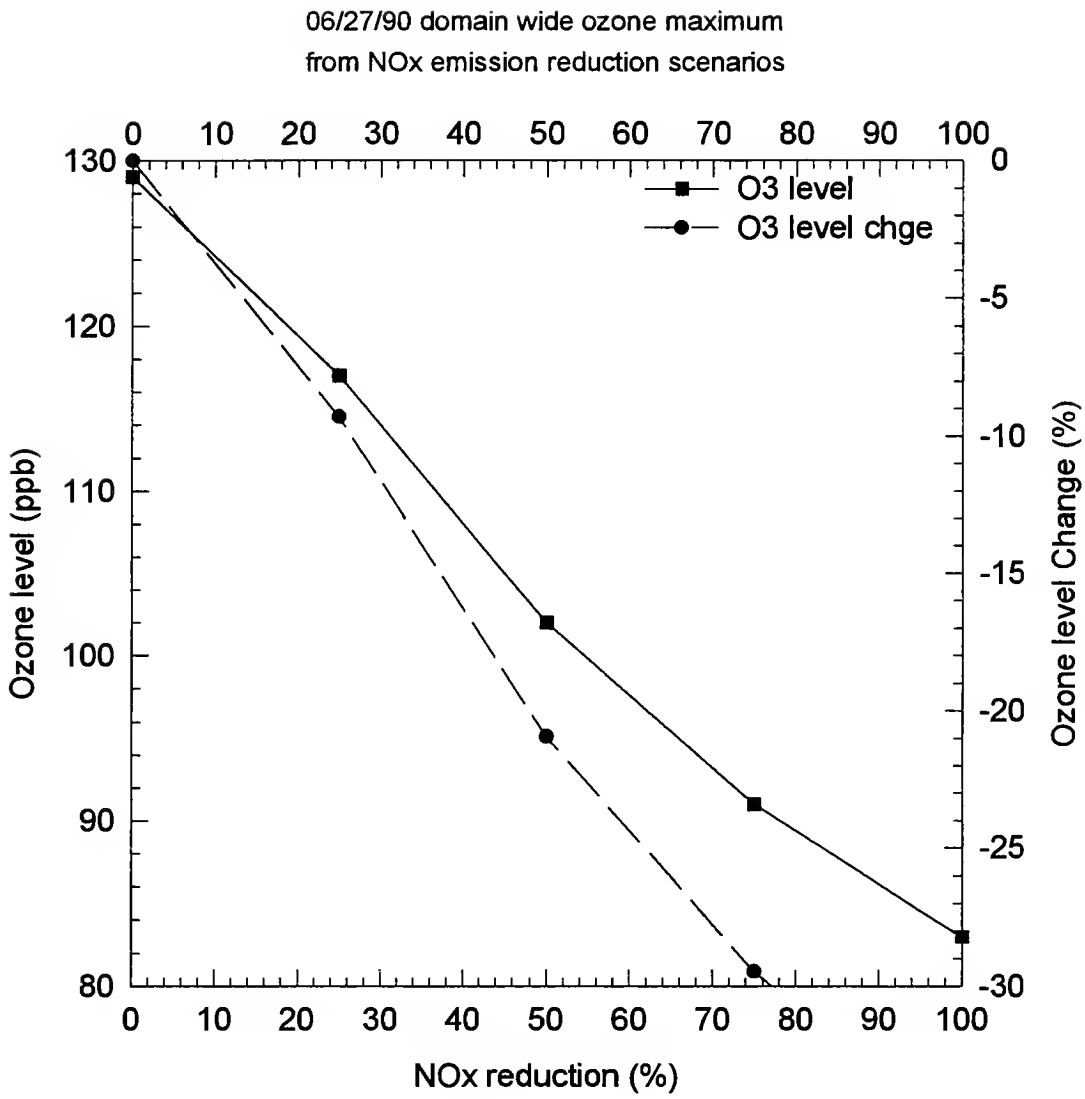

Figure 3.9.b. Changes in predicted domain-wide one-hour average ozone concentration daily peak (ppb) following NO_x emissions reduction scenarios on June 27, 1990.

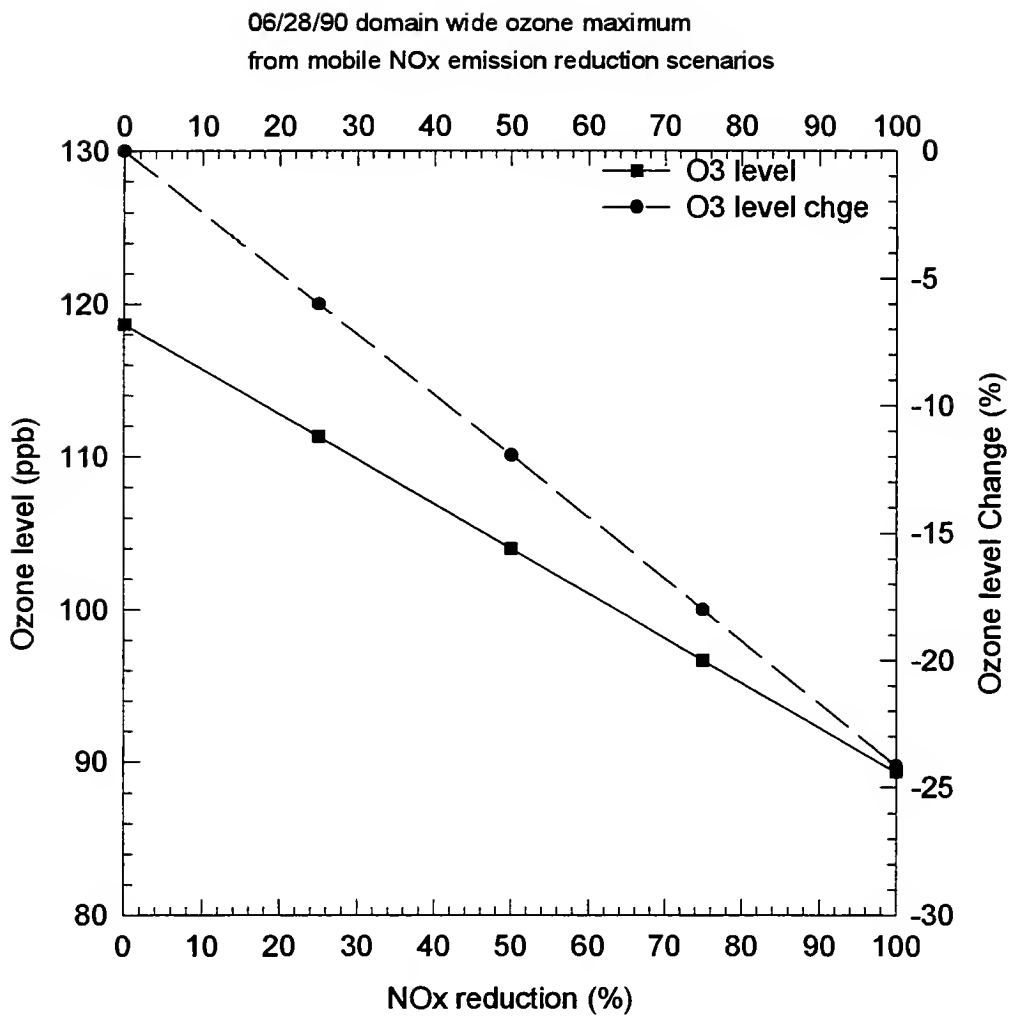

Figure 3.9.c. Changes in predicted domain-wide one-hour average ozone concentration daily peak (ppb) following NO_x emissions reduction scenarios on June 28, 1990.

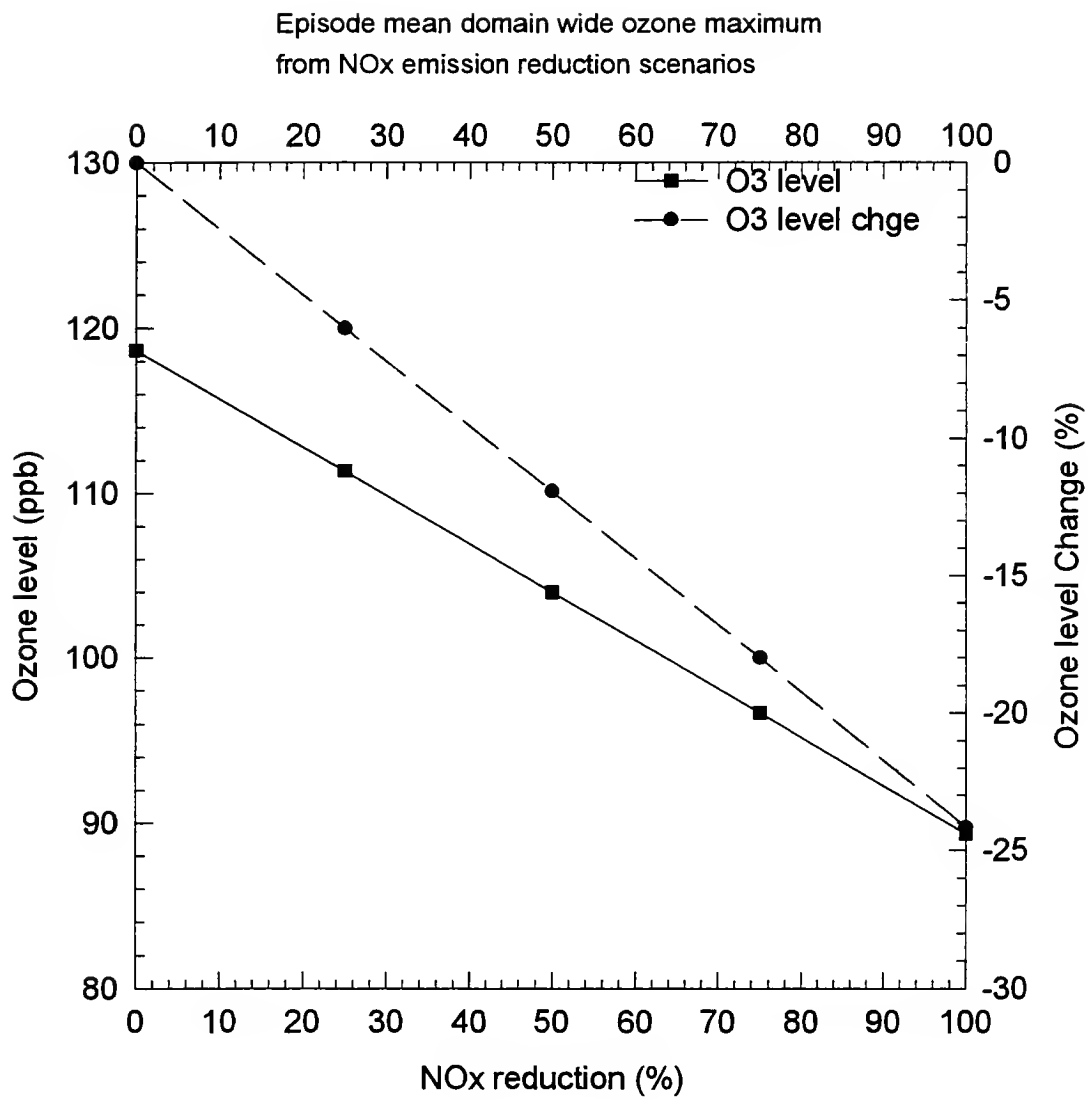

Figure 3.9.d. Episodic mean episodic changes in predicted domain-wide one-hour average ozone concentration daily peak (ppb) following NO_x emissions reduction scenarios.

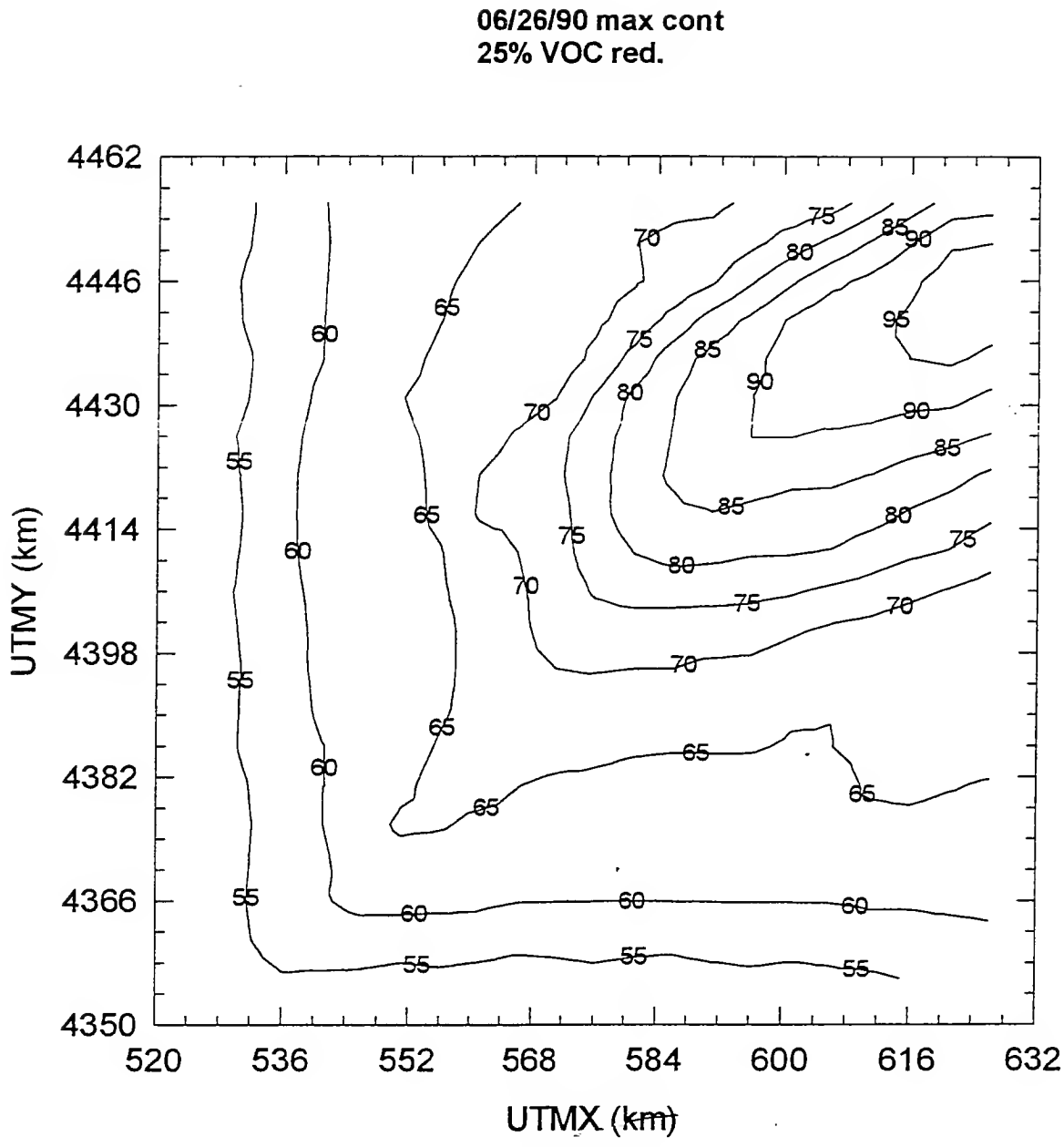

Figure 3.10.a. Predicted one-hour average ozone concentration daily peak (ppb) contour map for 25% VOCs emissions reduction on June 26, 1990.

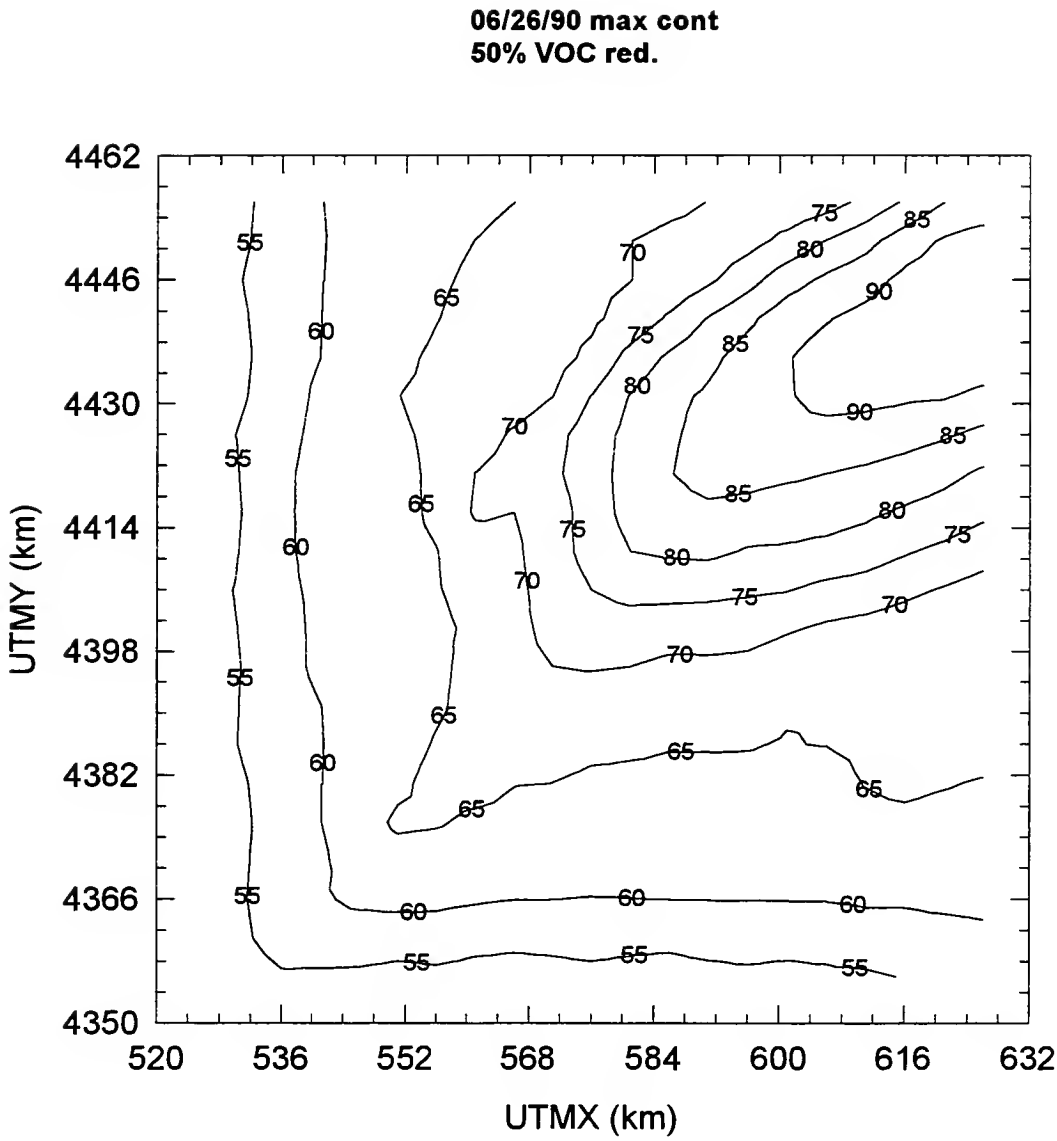

Figure 3.10.b. Predicted one-hour average ozone concentration daily peak (ppb) contour map for 50% VOCs emissions reduction on June 26, 1990.

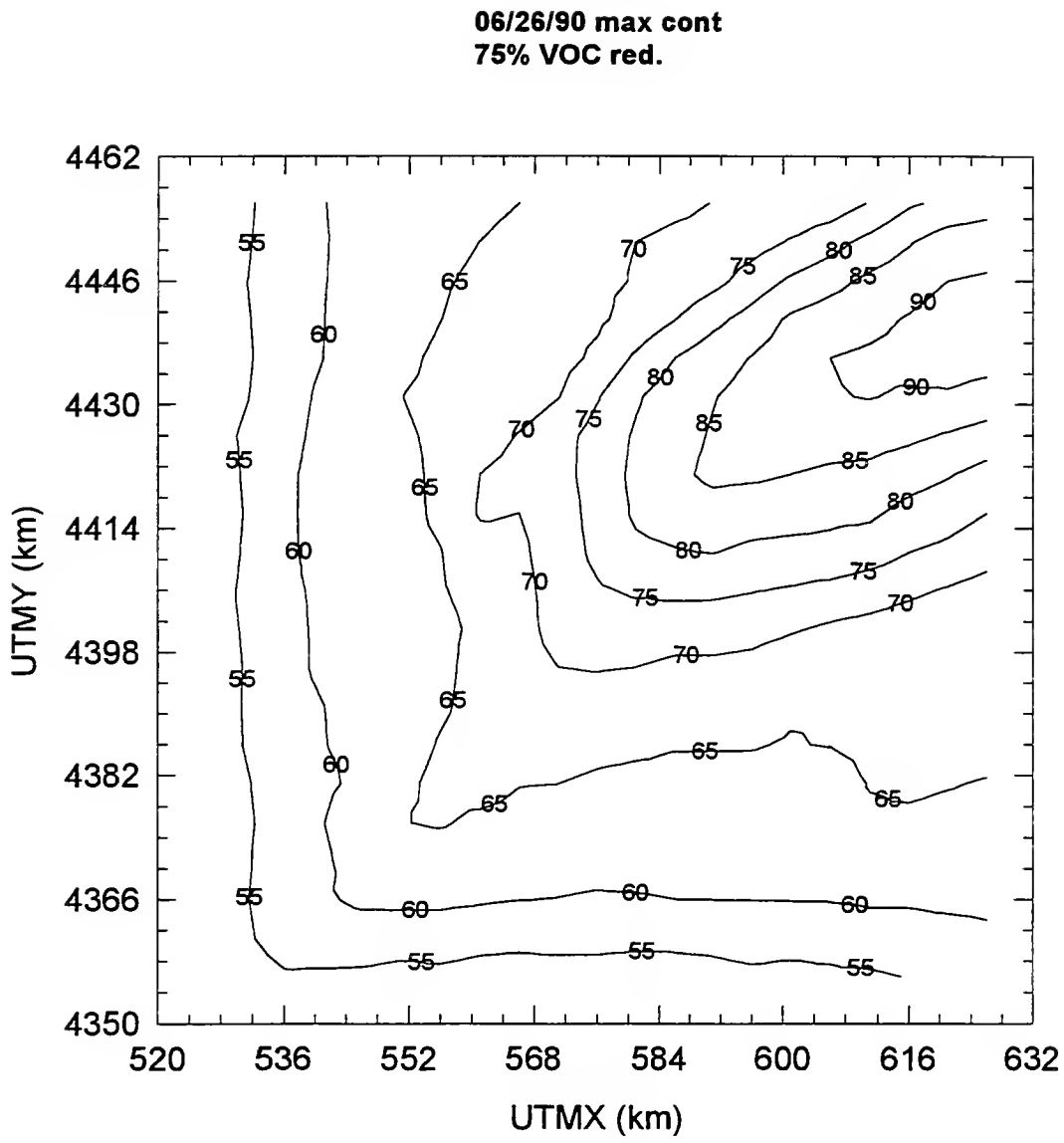

Figure 3.10.c. Predicted one-hour average ozone concentration daily peak (ppb) contour map for 75% VOCs emissions reduction on June 26, 1990.

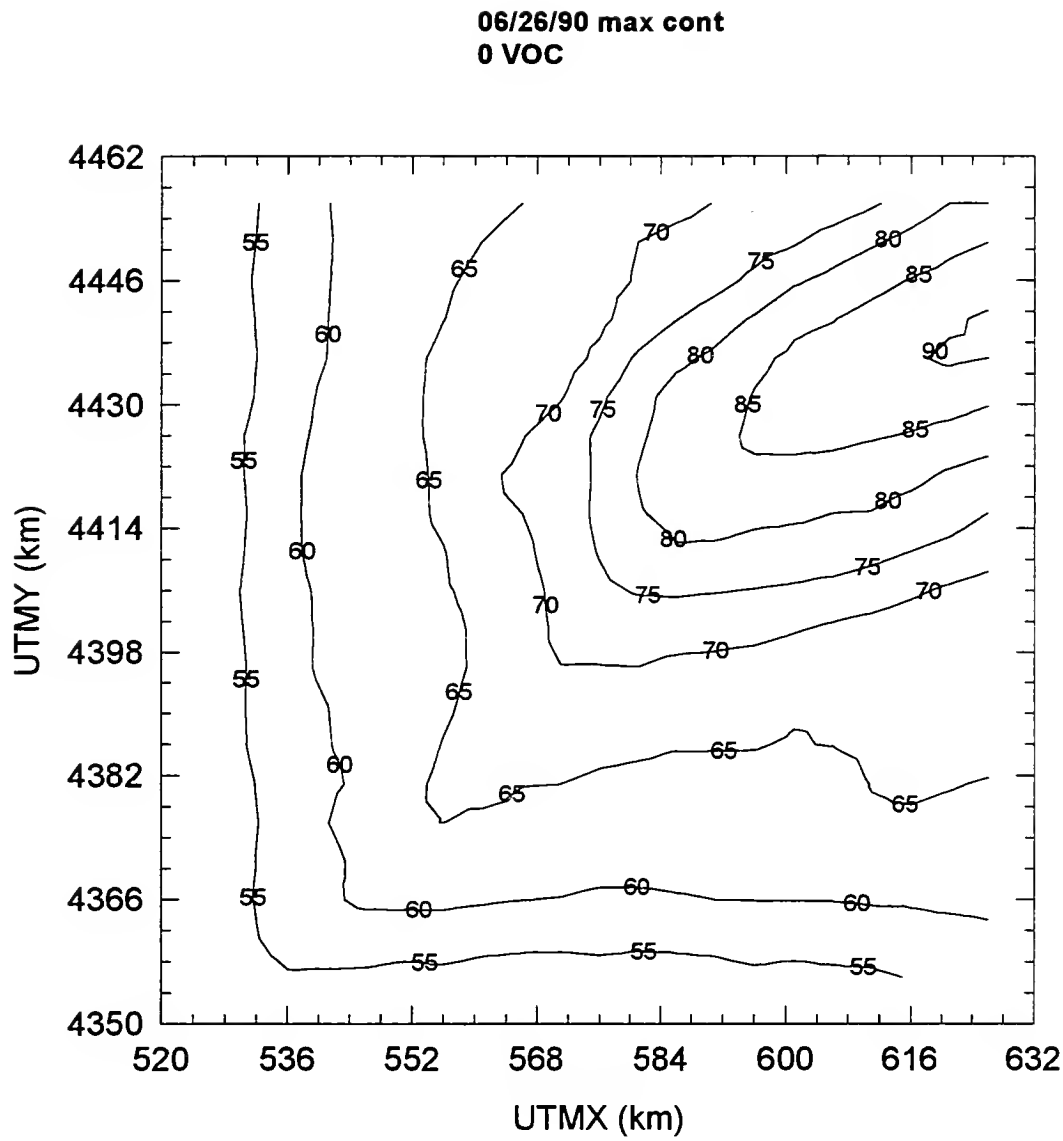

Figure 3.10.d. Predicted one-hour average ozone concentration daily peak (ppb) contour map for 100% VOCs emissions reduction on June 26, 1990.

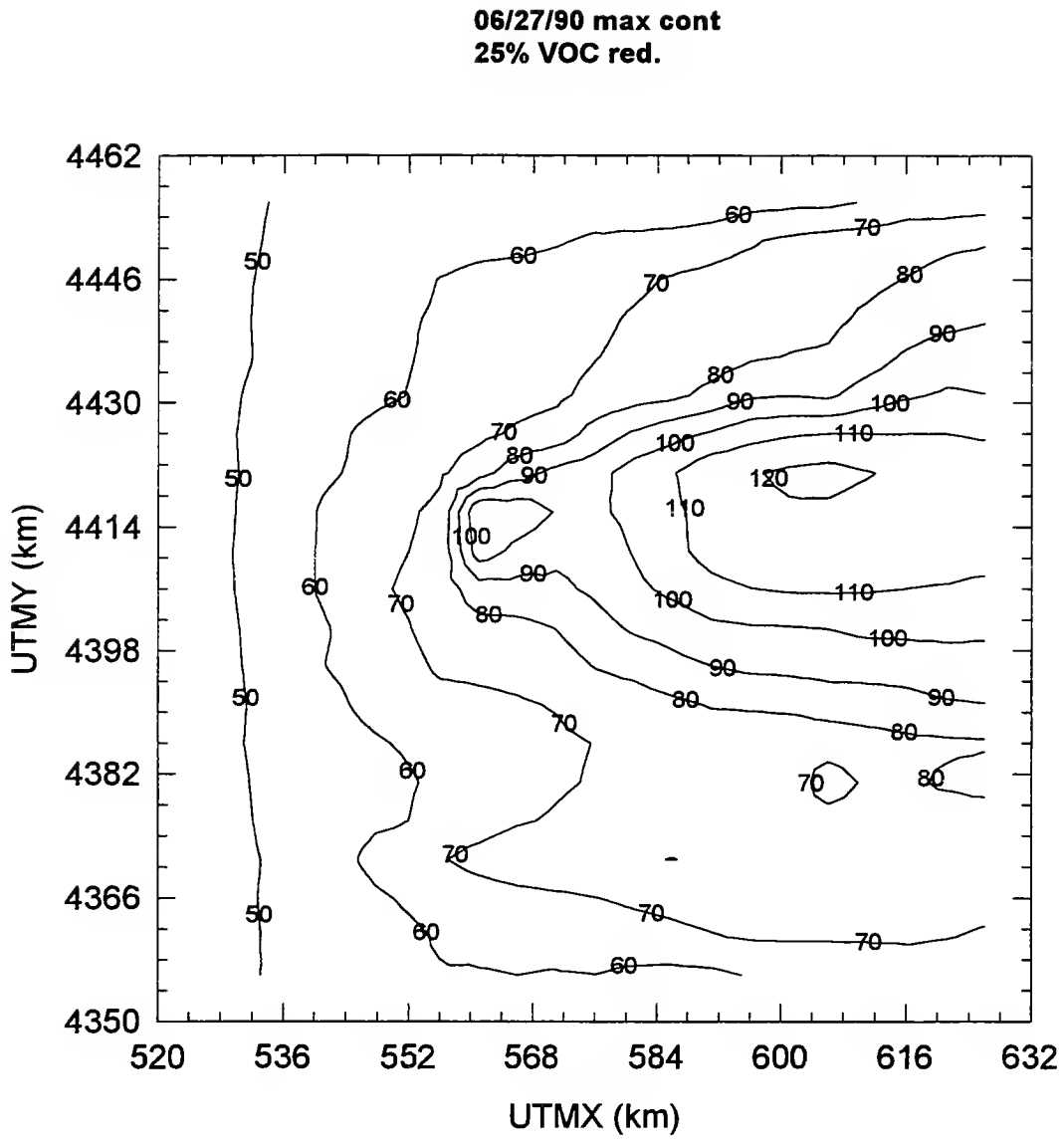

Figure 3.10.e. Predicted one-hour average ozone concentration daily peak (ppb) contour map for 25% VOCs emissions reduction on June 27, 1990.

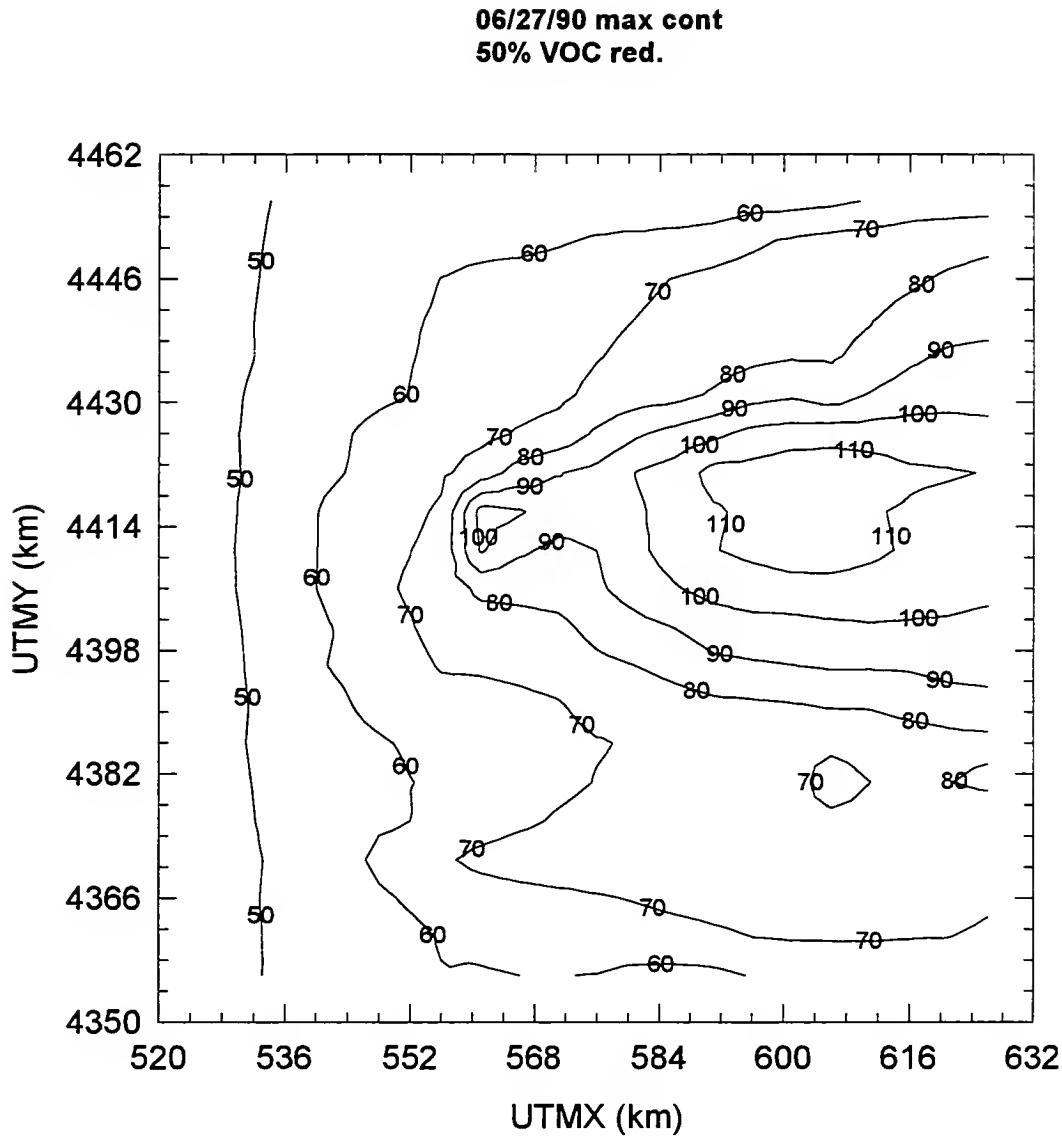

Figure 3.10.f. Predicted one-hour average ozone concentration daily peak (ppb) contour map for 50% VOCs emissions reduction on June 27, 1990.

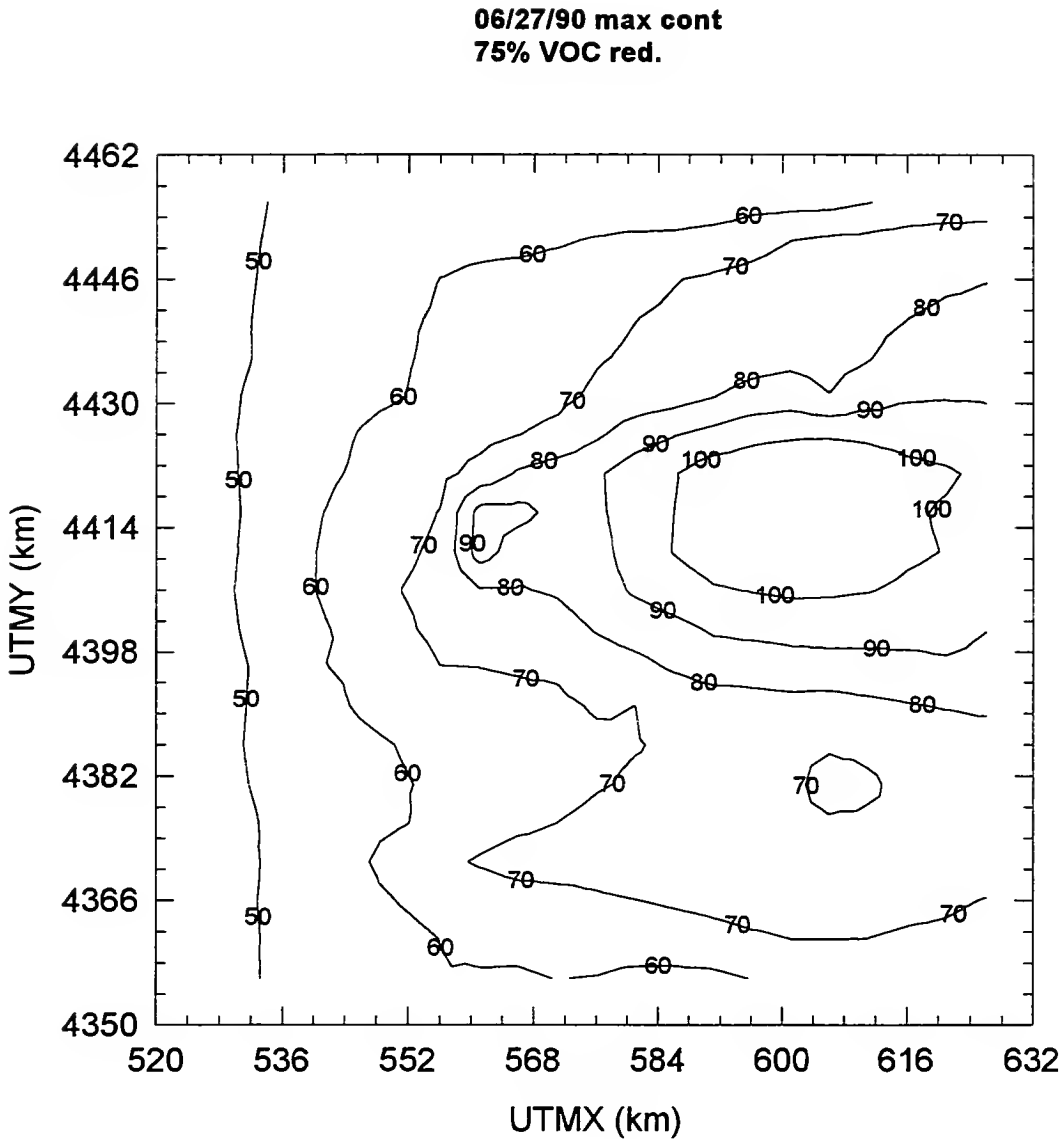

Figure 3.10.g. Predicted one-hour average ozone concentration daily peak (ppb) contour map for 75% VOCs emissions reduction on June 27, 1990.

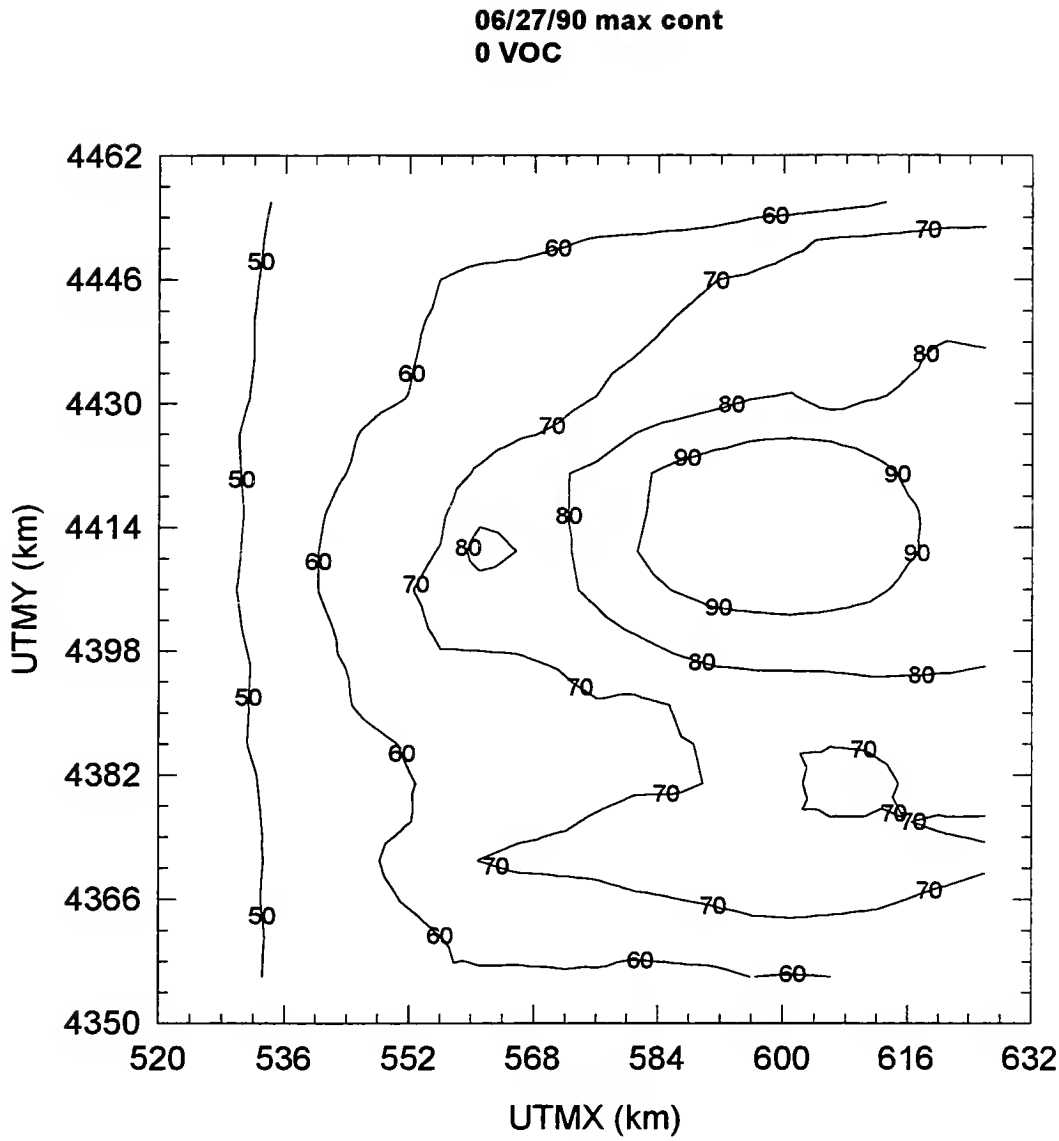

Figure 3.10.h. Predicted one-hour average ozone concentration daily peak (ppb) contour map for 100% VOCs emissions reduction on June 27, 1990.

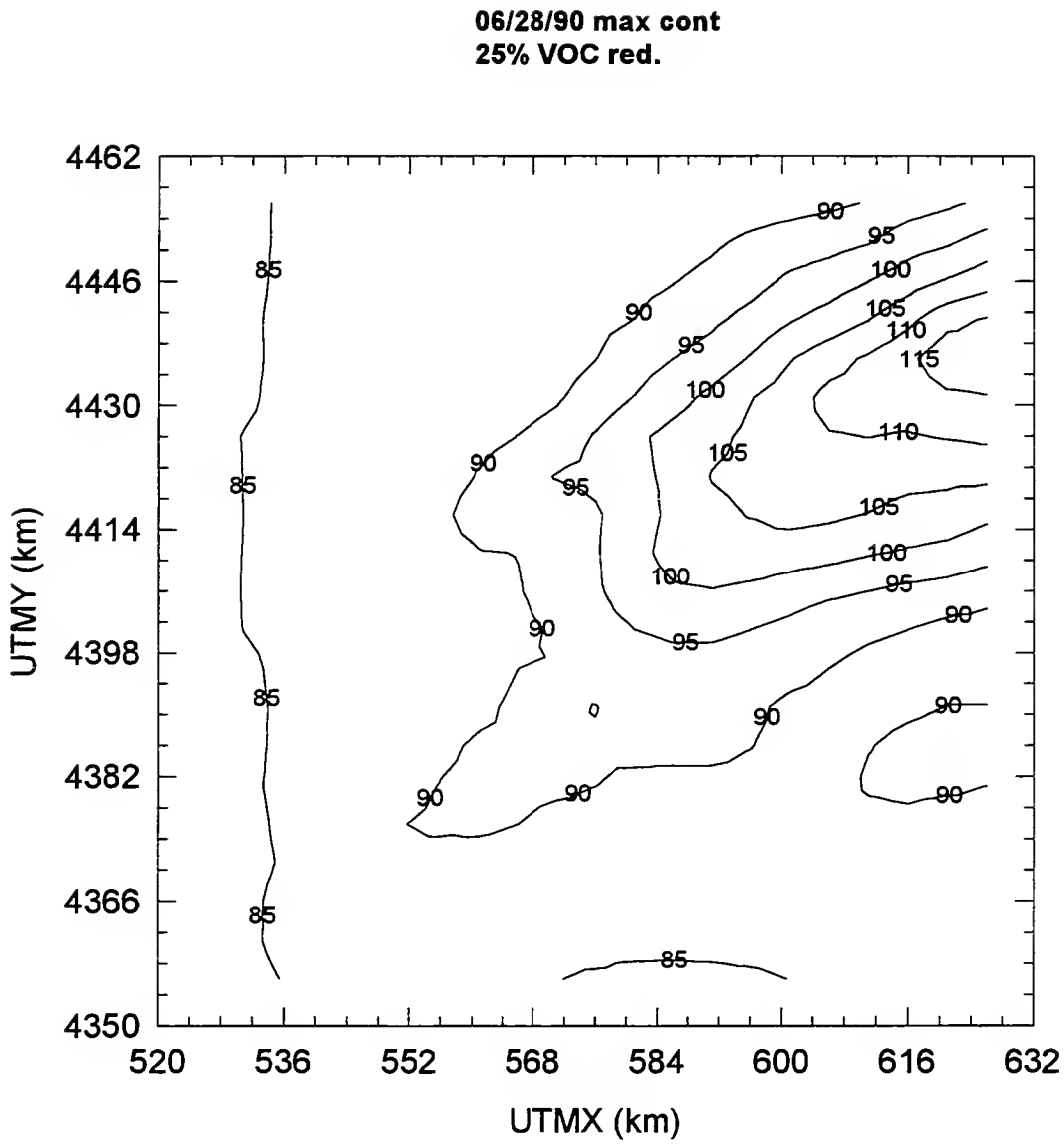

Figure 3.10.i. Predicted one-hour average ozone concentration daily peak (ppb) contour map for 25% VOCs emissions reduction on June 28, 1990.

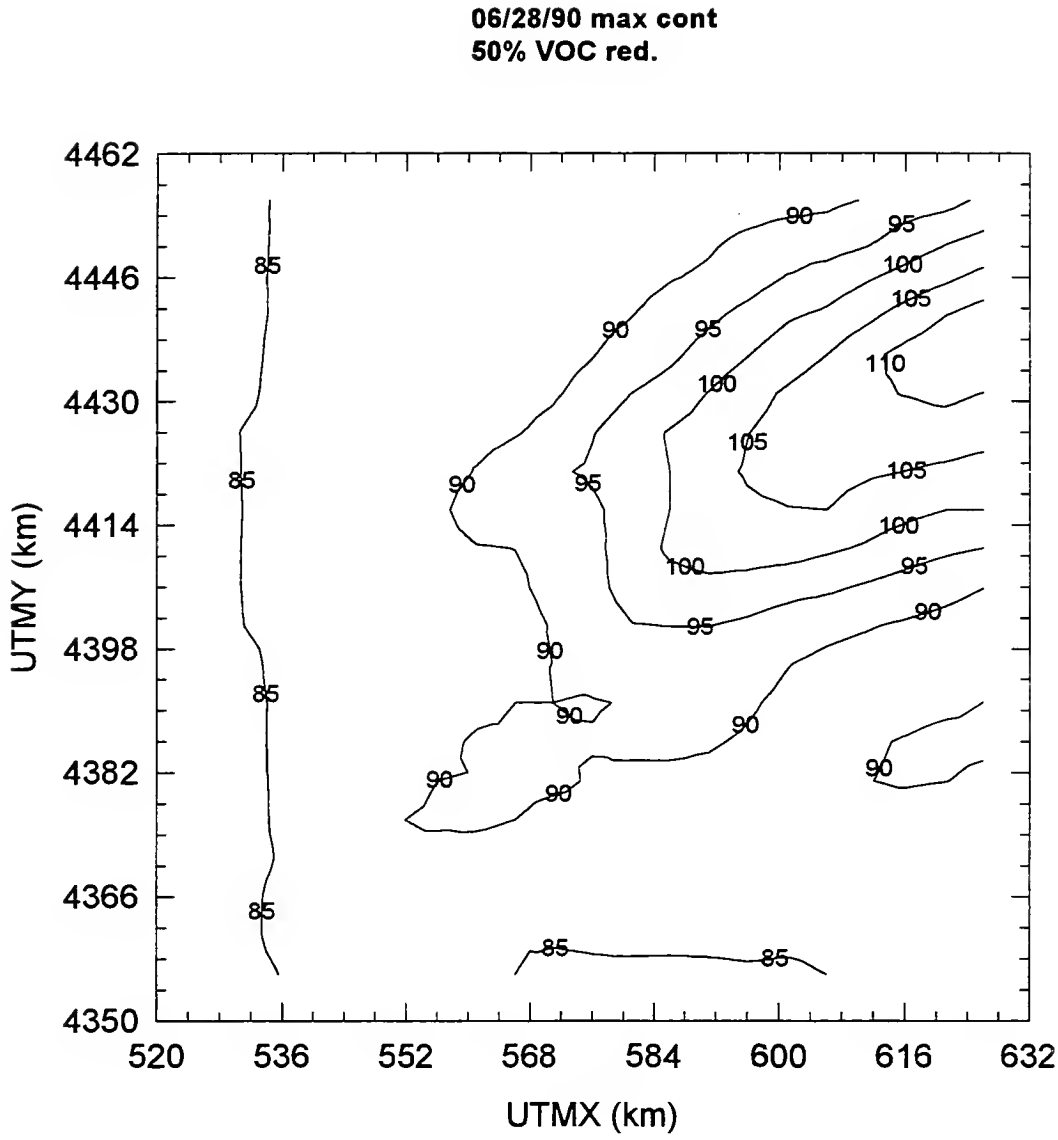

Figure 3.10.j. Predicted one-hour average ozone concentration daily peak (ppb) contour map for 50% VOCs emissions reduction on June 28, 1990.

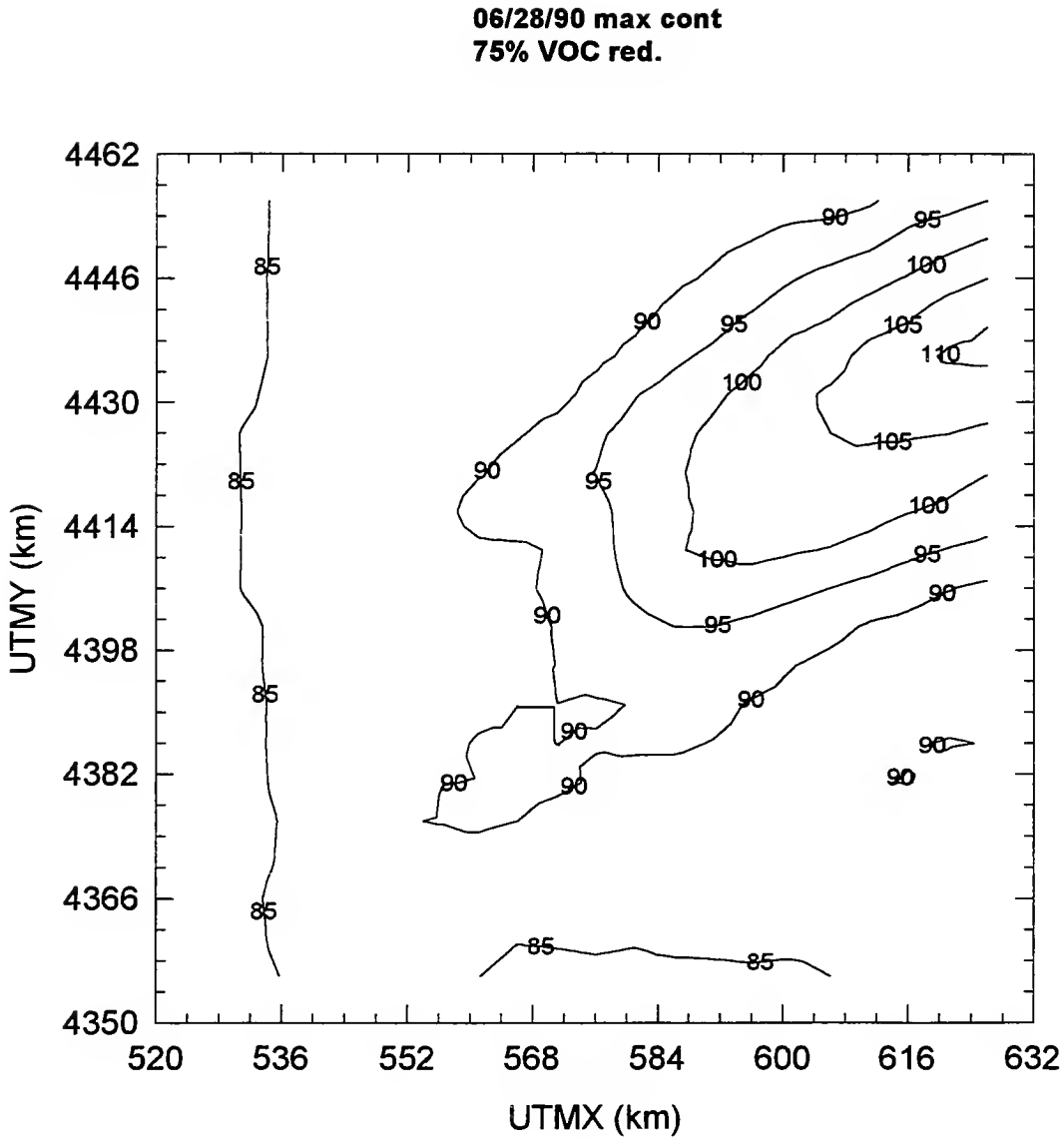

Figure 3.10.k. Predicted one-hour average ozone concentration daily peak (ppb) contour map for 75% VOCs emissions reduction on June 28, 1990.

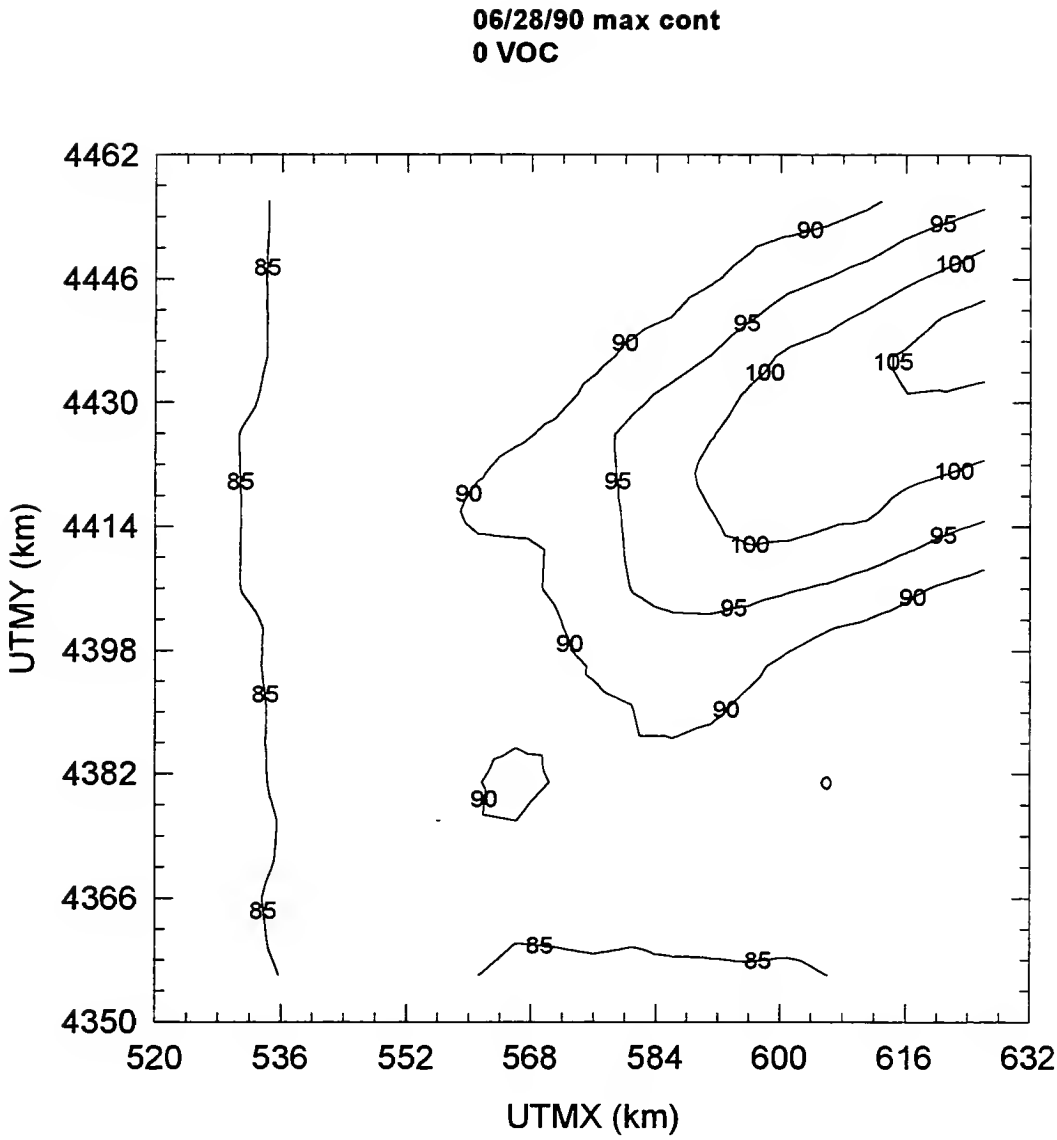

Figure 3.10.1. Predicted one-hour average ozone concentration daily peak (ppb) contour map for 100% VOCs emissions reduction on June 28, 1990.

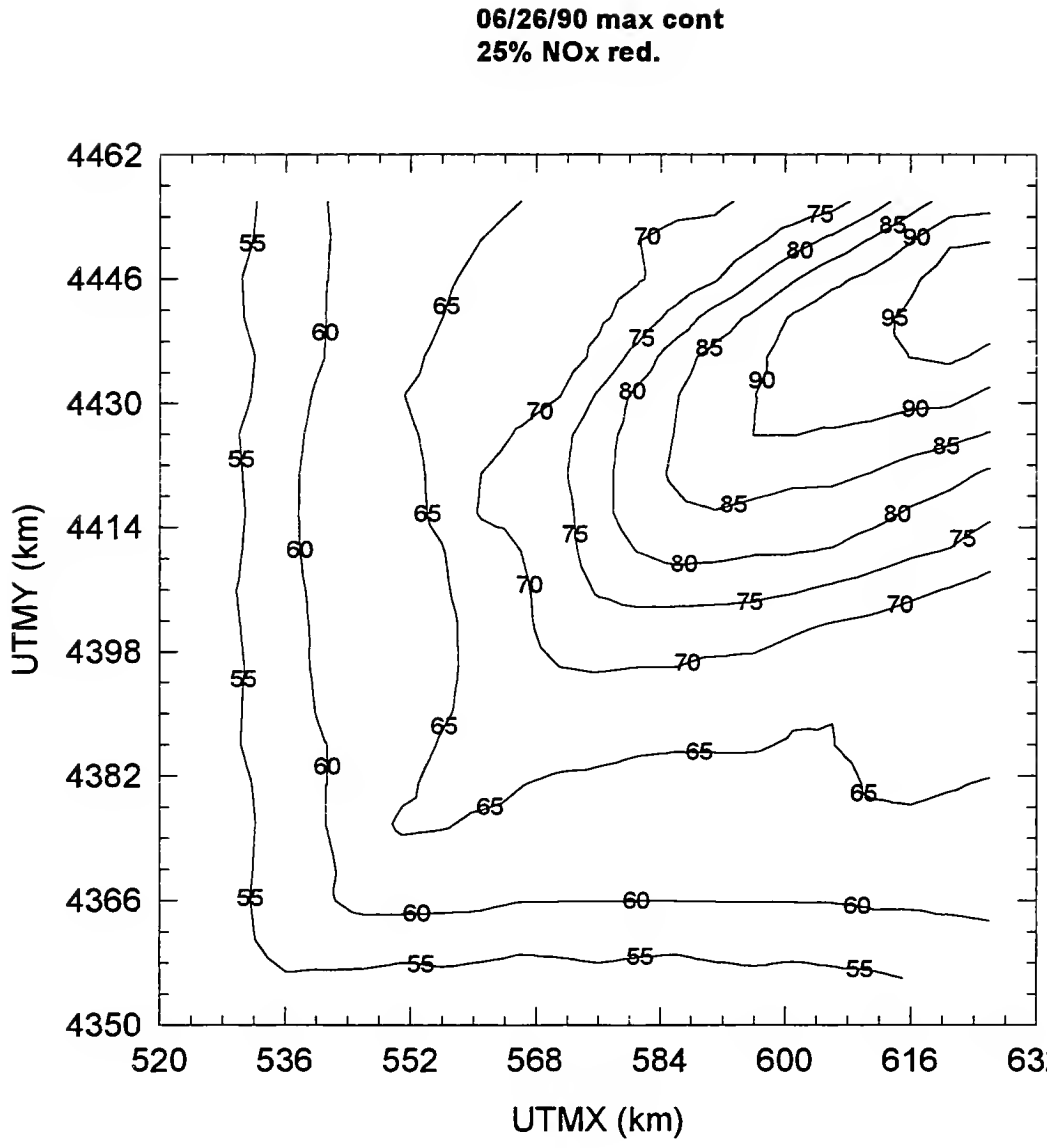

Figure 3.11.a. Predicted one-hour average ozone concentration daily peak (ppb) contour map for 25% NO_x emissions reduction on June 26, 1990.

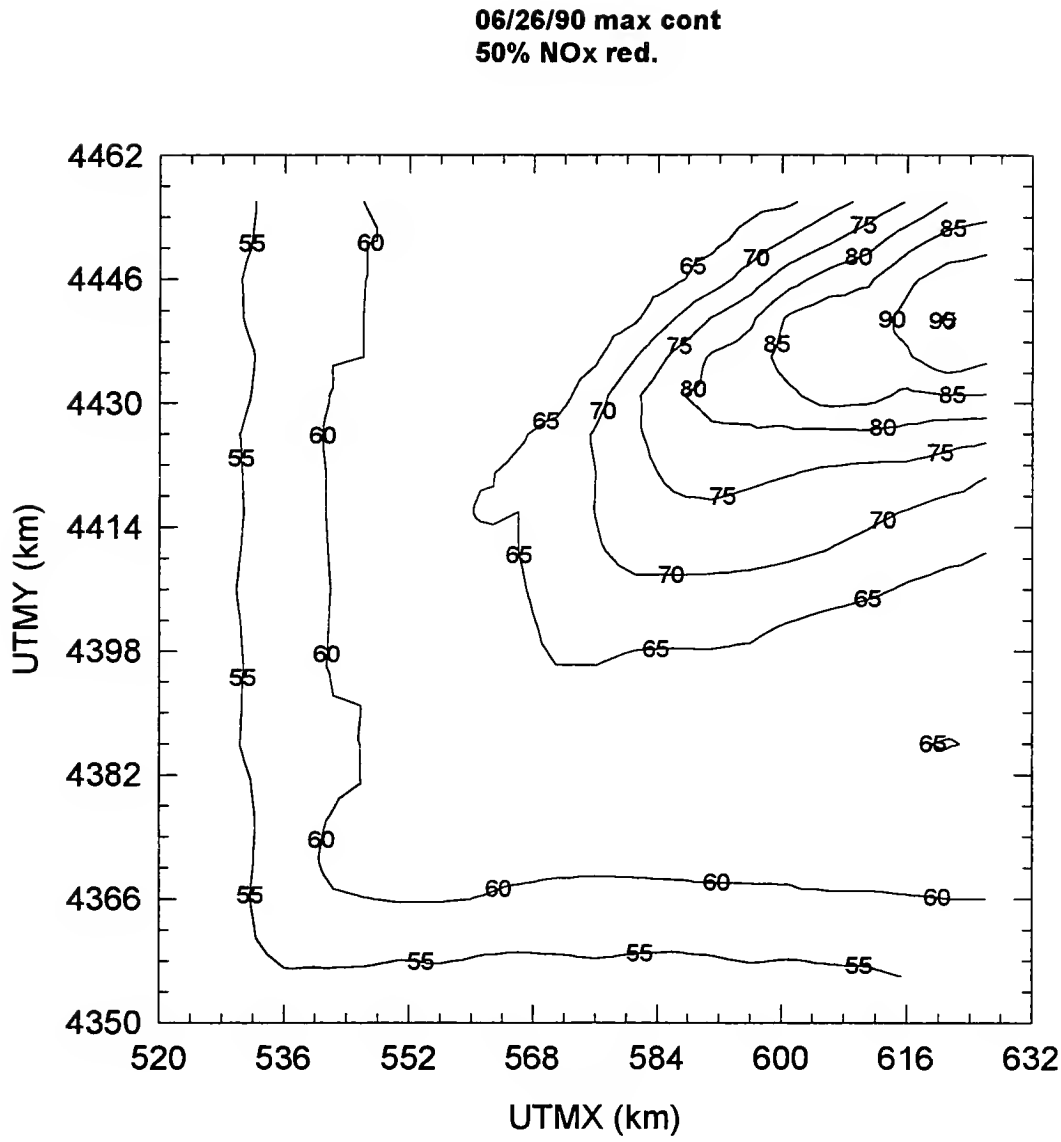

Figure 3.11.b. Predicted one-hour average ozone concentration daily peak (ppb) contour map for 50% NO_x emissions reduction on June 26, 1990.

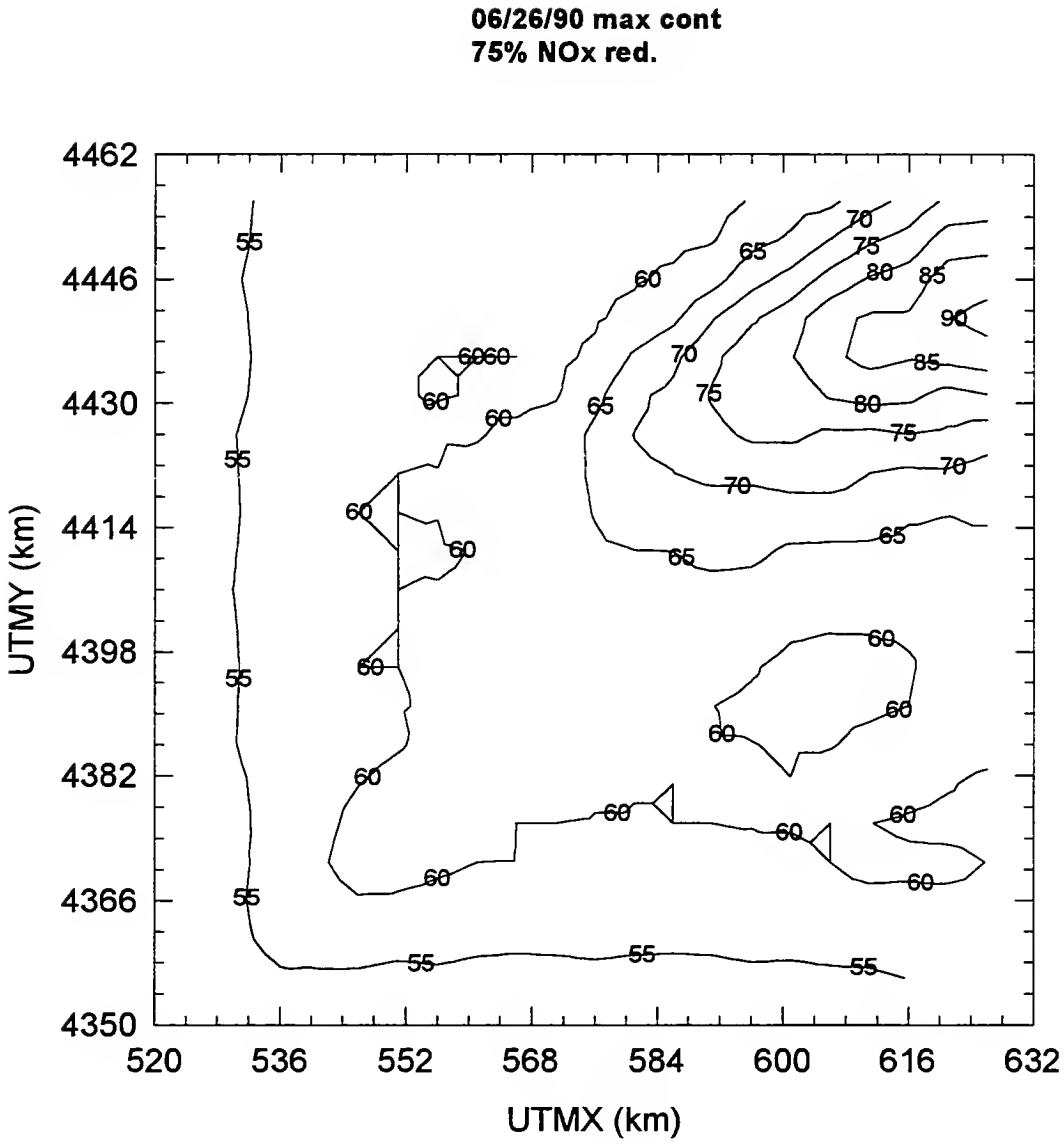

Figure 3.11.c. Predicted one-hour average ozone concentration daily peak (ppb) contour map for 75% NO_x emissions reduction on June 26, 1990.

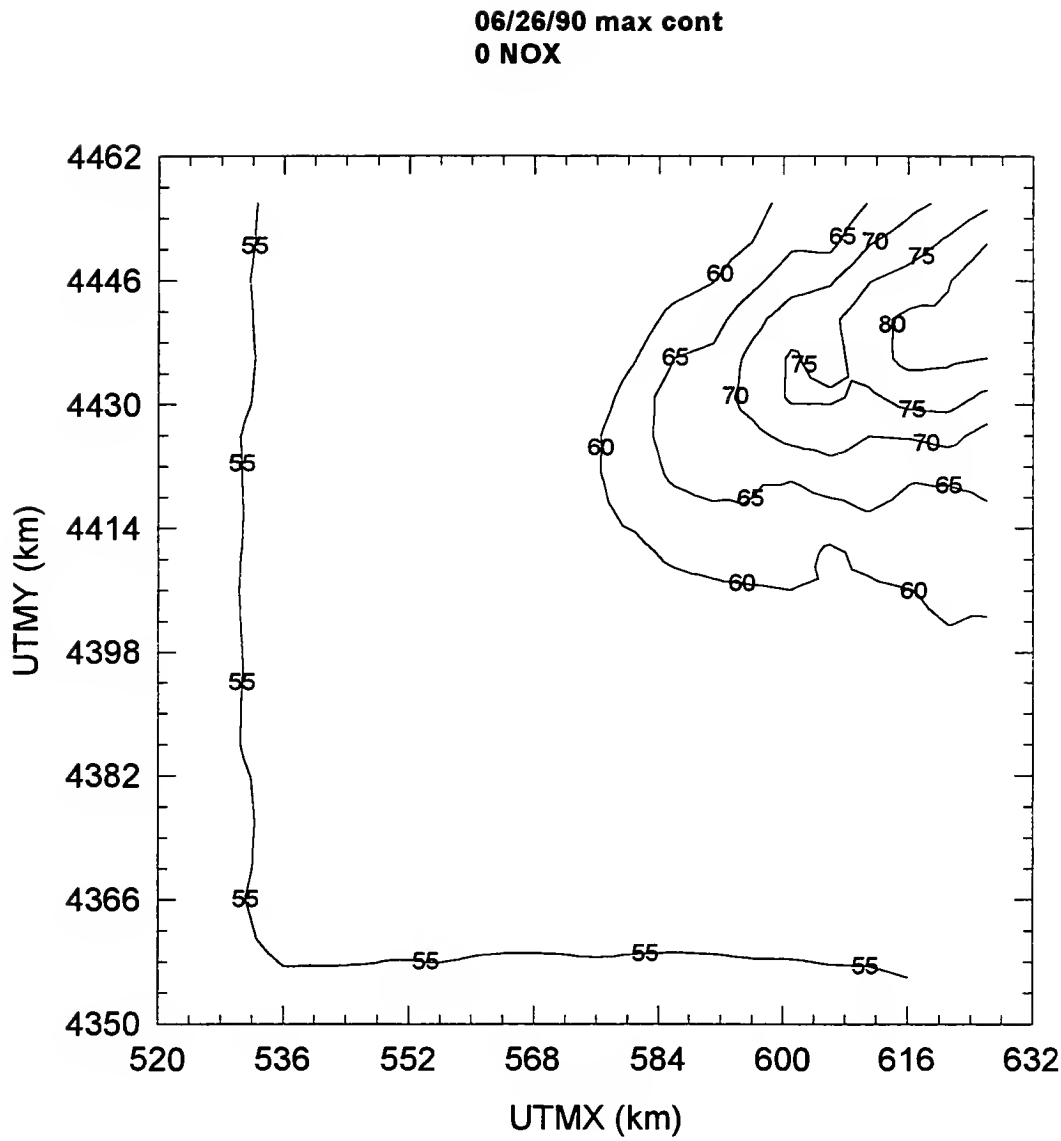

Figure 3.11.d. Predicted one-hour average ozone concentration daily peak (ppb) contour map for 100% NO_x emissions reduction on June 26, 1990.

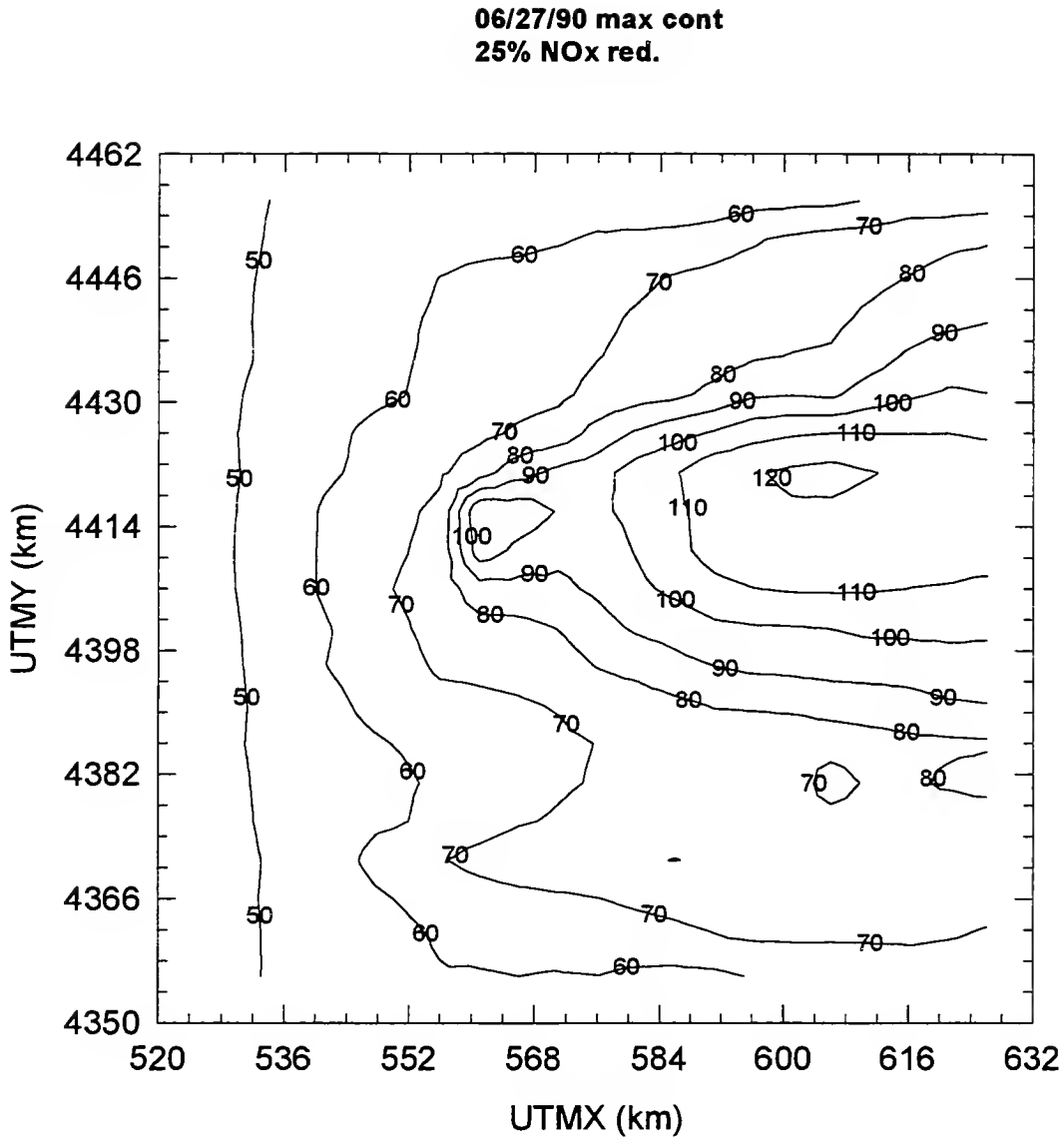

Figure 3.11.e. Predicted one-hour average ozone concentration daily peak (ppb) contour map for 25% NO_x emissions reduction on June 27, 1990.

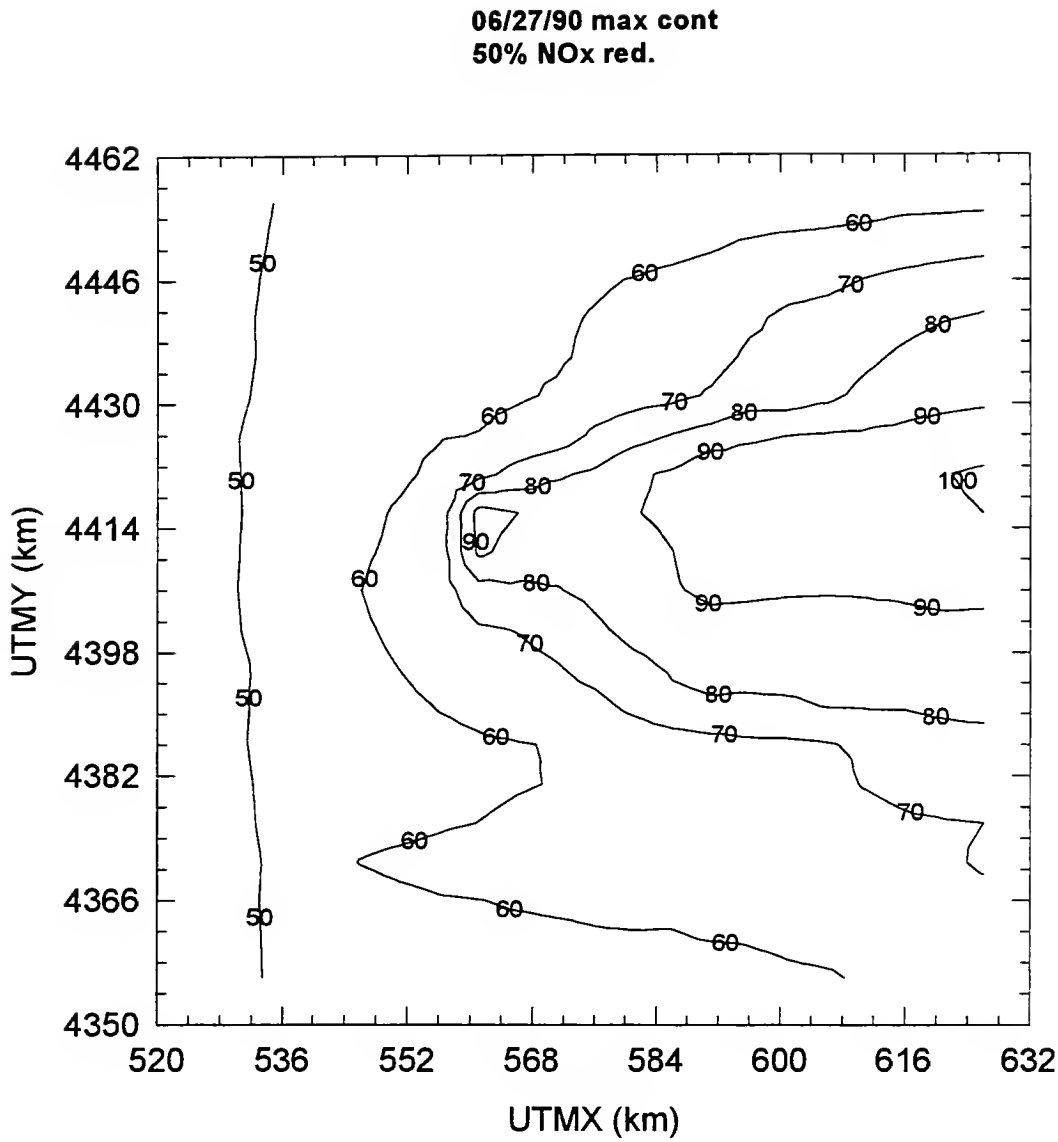

Figure 3.11.f. Predicted one-hour average ozone concentration daily peak (ppb) contour map for 50% NO_x emissions reduction on June 27, 1990.

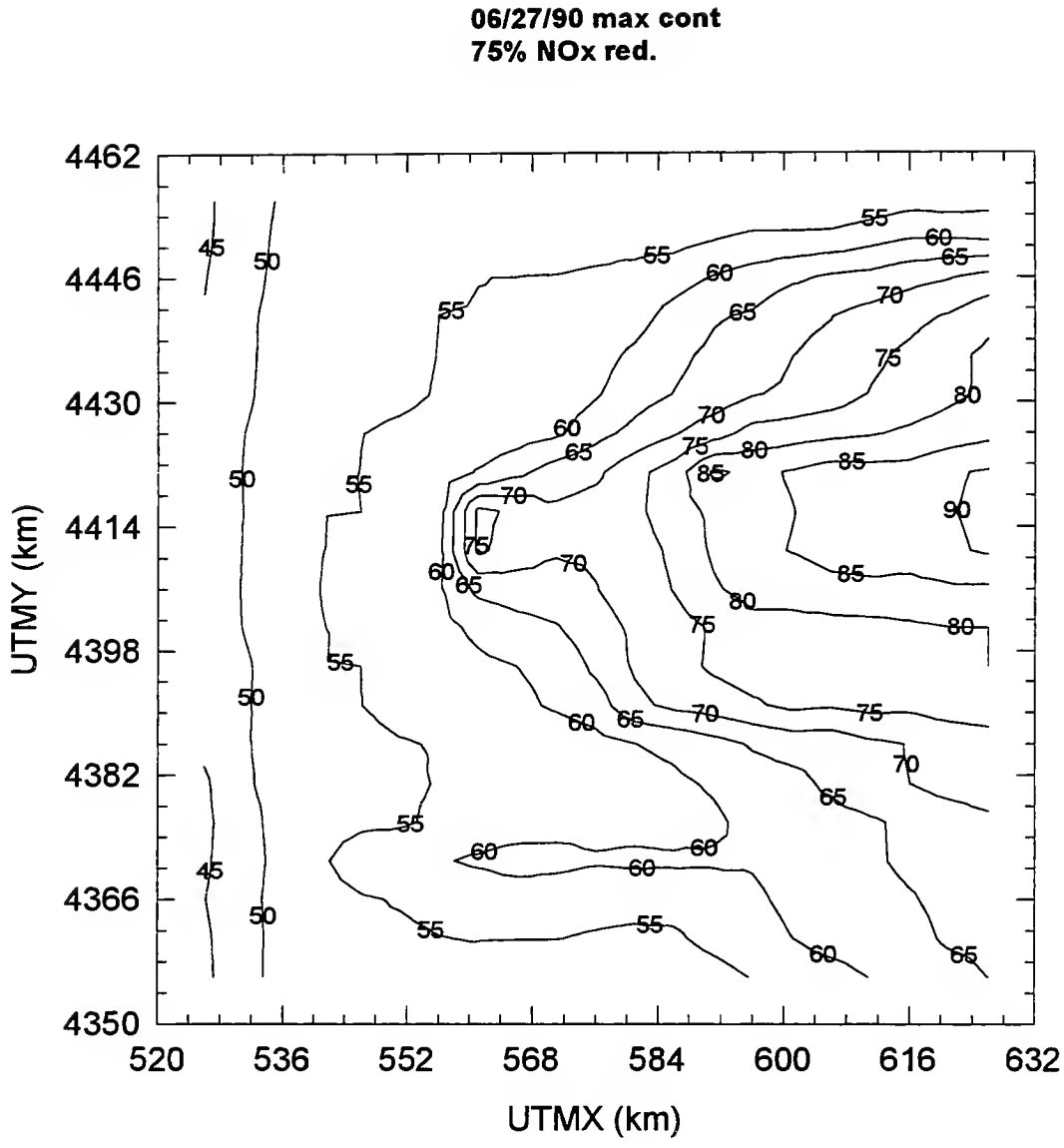

Figure 3.11.g. Predicted one-hour average ozone concentration daily peak (ppb) contour map for 75% NO_x emissions reduction on June 27, 1990.

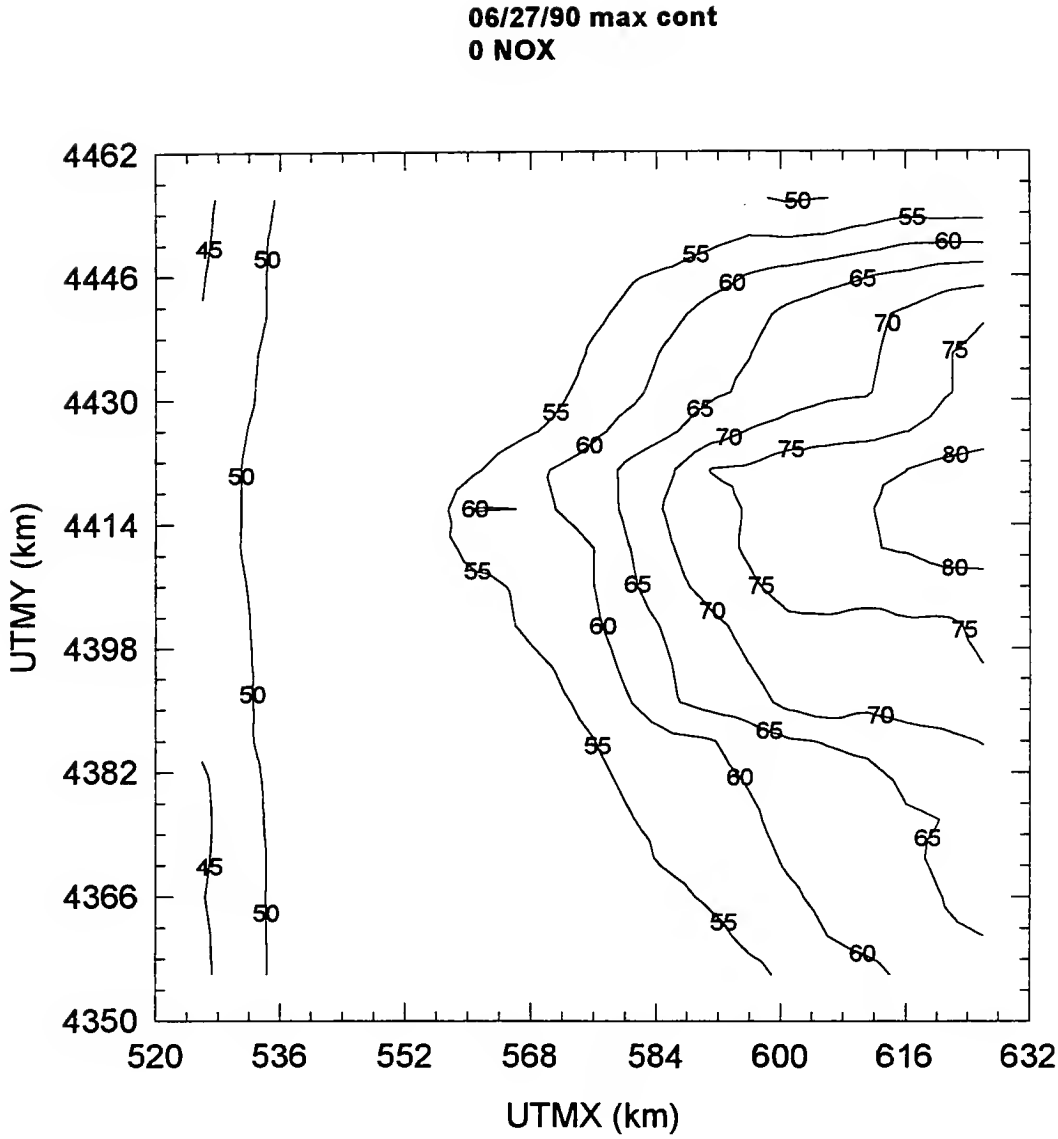

Figure 3.11.h. Predicted one-hour average ozone concentration daily peak (ppb) contour map for 100% NO_x emissions reduction on June 27, 1990.

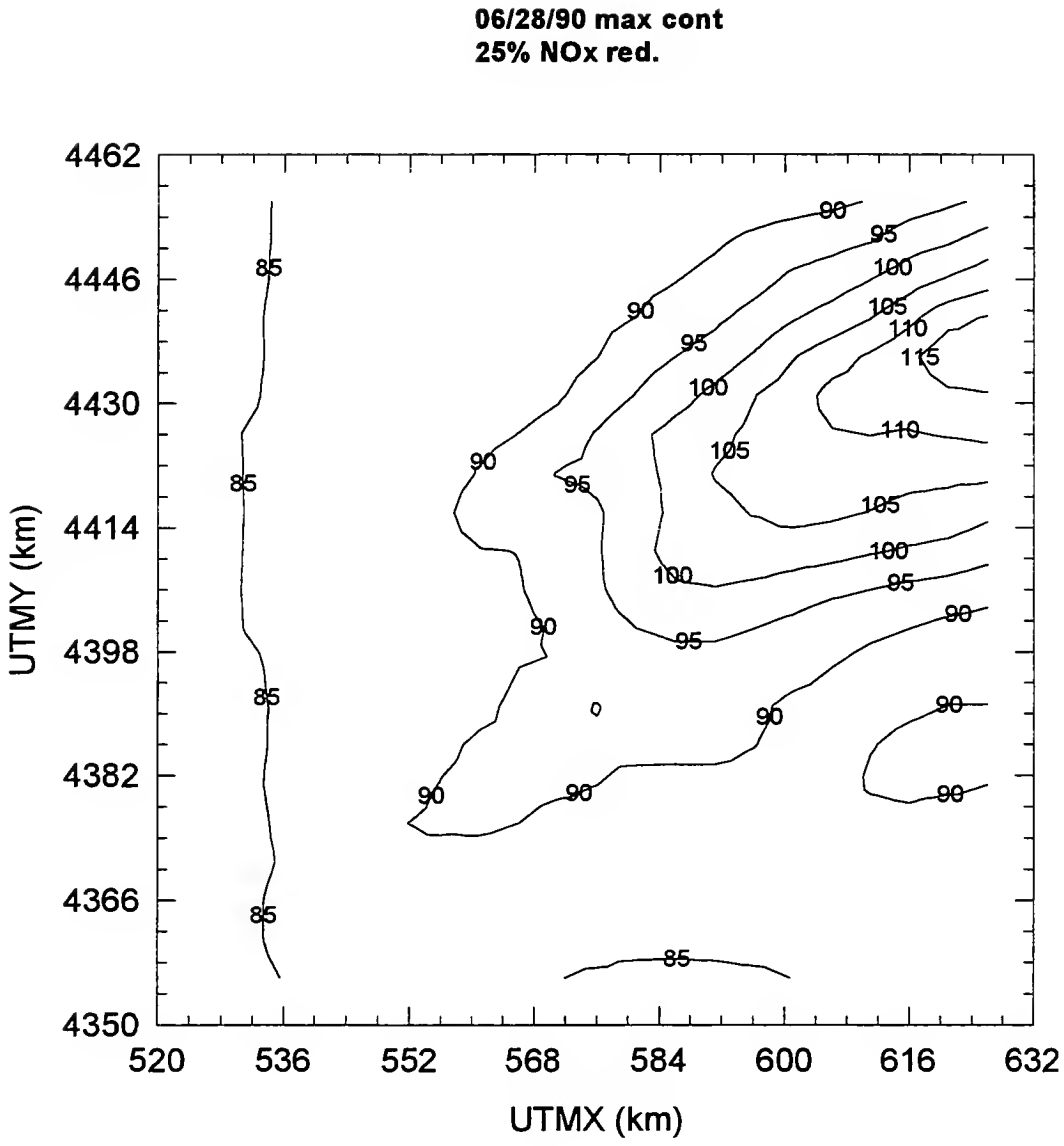

Figure 3.11.i. Predicted one-hour average ozone concentration daily peak (ppb) contour map for 25% NO_x emissions reduction on June 28, 1990.

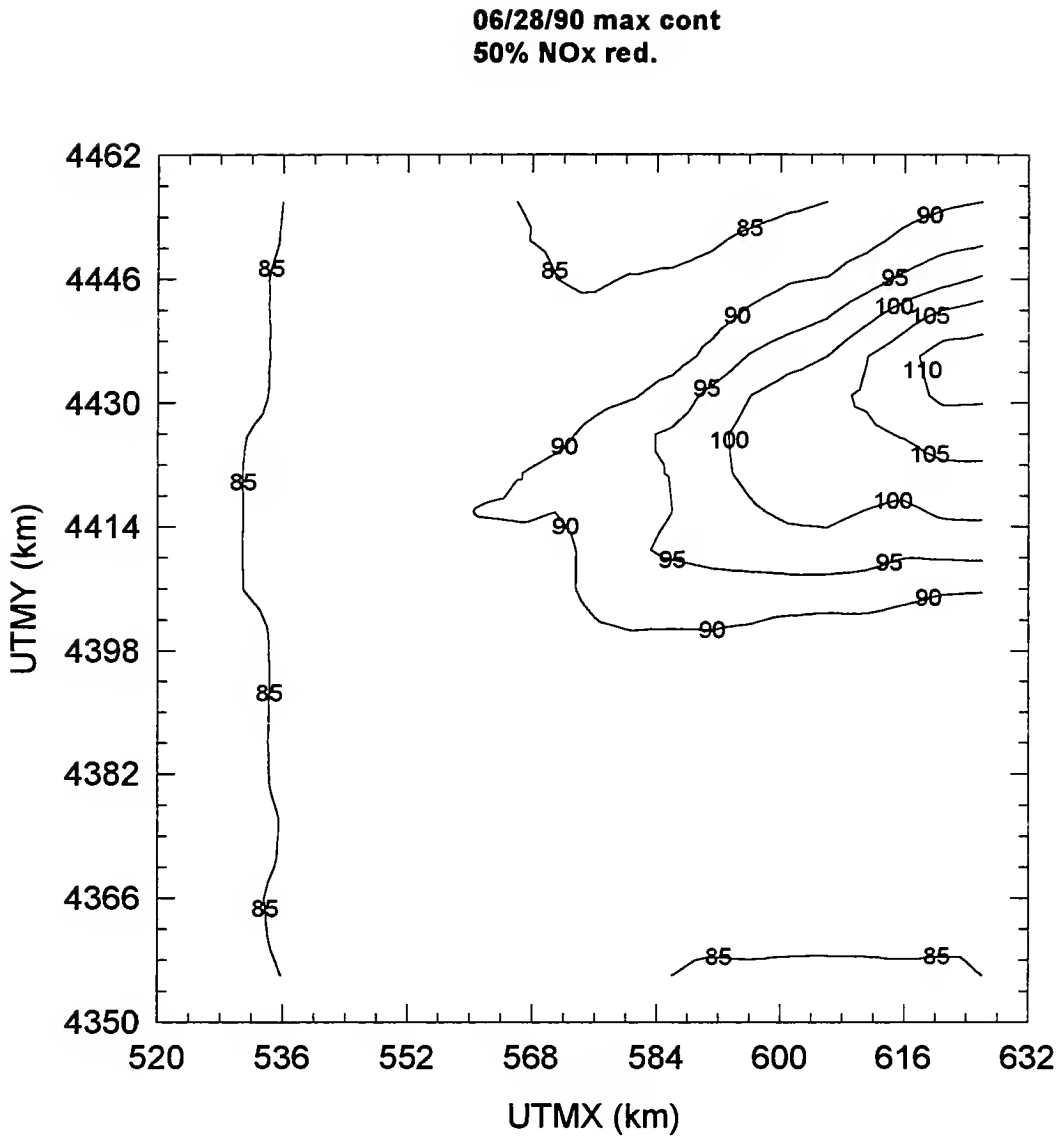

Figure 3.11.j. Predicted one-hour average ozone concentration daily peak (ppb) contour map for 50% NO_x emissions reduction on June 28, 1990

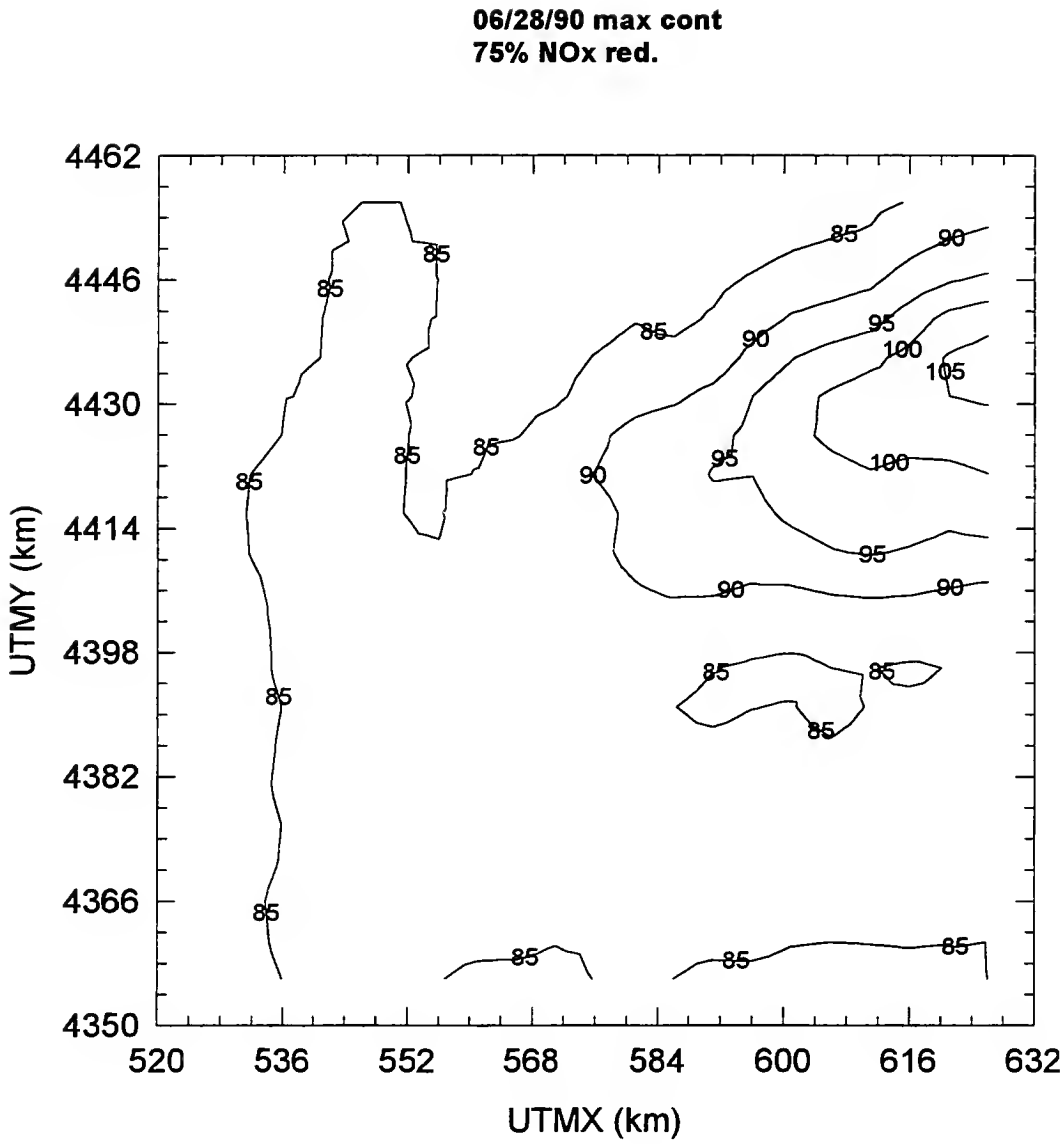

Figure 3.11.k. Predicted one-hour average ozone concentration daily peak (ppb) contour map for 75% NO_x emissions reduction on June 28, 1990.

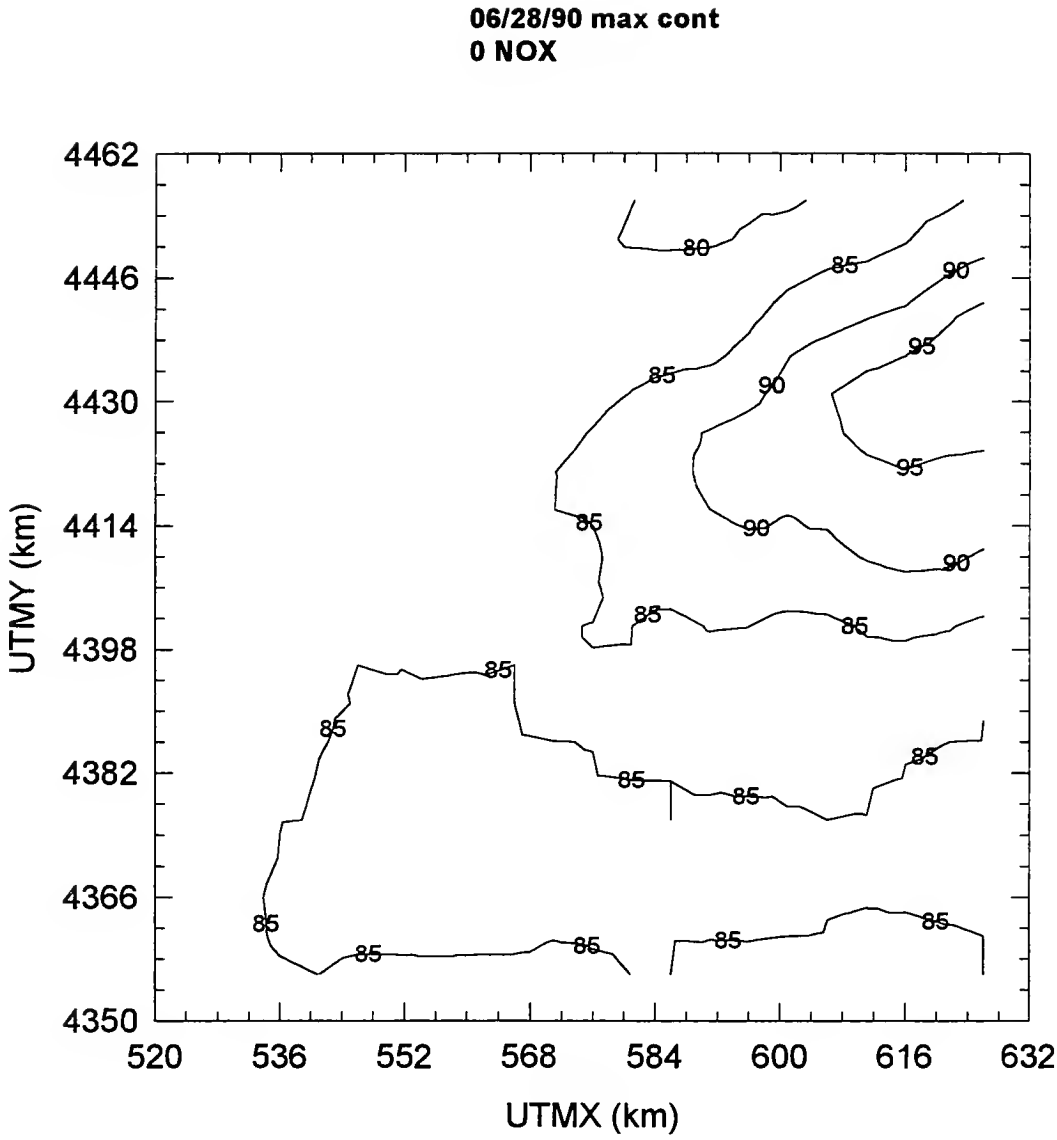

Figure 3.11.1. Predicted one-hour average ozone concentration daily peak (ppb) contour map for 100% NO_x emissions reduction on June 28, 1990.

4. Summary and Conclusion

In this research study, the UAM-IV was operated in order to simulate one-hour average ground-level ozone concentrations and to study the relative effects of mobile source emissions on the generation of ground-level ozone in the Indianapolis MSA. Available and calculated emission inventories and routine measurements of one-hour average ozone concentrations and meteorological parameters were used to define the modeling domain and episodes, develop the required input files of the UAM-IV, evaluate the performance of the UAM-IV, and analyze the emission reduction scenarios. The modeling domain was 112 km long and 112 km wide, divided into a grid cell array of 4 km by 4 km, and centered on the city of Indianapolis. The modeling episode was June 25-28, 1990.

Statistical studies and visual inspections of the modeling results showed that the model performed very well with the base case inputs. The emission control sensitivity analyses showed that the elevated point source (effective stack height > 25 m) emissions originated within the modeling domain had a minimal effect on the generation of ground-level ozone concentration. However, ground-level ozone concentration was found to be very sensitive to the low-level emissions as expected. These emissions are largely emitted by mobile sources. Furthermore, the domain-wide one-hour average ground-level ozone concentration daily peaks were shown to decrease linearly when both anthropogenic VOCs and NO_x emissions were reduced. The same trend was observed when the contributions of mobile source emissions of VOCs and NO_x only were assessed. The decreases in the domain-wide one-hour average ground-level ozone concentration daily peaks were more sensitive to NO_x emissions reductions than VOCs emissions reductions.

The percent decreases in ground-level ozone concentrations with for example 20% reduction in mobile source emissions of VOCs and NO_x appear small, these are about 3% and 5% respectively. This would suggest that imposed control measure benefits outweigh the reductions. However, overwhelming new evidence show that Mobile5a underestimates mobile emissions by a factor of 1.5 to 2.5. Therefore, the percent decreases determined in this study are very conservative. Furthermore, a 3% or 5% drop in ozone concentration level is significant relative to achieving the national ambient air quality standards (NAAQS) for ozone.

These conservative and relatively low percent decreases in ground-level ozone concentration can make the difference between achieving or exceeding the NAAQS for ozone.

An operational UAM-IV model that is calibrated and for which a satisfactory model performance evaluation was done for the Indianapolis MSA is now available and stored on the Purdue IBM 3090 mainframe computer. This is a first of its kind. Along with the results of this study, the deployed UAM-IV can be used to estimate changes in ground-level ozone concentration following targeted emissions reductions imposed by various control strategies. It can also assist various urban and environmental planners in shaping and developing appropriate policies and regulations in term of future growth in industrial and transportation activities.

5. References

Businger, J.A., J.C. Wyngaard, Y. Izumi, and E.F. Bradley, 1971: Flux-Profile Relationships in Atmospheric Surface Layer, *J. Atmos. Sci.*, **28**, 181.

Fatogoma, O, 1996: The Estimation Of Mixing Height And Its Effects On The Urban Airshed Model's Prediction Of Tropospheric Ozone Concentration. Ph.D. Thesis, Purdue Univ., W. Lafayette, IN.

Fatogoma, O and R.B. Jacko, 1995: Impact Analysis of Vehicles on Ozone Generation in the Indianapolis Metropolitan Statistical Area. Draft Final Report, HPR-2108.

Ferris, B. G., 1978: Health Effects of Exposure to Low Levels of Regulated Air Pollutants. *J. Air Poll. Control Assoc.*, **28**, 482.

Gery, M.W., G.Z. Whitten, J.P. Killus and M.C. Dodge, 1989. A Photochemical Kinetics Mechanism For Urban And Regional Scale Computer Modeling. *J. Geophys. Res.*, **94**, 12925.

Indiana Department Of Environmental Management, 1993. Revised 1990 Emission Inventory. Indianapolis, IN.

Indianapolis Air Pollution Control Section, 1992: 1990 Base Year Inventory of Ozone Precursor Emissions for Marion County. Indianapolis, IN.

Killus, J.P., J.P. Meyer, D.R. Duran, G.E. Anderson, T.N. Jerskey, S.D. Reynolds and J. Ames, 1984: Continued research in mesoscale air pollution simulation modeling, Vol. V: Refinements in numerical analysis, transport, chemistry, and pollutant removal. EPA 600/3-84-095a.

Lamb, R.G. and Seinfeld J.H., 1973: Mathematical Modeling of Urban Air Pollution-General Theory, *Environ. Sci. Technol.*, **7**, 235.

Milford, J.B., A.G. Russell And G.J. Mcrae, 1989. A New Approach To Photochemical Pollution Control: Implications Of Spatial Patterns In Pollutant Responses To Reductions In Nitrogen Oxides And Reactive Organic Gas Emissions. *Environ. Sci. Technol.*, **23**, 1290.

National Oceanic And Atmospheric Administration, 1990. *Daily Weather Maps.* Climate Analysis Center, Washington, DC.

Smolarkiewicz, P.K., 1983. A Simple Positive Definite Advection Scheme With Small Implicit Diffusion. *Monthly Weather Review*, **111**, 479-486.

U.S. Congress, 1990: Clean Air Act Amendment, Title I and II.

USEPA, 1990a. User's Guide For The Urban Airshed Model, Volume I: User's Manual For UAM (CB-IV). EPA-450/4-90-007A, Research Triangle Park, NC.

USEPA, 1990b. User's Guide For The Urban Airshed Model, Volume II: User's Manual For UAM (CB-IV) Modeling System. EPA-450/4-90-007B, Research Triangle Park, NC.

USEPA, 1990c. User's Guide For The Urban Airshed Model, Volume III: User's Manual For The Diagnostic Wind Model. EPA-450/4-90-007C, Research Triangle Park, NC.

USEPA, 1990d. User's Guide For The Urban Airshed Model, Volume IV: User's Manual For The Emission Processor System. EPA-450/4-90-007d, Research Triangle Park, NC.

USEPA, 1991. Guideline For Regulatory Application Of The Urban Airshed Model. Office Of Air Quality Planning And Standards, Research Triangle Park, NC.

Wang R.T., S.C. Gerry., J.S. Newson, A.R. Van meter, R.A. Wayland, J.M. Godowitch and K. Shere, 1990. Biogenic Emissions Inventory System (BEIS).

Zanneti, P., 1990: Air Pollution Modeling. Van Nostrand Reinhold, New York, NY.

COVER DESIGN BY ALDO GIORGINI